VILNIUS UNIVERSITY

CENTER FOR PHYSICAL SCIENCES AND TECHNOLOGIES

IEVA KULAKAUSKAITĖ

SYNTHESIS OF MAGNETIC NANO-SORBENTS, THEIR CHARACTERIZATION AND INVESTIGATION OF SORPTIVE PROPERTIES

Doctoral Dissertation

Physical sciences, Chemistry (03P)

Vilnius, 2018

The dissertation was prepared at the Institute of Physics of the Center for Physical Sciences and Technology in 2013-2017.

Supervisor:

Dr. Galina Lujanienė (Center for Physical Sciences and Technology, Physical sciences, Chemistry 03P)

VILNIAUS UNIVERSITETAS

FIZINIŲ IR TECHNOLOGIJOS MOKSLŲ CENTRAS

IEVA KULAKAUSKAITĖ

**MAGNETINIŲ NANO-SORBENTŲ SINTEZĖ,
APIBŪDINIMAS IR SORBCINIŲ SAVYBIŲ TYRIMAS**

Daktaro disertacija,

Fiziniai mokslai, Chemija 03P

Vilnius 2018

Disertacija rengta Fizinių ir technologijos mokslų centro Fizikos institute 2013-2017 metais.

Darbo vadovas:

Dr. Galina Lujanienė (Fizinių ir technologijos mokslų centras, fiziniai mokslai, chemija – 03P)

Content

Abbreviations

Chi-CG – chitosan magnetic beads modified with cysteine-glutaraldehyde schiff's base

CNT – Carbon nanotubes

Cys-Fe_3O_4 MNP – L-Cysteine functionalized magnetic nanoparticles

Fe_3O_4/montmorillonite – magnetite/montmorillonite nanocomposite

Fe_3O_4/talc – magnetite/talc nanocomposite

Fe_3O_4@TSTC[4]AS-s-SA – sodium alginate supported tetrasodium thiacalix[4]arene tetrasulfonate nanogel

FTIR – fourier-transform infrared spectroscopy

GO – graphene oxide

ICP-MS – Inductively coupled plasma mass spectrometry

INS – iron-oxide nano-particles-immobilized sand

M – magnetite

MGO – magnetic graphene oxide

MNP – magnetic nanoparticles

MPB – magnetic Prussian Blue

MPBGO – magnetic Prussian blue-graphene oxide

PB – Prussian blue

PB-MNC – Prussian blue-functionalized magnetic nanoclusters

PZC – point of zero charge

SEM – scanning electron microscope

TEM – transmission electron microscopy

TEPA – tetraethylenepentamine

WHO – World Health Organization

XRD – X-ray diffraction

γ-Fe_2O_3-2-HEAS – 2-hydroxyethylammonium sulfonate immobilized on c-Fe_2O_3 nanoparticles

INTRODUCTION

Currently, water is one of the most vital human resources and has economic, social, political and environmental importance in the world. The major water sources include groundwater, lakes and reservoirs, canals, atmospheric water generation, rainwater harvesting, fog collection and sea water. Their contamination could be varied depending on the source of pollutant. With the rapid development of the economy and industry, large amounts of wastewater containing different kinds of heavy metal ions and organic pollutants are generated (Liu et al., 2016). Heavy metals are toxic, carcinogenic and prone to accumulate in living organisms. Toxic heavy metals are a big concern in the treatment of wastewater (Fu et al., 2011).

The poisoning of copper (Cu(II)) causes keratinization, dramatization, itching of hands and feet (Huang et al., 2007, Zhou et al., 2009). Copper is essential for animal metabolism, yet the excessive ingestion of it can bring serious toxicological effects, such as vomiting, cramps, convulsions, or even death (Paulino et al., 2006). According to United States Environmental Protection Agency (USEPA) provisions, the maximum content of copper in the water is 1.3 mg/L. Thereby, the concentration of Cu(II) in wastewater should be reduced to a bare minimum before it is discharged into the environment (Liu et al., 2016).

Cobalt (Co(II)) can be accumulated through the food and do a lot of damage to human health. The excess intake of cobalt can result bone defects, low blood pressure and even genetic mutation in living cells.

Nickel (Ni(II)) finds its way into the water systems through effluents from industries. The nickel salts are known to be toxic to human health. Strong poisoning of Ni(II) causes headache, dizziness, nausea, and tightness in chest, chest pain, shortness of breath, dry cough, cyanosis, and heavy weakness (Parker et al., 1980). At higher concentrations it is a potential carcinogenic and causes

cancer of the lungs, nose and bone. (Knishna et al., 2011). According to the WHO (World Health Organization), the maximum toxicity value for nickel is 130 µg/L, assuming a 60 kg adult drinks two litres of water per day (Singh et al., 2013). Nickel carbonyl [Ni(CO)$_4$] has been estimated as fatal for humans at atmospheric exposure of 30 ppm for 30 min (Namasivayam et al., 1994).

Lead (Pb(II)), if present, with a concentration of >70µg/dL (WHO) (Singh et al., 2013) in blood vessels can cause damage to central nervous system, kidney, liver, reproductive system, basic cellular processes and brain functions. The toxic symptoms are anaemia, insomnia, headache, dizziness, irritability, weakness of muscles, hallucination and kidney damages (Naseem and Tahir, 2001).

A variety of the treatment technologies have been proposed and used to eliminate heavy metals from polluted water. Such technologies are mostly based on adsorption, chemical precipitation, ion exchange, membrane filtration, reverse osmosis, and electrolysis (Fu et al., 2011). Among those, adsorption can be ranked as one of the most preferred methods for treating heavy metals, because of its high efficiency, low cost and easy operation (Hur et al., 2015). Furthermore, process can be reversed under certain circumstances via desorbtion.

The choice of adsorbents is key to successful application of adsorption-based treatments. Number of materials have been investigated extensively for this purpose (Ahmaruzzaman et al., 2011, Rao et al., 2009, Crini et al., 2006). A number of researchers have studied the use of activated carbon sorbents in heavy metals removal process (Jusoh et al., 2007; Kang et al., 2008). Carbon nanotubes (CNTs) were discovered by Iijima (1991) in 1991. They have been proven to possess great potential for removing heavy metal ions, such as lead (Wang et al., 2007a; Kabbashi et al., 2009), cadmium (Kuo and Lin, 2009), chromium (Pillay et al., 2009), copper (Li et al., 2010), and nickel (Kandah and Meunier, 2007) from wastewater. Searching for low-cost and easily available sorbents Bhattacharyya and Gupta (2008) reviewed sorption of heavy metals on

natural and modified kaolinite and montmorillonite. Multiple polymers containing free amino and hydroxyl groups – like chitosan – were used. Since being discovered in 2004, graphene and later graphene oxide-based nanomaterials gained attention for their ability of removing different pollutants from water (Novoselov et al., 2004).

After adsorption, it can be difficult to separate sorbents from the aqueous solution using traditional separation methods, such as filtration and sedimentation, as sorbents may block filters or be lost. Furthermore, the sorbents are discarded with the process sludge, which generates secondary pollution. To overcome the problems related to the ease of separation and regeneration of sorbents, recent research has been focused on magnetic separation technology. Separation technologies employing magnetic sorbents are an alternative method for treating water/wastewater (Barquist et al., 2010, Zhang et al., 2007, Oliveira et al., 2004 and etc.). Magnetic separation was first described by William Fullarton in 1792 as a method of separating iron minerals. Simple scheme of magnetic separation is shown in Figure 1.
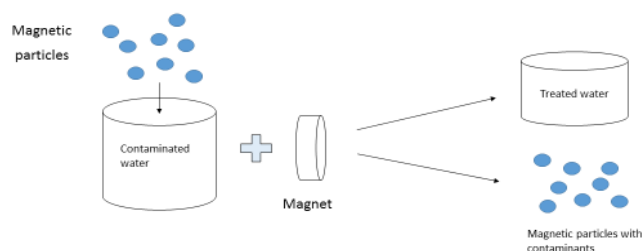
Fig. 1. Simple scheme of magnetic separation

During the 1970s and 1980s, scientists were beginning to realize that materials with magnetic properties were useful for the separation of metal pollutants that are sensitive to magnetic fields from a variety of matrices. Many of these reports deal with the influence of different parameters on the removal of metal ions by Fe_3O_4 magnetic nanoparticles (Shen et al., 2009, Yavuz et al., 2006, Yean et al., 2005, Mayo et al., 2007). As an example, Shen has observed that the adsorption efficiency of Ni(II), Cu(II), Cd(II) and Cr(VI) ions by Fe_3O_4

nanoparticles is strongly dependent on pH, temperature, the amount of the sorbent and the length of exposure. Further, Shen has also identified higher removal efficiency of these metal ions at a 3.5 mg/ml dose of nano-sorbent with an optimum pH of 4.

In order to increase the chemical stability of Fe_3O_4 nanoparticles, the surface modification of Fe_3O_4 nanoparticles is necessary. In 1996, Towler et al. reported the recovery of radium, lead, and polonium from seawater samples using a magnetic adsorbent consisting of manganese dioxide coated magnetite. Since then, other modifications of magnetic materials have been reported (Warner et al., 2010, Wang et al., 2010, Kumar et al., 2013). The main advantage of this technology is that a large amount of wastewater can be purified in a very short period of time using less energy and compared to other methods producing no contaminants (Ge et al., 2012)

Aim and objectives of this study

The main task of this work was to estimate application of synthetic magnetic nanocomposites for removal of heavy metals from liquid media.

The objectives of the study were:

1. To synthesize magnetite (M), magnetic graphene oxide (MGO), magnetic Prussian blue (MPB) and magnetic Prussian blue with graphene oxide (MPBGO) using precipitation method
2. To investigate structural, morphological and magnetic properties of the synthesized nanosorbents
3. To investigate the mechanisms of heavy metals (Cu (II), Co (II), Ni (II) and Pb (II)) sorption by nanosorbents as well as estimate the equilibrium and kinetic sorption parameters, sorption dependences on pH, heavy metal initial concentration, sorbent dosage and contact time
4. To apply theoretical isotherms and kinetic models for the analysis of experimental data

5. To estimate the suitability of synthesized nanosorbents for removal of heavy metals from the Baltic Sea water

Novelty of the study

1. The removal of Cu(II), Co(II), Ni(II), Pb(II) elements from liquid media using magnetic Prussian blue nanosorbents was studied for the first time
2. In this study, the parameters of magnetic nanosorbents affecting the sorption efficiency was estimated. The calculated parameters revealed mechanisms of sorption of heavy metals
3. Synthesized nanosorbents applied to remove the heavy metals from the Baltic Sea water

Scientific and practical significance of the results

1. Magnetic nanosorbents will have a wide range of applications not only in water treatment technologies, protecting the environment from toxic elements, but also in concentrating metals from various media
2. Automatic sorbent separation can be used in technology with studied nanosorbents
3. The results of this study are significant in the use of nanosorbents in water purification technologies, since it has made it possible to better understand toxic element sorption mechanisms, possibilities to use them across a wide pH range and their rapid kinetics
4. Complex nanosorbents are characterized by greater stability and possible reusability

Author's contribution

        Planning research, synthesizing nanosorbents, applying it in sorption experiments, evaluation and publication of results.

Statements to be defined

1. Magnetic Prussian blue nanocomposites are suitable for Cu(II), Co(II), Ni(II) and Pb(II) removal from liquid media and poses high sorption capacities (Q_{max} Cu (II) – 138 mg / g, Co(II) - 115 mg / g, Ni (II) - 155 mg / g, Pb (II) - 778 mg / g).

2. Nano-sorbents efficiently sorb Cu (II), Co (II), Ni (II) and Pb (II) at high concentrations of competing ions in complex natural waters (such as seawater).

3. The magnetic properties of the synthesized nanosorbents decrease from magnetite to more complex sorbents (M>MPB>MGO>MPBGO).

4. The different nature of sorption mechanism – chemical for Cu (II), Co (II), Ni (II), as well as physical for Pb (II) – was determined using the Dubinin-Radushkevich isotherm.

  Scientific approval

List of publications (Disertation theme):

1. **Kulakauskaitė I.,** Lujanienė G., Valiulis D. *Dependences of heavy metals sorption on nano-magnetic sorbents.* Proceedings of the 4ᵗʰ international conference on enviromental radioactivity „Radionuclides as tracers of enviromental proceses" (ENVIRA 2017). (2017) 109-112

2. Lujanienė G., Šemčuk S., Lečinskytė A., **Kulakauskaitė I**., Mažeika K., Valiulis D., Pakštas V., Skapas M., Tumėnas S. *Magnetic graphene oxide based nano-composites for removal of radionuclides and metals from contaminated solutions.* Journal of Enviromental Radioactivity. 166 (2017) 166-174

3. Lujanienė G., Šemčuk S., **Kulakauskaitė I**., Mažeika K., Valiulis D., Juškėnas R., Tautkus S. *Sorption of radionuclides and metals to graphene oxide and magnetic graphene oxide*. Journal of Radioanalytical and Nuclear chemistry 307 (2016) 2267-2275.

Other publications:

1. Lujanienė G., Štamberg K., Pakštas V., Juškėnas R., **Kulakauskaitė I**., Šemčuk S., Mažeika K., Vopalka D. *Study of Pu sorption behavior in natural clay*. Journal of Radioanalytical and Nuclear chemistry. 304 (2015) 53-59

2. Lujanienė G., Mažeika J., Li H.C., Petrošius R., Barisevičiūtė R., Jokšas K., Remeikaitė-Nikienė N., Malejevas V., Garnaga G., Stankevičius A., **Kulakauskaitė I**. Povinec P.P. *^{14}C and ^{13}C variations in organic fractions of Baltic Sea sediments*. Radiocarbon Vol 57 Nr. 3 (2015) 1-12.

3. Lujanienė G., Remeikaitė-Nikienė N., Garnaga G., Jokšas K., Šilobritienė B., Stankevičius A., Šemčuk S., **Kulakauskaitė I**. *Transport of ^{137}Cs, ^{241}Am and Pu isotopes in Curonian Lagoon and the Baltic Sea*. Journal of Enviromental Radioactivity. 127 (2014) 40-49

4. Lujanienė G., Garnaga G., Remeikaitė-Nikienė N., Jokšas K., Garbaras A., Skipitytė R., Barisevičiūtė R., Šilobritienė B. **Kulakauskaitė I**. and etc. *Cs, Am and Pu isotopes as trasers of sedimentation processes in the Curonian Lagoon-Baltic Sea system*. Journal of Radioanalytical and Nuclear chemistry. 296 (2013) 787-792

5. Lujanienė G., Beneš P., Štamberg K., Jokšas K., **Kulakauskaitė I**. *Pu and Am sorption to the Baltic Sea bottom sediments*. Journal of Radioanalytical and Nuclear chemistry. 295 (2013) 1957-1967

List of conferences and seminars:

Disertation theme:

1. **Kulakauskaitė I.,** Lujanienė G. *Lead removal from waste waters using nano-magnetic sorbent.* International conference on chemistry and material science: October 18 - 20 2017 Rome Italy. p 54

2. **Kulakauskaitė I**., Lujanienė G., Valiulis D. *Dependences of heavy metals sorption on nano-magnetic sorbents.* 4th international conference on environmental radioactivity: Radionuclides as tracers of environmental proceses (ENVIRA 2017): 29 May- 2 June 2017. p 146.

3. **Kulakauskaitė I**, Lujanienė G, Mažeika K, Valiulis D, Šemčuk S, Pakštas V, Skapas M, Tumėnas S. *Sorption of toxic metals by magnetic nanocomposites.* 9th international conference on nuclear and radiochemistry: August 29-September 2, 2016 Helsinki Finland. p 192.

4. Šemčuk S., Lujanienė G., Leščinskytė A., Tautkus S., **Kulakauskaitė I**., Juškėnas R. *Sorption of Cs, Pu and Am to graphene oxide based nanosorbents.* 9th international conference on nuclear and radiochemistry: August 29-September 2, 2016 Helsinki Finland. p 179.

5. **Kulakauskaitė I,** Lujanienė G. *Nickel sorption by magnetic nanocomposites.*
   International conference of Lithuanian Society of Chemistry "Chemistry and Chemical Technology 2016": Lithuanian Academy of Sciences Vilnius Lithuania April 28 - 29 2016. p 148

6. Lujanienė G., Šemčuk S., **Kulakauskaitė I.,** Mažeika K., Tautkus S., Valiulis D., Juškėnas R. *Application of graphene oxide and magnetic graphene oxide for removal of radionuclides and heavy metals from contaminated wastewater* International conference "Environmental radioactivity" (ENVIRA2015): Thessaloniki Greece September 21- 25 2015. p 281.

7. Lujanienė G., **Kulakauskaitė I**., Šemčuk S,, Tautkus S., Valiulis D., Mažeika K., Motiejūnas S. *Sorption of radionuclides and heavy metals to natural clay, graphene oxide and graphene oxide-ferrous oxide composite*. Tenth international conference on methods and applications of radioanalytical chemistry (MARC X): Kailua-Kona USA April 12-17 2015. p 207

8. **Kulakauskaitė I**., Lujanienė G., Šemčuk S., Mažeika K., Tautkus S. *Synthesis and characterization of graphene oxide and graphene oxide-ferrous oxide composite*. Radiation interaction with materials: fundamentals and applications. 5th international conference, Kaunas, May 12-15, 2014. p 254-255

9. Šemčuk S., Lujanienė G., **Kulakauskaitė I**., Tautkus S. *Kinetics of Pu and Am sorption to graphene oxide and graphene oxide-ferrous oxide composite*. Radiation interaction with materials: fundamentals and applications. 5th international conference, Kaunas, May 12-15, 2014. p 256-257

10. **Kulakauskaitė I**., Lujanienė G., Mažeika K. *Study of Am(III) and Pu(IV) sorption to maghemite*. Chemija 2013: 11-oji Lietuvos chemikų tarptautinė konferencija = 11th International conference of Lithuania's Chemists: Vilnius, 2013 m. rugsėjo 27 d. p 1

Other:

1. Lujanienė G., Levinskaitė L., Juškėnas R., Štamberg K., Kačergius A., **Kulakauskaitė I.**, Šemčuk S., Vodopalka D. *Study of Cs, Pu and Am sorption to natural clay and bottom sediments*. 9th international conference on nuclear and radiochemistry: August 29-September 2 2016 Helsinki Finland. p 65

2. Lujanienė G., Levinskaitė L., Juškėnas R., Štamberg K., Kačergius A., **Kulakauskaitė I.**, Gavutis M., Šemčuk S,, Vopalka D. *Sorption behavior of Cs, Pu and Am to natural clay: effect of various components.*

International conference on radioanalytical and nuclear chemistry (RANC-2016): April 10-15 2016 Budapest Hungary. p 56

3. Lujanienė G., Mažeika J., Li, H.C., Petrošius R., Valiulis D., Remeikaitė-Nikienė N., Barisevičiūtė R., Jokšas K., Garnaga-Budrė G., Stankevičius A., **Kulakauskaitė I**., Povinec, P.P. *Application of radioactive and stable isotopes to trace anthropogenic pollution in the Baltic Sea*. 23rd WiN global annual conference: women in nuclear meet atoms for peace: Vienna Austria 24-28 August 2015. p 131

4. Lujanienė G., Mažeika J., Li, H.C., Petrošius R., Valiulis D., Remeikaitė-Nikienė N., Barisevičiūtė R., Jokšas K., Garnaga-Budrė G., Stankevičius A., **Kulakauskaitė I.**, Šemčuk S., Povinec, P.P. *Application of 137Cs, 14C and Pu isotopes to trace pollutants in the Baltic Sea*. International conference "Environmental radioactivity" (ENVIRA2015): Thessaloniki, Greece, September 21- 25, 2015. p 30

5. Lujanienė G., Remeikaitė-Nikienė N., Barisevičiūtė R., **Kulakauskaitė I.**, Šemčuk S., Mažeika J., Petrošius R., Jokšas K., Li, H.C., Garnaga-Budrė G., Stankevičius A., Povinec, P.P.*The Δ14C, δ13C, δ15N and plutonium isotopes signatures in the Baltic Sea suspended particulate matter and bottom sediments*. International symposium on isotope hydrology: revisiting foundations and exploring frontiers: Vienna Austria, 11-15 May 2015. p 123-126

6. Lujanienė G., Mažeika J., **Kulakauskaitė I.**, Šemčuk S., Povinec P.P. ir kt. *Study of organic matter sources using Δ14C, δ13C and plutonium isotopes signatures*. Tenth international conference on methods and applications of Radioanalytical Chemistry (MARC X): Kailua-Kona USA April 12 - 17 2015. p 206

7. Lujanienė G., Mažeika J., Li, H.C., Petrošius R., Remeikaitė-Nikienė N., Barisevičiūtė R., Jokšas K., Garnaga G., Stankevičius A., **Kulakauskaitė I.**, Šemčuk S., Povinec, P.P. *Study of Δ14C and δ13C variations in*

organic fractions of the Baltic Sea sediments. Radiocarbon in the environment conference: Belfast, UK, August 18-22, 2014. p 66

8. Lujanienė G., Štamberg, K., Juškėnas R., **Kulakauskaitė I**., Vopalka, D. *Pu(V) and Pu(IV) oxidation state distribution in natural clay*. 17th radiochemical conference: Marianske Lazne, Czech Republic, May 11-16, 2014. p 61

9. Lujanienė G., Juškėnas R., Levinskaitė L., **Kulakauskaitė I**., Gavutis M., Šemčuk S. *Pu oxidation state transformation by natural clay and their various component* 18th international scientific conference "EcoBalt 2013" Vilnius, Lithuania, October 25-27, 2013. p 32

1. LITERATURE REVIEW

1.1. Nano sorbents

The choice of adsorbents is the key to successful application for the sorption-based treatments. Several types of materials, such as activated carbons, clay minerals, chelating materials, and chitosan/natural zeolites have been researched to adsorb metal ions from aqueous solutions. Although traditional sorbents could remove heavy metal ions from wastewater, the low sorption capacities and efficiencies severely limit their application. To solve these aforementioned limitations of traditional sorbents, nanomaterials are used as superior choice for remove heavy metal ions in wastewater. Materials with the particle size between 1 nm to 100 nm are defined as nanomaterials. Used as sorbents for removing heavy metal ions in wastewater, nanomaterials should satisfy the following criterions:

1. The nanosorbents themselves should be non-toxic.
2. The sorbents present relatively high sorption capacities and selectivity to the low concentration of pollutants,
3. The adsorbed pollutants could be removed from the surface of the nano adsorbent easily,
4. The sorbents could be infinitely recycled.

So far, a variety of nanomaterials such as carbon nanotubes, carbon based material composites, graphene, nano metal or metal oxides, and polymeric sorbents have been studied in the removal of heavy metal ions from aqueous solution, and the results indicate that these nanomaterials show high adsorption capacity (Table 1).

Table 1. Maximum sorption capacities (Q_{max}) for various sorbents

Sorbent	$Cu^{2+} Q_{max}$	$Co^{2+} Q_{max}$	$Ni^{2+} Q_{max}$	$Pb^{2+} Q_{max}$	$Cs^+ Q_{max}$	References
MGO	6.58mg/g	1.28mg/g	1.55mg/g	9.71mg/g	-	(Sun et al., 2015)
Nano-Fe3O4–SiO2–TETA	480μmol/g	-	-	680 μmol/g	-	(Mahmeda et al., 2014)
INS	1.26mg/g	-	-	2.08mg/g	-	(Lee et al., 2012)
MPB	-	-	-	-	96mg/g	(Thammawong et al., 2013)
MGO	-	-	-	-	9.25mg/g	(Li et al., 2015)
PB-MNC	-	-	-	-	45.87mg/g	(Roh et al., 2016)
Fe$_3$O$_4$/talc	21.05mg/g	-	33.33mg/g	74.62mg/g	-	(Kalantari et al., 2014)
Fe$_3$O$_4$/montmorillonite	70.92mg/g	-	65.78mg/g	263.15mg/g	-	(Kalantari et a., 2015)
PB/Fe3O4/GO	-	-	-	-	55.56mg/g	(Yang et al., 2014)
Magnetic Prussian blue/Fe3O4 core/shell	-	-	-	-	132.6mg/g	(Chang et al., 2016)
Graphene oxide (GO) aerogels	29.59mg/g	-	-	-	-	(Mi et al., 2012)
graphene oxide	294mg/g	-	-	1119mg/g	-	(Sitko et al., 2013)
γ-Fe$_2$O$_3$-2-HEAS.	-	-	-	330mg/g	-	(Khani et al., 2016)
Chi-CG	156.49mg/g	-	-	-	-	(Abou et al., 2016)
TEPA modified chitosan/CoFe2O4	168mg/g	-	-	228mg/g	-	(Fan et al., 2017)
chitosan/magnetite	-	-	52.55mg/g	63.3mg/g	-	(Vinh Tran et al., 2010)
Cys–Fe$_3$O$_4$ MNPs	-	-	-	183.5mg/g	-	(Fan et al., 2016)
magnetite nanorods	79.1mg/g	-	95.4mg/g	112.8mg/g	-	(Karami et al., 2013)
Magnetite koalite	98mg/g	-	95.2mg/g	106mg/g	-	(Lasheen et al., 2015)
Fe$_3$O$_4$@TSTC[4]AS-s-SA	90.56mg/g	74.9mg/g	97.4mg/g	99.8mg/g	-	(Lakouraj et al., 2014)

Graphene oxide (GO) based nano-composites belong to the group of the most promising sorbents capable of efficiently removing heavy metals. (Mauter and Elimelech, 2008; Zhu et al., 2010). GO was applied to the removal of Cu(II) and Pb(II) ions with the maximum adsorption capacities at pH = 5 - 294 and 1119 mg/g (Sitko et al., 2013). Nano-composites possessing magnetic properties

are especially useful since they can be easily eliminated from the solutions after the treatment procedures. Various kinds of magnetic composites were used, e.g., chitosan/magnetite nanocomposite beads were prepared, characterized and used for removal of toxic metal ions such as Pb(II), Ni(II) in the pH range from 4 to 6 (Q_{max} – 63.33 mg/g and 52.55 mg/g) (Vinh Tran et al., 2010), as well as the magnetic GO composite for Cu(II), Co(II), Ni(II) and Pb(II) (the obtained Q_{max} - 6.58 mg/g, 1.28 mg/g, 1.55 mg/g and 9.71 mg/g) (Sun et al., 2015).

Since Fukushima accident Prussian blue (PB) sorbents were widely used for the Cs elimination of contaminated water. According to Yang, sorption of the 70.25% Cs(I) to $PB/Fe_3O_4/GO$ was finished in less than 30 min (Yang et al., 2014), and the maximum adsorption capacity was 55.56 mg/g. Chang successfully fabricated magnetic Prussian blue/Fe_3O_4 core/shell nanoparticles for cesium removal with absorption maximum of 132.2 mg/g (Chang et al., 2016).

1.1.1. Iron oxides

Iron oxide nanostructures play an important role in science from technology to biotechnology. Iron oxides were widespread in nature. These compounds are ubiquitous in soils and sediments and have a profound influence on the water chemistry of aquifers and subsurface waters. Moreover, the formation of various iron oxides is dependent on abundance of water (Cornell et al., 2000, Lanf et al., 2009). The iron oxides have been known for millennia. Such minerals were used originally as pigments for paints during the Paleolithic, since then uses of iron oxides have expanded. Nowadays, iron oxides are used vastly in various fields; not only as pigments in paint, but also as catalysts, sensors, recording media material and ferrofluids (Yang et al., 2009, Saha et al., 2011, Kong et al., 2001 and etc.). Magnetic nanoparticles have many unique magnetic properties such as superparamagnetic, low Curie temperature, high magnetic susceptibility, high coercivity, etc. Various methods for synthesis and

control of shape, size, stability and dispersibility of nanoparticles have been reported (Bakhshayesh et al., 2013).

Iron oxides exist in many forms in nature, with magnetite (Fe_3O_4), maghemite (γ-Fe_2O_3), and hematite (α-Fe_2O_3) being probably the most common (Cornell et al., 2003). Some of their physical and magnetic properties are summarized in Table 2.

Table 2. Physical and magnetic properties of iron oxides (Teja et al., 2009)

Property	Oxide		
	Hematite	**Magnetite**	**Maghemite**
Molecular formula	α-Fe_2O_3	Fe_3O_4	γ-Fe_2O_3
Density (g/cm^3)	5,26	5,18	4,87
Melting point (^{o}C)	1350	1583-1597	-
Hardness	6,5	5,5	5
Type of magnetism	Weekly ferromagnetic or antiferromagnetic	Ferromagnetic	Ferrimagnetic
Curie temperature (K)	956	850	820-986
M_s at 300K (A-m^2/kg)	0,3	92-100	60-80
Standard free energy of formation ΔG_t° (KJ/mol)	-742,7	-1012.6	-711,1
Crystallographic system	Rhombohedral, hexagonal	Cubic	Cubic or tetrahedral
Structural type	Corundum	Inverse spinel	Defect spinel
Space group	R3c (hexagonal)	Fd3m	P4$_3$32 (cubic) P4$_1$2$_1$2 (tetragonal)

Lattice parameter, nm	A=0,5034 c=1,375 a_R=0,5427 α=55,3°	A=0.8396	A=0.83474 (cubic) A=0.8347, c=2.501 (tetragonal)

The most important is magnetite, which exhibits the strongest magnetism of any transition metal oxide. It is non-porous material with specific surface area, which ranges relative to preparation manner from 4 m^2/g^{-1} to 100 m^2/g^{-1} (Cornell et al., 2003). Due to their high surface area, iron oxides are used as sorbent to control the aqueous concentration of dissolved species (Bakhshayesh et al., 2013).

In magnetite crystal structure, 32 O^{2-} the oxygen ions are in a cubic close-packed arrangement (Figure 2). The unit cell edge length is a=0,839 nm. Magnetite differs from most other iron oxides in that it contains both divalent and trivalent iron ions. It has an inverse spinel structure with Fe(III) ions distributed randomly between octahedral and tetrahedral sites, and Fe(II) ions in octahedral sites (Klotz et al., 2008).
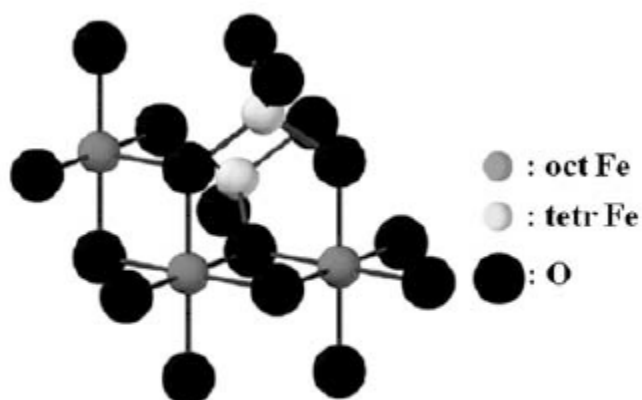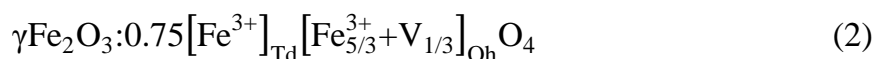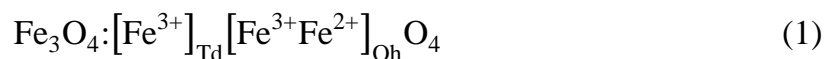

Fig. 2. Crystal structure of magnetite (Teja et al., 2009)

Magnetite is frequently non-stoichiometric in which case it has a cation deficient Fe(III) sublattice. In stoiciometric magnetite Fe(II)/Fe(III)=0.5.

The divalent ion may also be partly or fully replaced by other divalent ions (e.g. Cu, Pb) (Cornell et al., 2003). The vacancies can be completely random or partially/totally ordered. It has been shown, essentially from combined IR spectroscopy and X-ray diffraction, that vacancy ordering occurs only for particles exceeding 5 nm (Morales et al., 1999).

$$Fe_3O_4 : \left[Fe^{3+} \right]_{Td} \left[Fe^{3+}Fe^{2+} \right]_{Oh} O_4 \qquad (1)$$

$$\gamma Fe_2O_3 : 0.75 \left[Fe^{3+} \right]_{Td} \left[Fe^{3+}_{5/3} + V_{1/3} \right]_{Oh} O_4 \qquad (2)$$

1.1.1.1. Magnetization of iron oxide particles

Iron oxide particles are classified by their response to an externally applied magnetic field. Description of orientations of the magnetic moments in a particle helps to identify different types of magnetism observed in nature. The magnetic properties of these particles can be described by the dependence of the magnetic induction B on the magnetic field H. Some materials, such as iron exhibit ferromagnetism, in that, they can be permanently magnetized. In most materials the relation between B and H is linear: $B=\mu H$; where μ is the magnetic permeability of the particles. Iron oxide particles exhibit paramagnetism if $\mu>1$; and diamagnetism if $\mu<1$. In vacuum, $\mu=1$. Alternatively, the magnetic susceptibility $\chi=\mu - 1$ is used. Hence, paramagnetic nanoparticles have $\chi>0$; diamagnetic particles $\chi<0$; and in vacuum $\chi=1$. One important advantage of the magnetic nanoparticle is their superparamagnetism. That enables their stability and dispersion upon removal of the magnetic field. as no residual magnetic force exist between the particles. Below approximately 15 nm, such particles are so small that the cooperative phenomenon of ferromagnetism is no longer observed, and no permanent magnetization remains after the particles have been subjected to an external magnetic field. However, the particles still exhibit very strong paramagnetic properties (hence the name of the phenomenon) with a very large susceptibility. Particles, whose unpaired electron spins align themselves

spontaneously so that the material can exhibit magnetization without being in a magnetic field are called ferromagnetic particles. Ferromagnetism is a so-called cooperative phenomenon, as single atom cannot exhibit ferromagnetism, but once a certain number of atoms are bound together in solid form, ferromagnetic properties arise. When the ferromagnetic particles are removed from the field, they exhibit permanent magnetization. Upon field reversal, the ferromagnetic material will initially oppose the field change, but eventually most domains will have switched their magnetization vectors and the same inverse magnetization is attained. Ferromagnetic materials, which are ground down to particle dimensions smaller than a particular domain, are no longer ferromagnetic but exhibit superparamagnetism (Elliott et al., 1998). In case of paramagnetic particles, a magnetic field is altered by the magnetic materials present in it. If a particle contains magnetic moments that can be aligned in an external magnetic field, this will amplify the field. Such substances exhibit the property of paramagnetism. In contrast to ferromagnetic materials (ferromagnetism), no permanent magnetization remains in paramagnetic materials, when they are removed from the magnetic field. Paramagnetism can be understood by postulating permanent atomic magnetic moments, which can be reoriented in an external field. These moments can be either due to orbiting electrons or due to atomic nuclei. The torque applied by an external magnetic field on these moments will tend to orientate them parallel to the field, which then reinforce it (Chen et al., 1986). The iron atom has a strong magnetic moment due to four unpaired electrons in its 3d orbital. When crystals are formed from iron atoms, different magnetic states can arise as shown in Figure 3. In the paramagnetic state, the individual atomic magnetic moments are randomly aligned with respect to each other, and the crystal has a zero-net magnetic moment. If this crystal is subjected to an external magnetic field, some of these moments will align, and the crystal will attain a small net magnetic moment. In a ferromagnetic crystal, all the individual moments are aligned even without an external field. A ferrimagnetic crystal, on the other hand, has a net magnetic moment from two types of atoms with moments of different strengths that are arranged in an

antiparallel fashion (see Figure 3). If the antiparallel magnetic moments are of the same magnitude, then the crystal is antiferromagnetic and possesses no net magnetic moment.
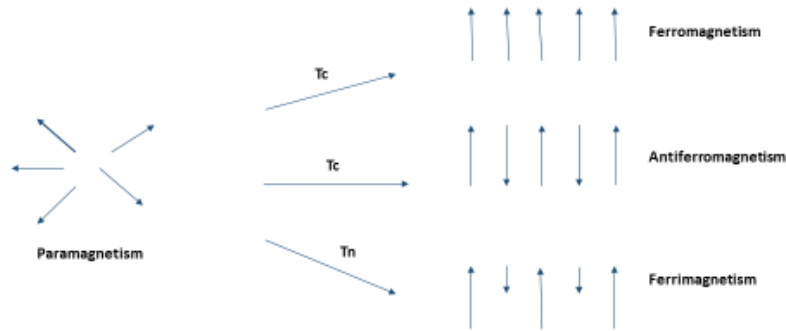

Fig. 3. Alignment of individual atomic magnetic moments in different types of materials (Teja et al., 2009)

In a bulk ferromagnetic material, the magnetization B is the vector sum of all the magnetic moments of the atoms in the material per unit volume of the material. The magnitude of B is generally less than its value when all atomic moments are perfectly aligned, because the bulk material consists of domains with each domain having its own magnetization vector arising from an alignment of atomic magnetic moments within the domain. The magnetization vectors of all the domains in the material may not be aligned, leading to a decrease in the overall magnetization. When the length scale of the material becomes small, however, the number of domains decreases until there is a single domain when the characteristic size of the material is below some critical size d_C.

If an external magnetic field of strength H is applied to a ferromagnet of magnetic strength B, the magnetization curve of Figure 4 is obtained showing B increases with H until a saturation value B_S is reached.
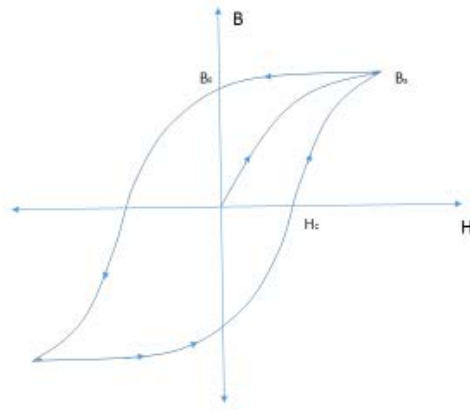
Fig. 4. Magnetization *B* as a function of an applied magnetic field *H*

The magnetization curve displays a hysteresis loop, because all domains do not return to their original orientations when *H* is decreased after the saturation magnetization value is attained. Thus, when *H* returns to zero, there is a remnant magnetization B_R which can only be removed by applying a coercive field H_C in the opposite direction of the initially applied field. A single domain magnetic material has no hysteresis loop and is said to be superparamagnetic. Iron oxide nanoparticles smaller than about 20 nm often display superparamagnetic behaviour at room temperature (Majewski et al., 2007). The ordered arrangement of magnetic moments decreases with increasing temperature due to thermal fluctuations of the individual moments. Beyond the Neel or Curie temperature, the material becomes disordered and loses its magnetization. The transition temperature is termed the Curie temperature T_C for ferromagnetic and ferrimagnetic substances, and the Neel temperature T_N for antiferromagnetic substances. Superparamagnetic particles are usually ordered below a blocking temperature, T_B.

Ferrous oxide (magnetite) can be synthesized by many methods, such as:

o   Gas phase methods (depends on thermal decomposition (pyrolysis), reduction, hydrolysis, disproportionation, oxidation, or other reactions to precipitate solid products from the gas phase);

o   Liquid phase methods (co-precipitation or other methods involving liquids/solvents);

o   Two phase methods (Water-in-oil (w/o) microemulsions consisting of nano-sized water droplets dispersed in an oil phase and stabilized by surfactant molecules at the water/oil interface);

o   Sol/gel methods (the hydrolysis and condensation of metal alkoxides or alkoxide precursors);

o   High pressure hydrothermal methods (relies on the ability of water at elevated pressures and temperatures to hydrolyze and dehydrate metal salts).
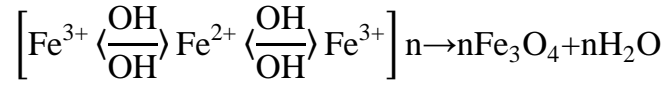
Several previous articles have covered the synthesis, protection, functionalization, and application of MNPs, as well as the magnetic properties of nanostructured systems (Lu et al., 2007, Wu et al., 2008, Unsoy et al., 2015). Unique shape magnetite nanoparticles, such as those of high aspect ratio, can be achieved in two main synthetic routes: (i) direct synthesis (in which the anisotropic growth is directed by tuning the reaction conditions or by using templates) and (ii) assembly methods (in which the high aspect ratio is achieved by the assembly from individual building blocks) (Fratila et al., 2014).

Most common, easiest and economic method for the controlled synthesis of large amounts of superparamagnetic nano-particles, without any stabilizing surfactant agents, is the chemical co-precipitation of iron salts in an alkaline environment, (Martinez-Mera et al., 2007, Sun et al., 2004, Lee et al., 2004, Qiu et al., 2005) known as the Massart process (Massart et al., 1982). In alkaline solutions, Fe(III) and Fe(II) precipitate spontaneously with a small

solubility product constant. If there are only divalent and trivalent ferrous ions in the solution, the precipitates are only the hydroxides of Fe(III) or Fe(II), which can be expressed as:

$$Fe^{3+}+3OH^{-}\rightarrow Fe(OH)_3\downarrow \tag{3}$$

$$Fe^{2+}+2OH^{-}\rightarrow Fe(OH)_2\downarrow \tag{4}$$

If these two kinds of ferrous ions are mixed together in alkaline conditions, the hydroxides formed may be adsorbed mutually producing a new kind of mixture that is highly unstable in normal conditions and can be stripped of water in its molecular structure. Reaction of producing magnetic nano-particles can be expressed as:

$$Fe^{2+}+Fe^{3+}+8OH^{-}\rightarrow Fe(OH)_2+2Fe(OH)_3$$

$$nFe(OH)_2+2nFe(OH)_3\rightarrow \left[Fe^{3+}\langle\tfrac{OH}{OH}\rangle Fe^{2+}\langle\tfrac{OH}{OH}\rangle Fe^{3+}\right]n \tag{5}$$

$$\left[Fe^{3+}\langle\frac{OH}{OH}\rangle Fe^{2+}\langle\frac{OH}{OH}\rangle Fe^{3+}\right]n\rightarrow nFe_3O_4+nH_2O$$
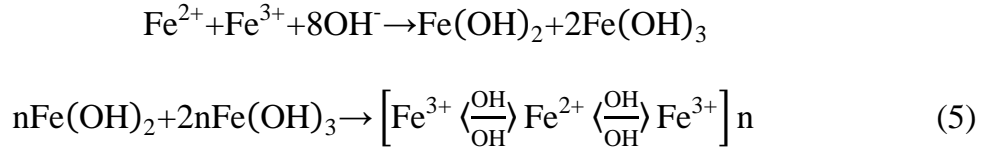
Once a core of Fe₃O₄ crystal is formed, the liquid phase becomes a two-phase system and because of the tremendous surface energy, small crystals tend to aggregate to form larger particles. The mechanism described by Eq. (5) indicates the formation process of the Fe₃O₄ core, which involves adsorption and dehydration of the hydroxides of Fe(II) and Fe(III). By this mechanism, the growth model is direct aggregation of particles. The stability of particles can be expressed as:

$$W=(a+b)\int_{a+b}^{\infty}\exp\left[\frac{V(R)}{k_BT}\right]\frac{dR}{R^2} \tag{6}$$

Where W is the stability factor of particles, a and b are the radius of the two particles, respectively, R is the distance between the two particles, and $V(R)$ is the function of potential energy of interaction, and kB is Boltzmann's constant. When the distance between particles is decreased to a certain extent, short-range reactions (such as van der Waals forces) may lead to the strong attraction

between particles. Generally, in the process of reaction without any external disturbance around the crystal, the particles of Fe_3O_4 can approach each other and aggregate easily, growing gradually into larger particles that reach the micrometer scale or larger. So, it is important to maintain adequate distance between particles for the stability of the multi-phase system (Tang et al., 2009).

As is well known, certain reaction conditions in this process and the dimensions of the nanocrystals have a significant impact on the chemical, physical, structural and magnetic properties of the nanoparticles (Roth et al., 2015). The control of shape, size and composition of nanoparticles depends on the type of salts used (e.g. sulphates, nitrates, chlorides, perchlorates, etc.), Fe(II) and Fe(III) ratio, pH and ionic strength of the solution (Gupta et al., 2005). When all these parameters are controlled, it is possible to synthesize particles with a size ranging from 4.2 to 16.6 nm (Massart et al., 1987). Other studies have showed that the modulation of ionic strength and acidity enables the tailoring of the particle size in the range of 2-15 nm. The shape variation is related to the variation of the electrostatic surface density of the nanoparticles (Jolivet et al., 2002, 2004). Organic ligands can influence co-precipitation products. For example, citrate helps produce smaller MNPs (8 nm) compared to MNP's size without citrate (14–28 nm), strongwe magnetic performance and better dispersion (Chem et al., 2015). It also prevents oxidation of magnetite to produce hematite. The effect of citrate can be explained by two processes: the chelation of citrate with iron ions prevents aggregation and the adsorption of citrate on the nuclei generate hydrolysis, inhibiting the growth of the nuclei (Bee et al., 1995).

According to the thermodynamics reaction Nr. 7, a complete precipitation of Fe_3O_4 should be expected between pH 9 and 14, while maintaining a molar ratio of Fe(III):Fe(II) at 2:1 under a non-oxidizing oxygen free environment. Otherwise, Fe_3O_4 might also be oxidized as:

$$Fe_3O_4 + 0.25O_2 + 4.5H_2O \rightarrow 3Fe(OH)_3 \qquad (7)$$

Jolivet has studied the influence of the Fe(II)/Fe(II) ratio on the size, composition, morphology, and magnetic properties of coprecipitated nanoscale particles (Jolivet et al., 1994). Small values of the x=Fe(II)/Fe(III) ratio are known to lead to goethite formation. For x=0.3, two distinct phases are coexisting: one that it is likely to be an oxy-hydroxide (made of 4 nm sized particles with a low Fe(II) content, (Fe(II)/Fe(III) about 0.07) and the other that is a non-stochiometric magnetite (consists of larger particles having a variable size and a composition Fe(II)/Fe(III) around 0.33). For x=0.35, the latter phase is the only constituent and its Fe(II)/Fe(III) ratio is equal to x. For x=0.5 corresponding to magnetite stoichiometry, particles are found to be homogeneous in size and composition (Jolivet et al., 1992).

Oxidation in the air can convert magnetite (Fe_3O_4) into maghemite (γFe_2O_3). Many electron or ion transfers depends upon the pH of the solution. Under acidic and anaerobic conditions, surface Fe(II) ions are desorbed as hexa-aqua complexes in solution, while, under basic conditions, the oxidation or reduction of the surface of magnetite may occur. The oxidation of ferrous ions is always correlated with the migration of cations through the lattice framework, creating cationic vacancies to maintain the charge balance. Two methods were reported to prevent the change of the ratio caused by air oxidation. One is that the synthesis of particles must be done without oxygen by passing N_2 gas. Using nitrogen gas not only protects critical oxidation of the magnetite, but also reduces the particle size when compared with the methods without removing the oxygen (Gupta et al., 2004, Kim et al., 2001). Another is to set the initial Fe(III)/Fe(II) molar ratio to less than 2:1, so that after the oxidation of Fe(II) to Fe(III), the ratio approaches to 2:1 (Fu et al., 2001).

Another very important factor influencing the synthesis is the iron concentration. The evolution of this factor is similar to the Fe(II)/Fe(III) ratio, with an optimum concentration between 39 and 78 mmol/L. The particle size of magnetite is strongly dependent upon the acidity and the ionic strength of the precipitation medium (Jiang et al., 2004, Jolivet et al., 2000). The higher the pH

and ionic strength, the smaller the particle size and size distribution will be, because these parameters determine the chemical composition of the crystal surface and consequently the electrostatic surface charge of the particles (Tartaj et al., 2006).

1.1.2. Graphene oxide

The study of graphene has been one of the most exciting topics in material science and many research fields since the first report of the preparation and isolation of a single graphene layer in 2004 (Showalter et al., 2016). It is a two-dimensional structure composed of a single layer of sp^2 networks of carbon atoms. Graphene has attracted tremendous attention and research interest, because of its exceptional physical properties, such as high electronic conductivity, good thermal stability, and excellent mechanical strength. For these reasons, graphene and its derivatives have been explored in a wide range of applications: electronics and optoelectronics (Avouris et al., 2012), chemical and biological sensors (Jiang et al., 2011), analytical chemistry (Li et al., 2012), electrochemistry (Brownson et al., 2010) energy-related areas including solar cells, lithium ion secondary batteries, supercapacitors, and catalysis (Luo et al., 2012). The hexagonal arrays of carbon atoms in graphene sheets are ideal for strong interactions with other molecules. However, graphene is insoluble and hard to disperse in all solvents due to strong van der Waals interactions, that can hamper sorption of organic compounds or metal ions. Therefore, the functionalization of graphene sheets can be important for their future applications (Georgakilas et al., 2012).

Graphene oxide (GO) is a precursor for graphene preparation that is prepared through the strong oxidation of graphite using e.g. $K_2Cr_2O_7$ or $KMnO_4$ like in the Hummer method.
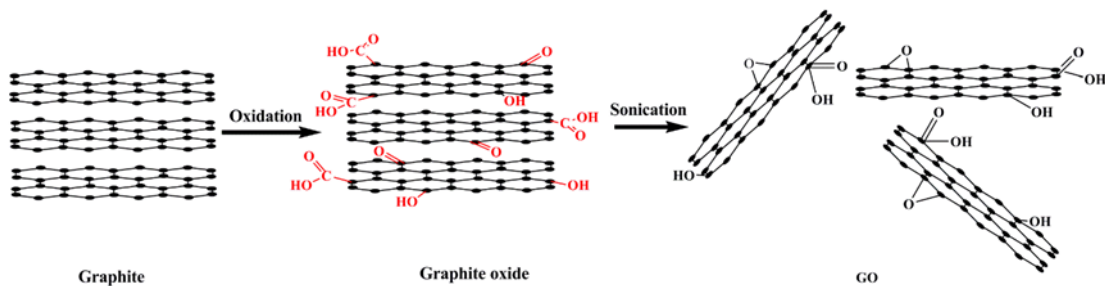
Fig. 5. Preparing graphene oxide (GO) (Li et al., 2014)

The oxidation process introduces large quantities of oxygen atoms on the surface of GO in the forms of epoxy, hydroxyl, and carboxyl groups (Fig. 6) (Showalter et al., 2016). In consequence, the interlayer spacing increases from 0.335 nm for graphite to more than 0.625 nm for GO. Moreover, GO is much more hydrophilic than the graphene. Functional groups containing oxygen atoms have a lone electron pair and, through sharing an electron pair, they can efficiently bind a metal ion to form a metal complex. In addition, the large surface area of GO (theoretical values of ~2620 m^2/g) enables it to have a large adsorption capacity. Zhao *et al*. applied GOs to remove U(VI), Cd(II) and Co(II) from aqueous solutions and found the sorption capacity of 97.5 mg/g for U(VI) at pH 5.0, 106.3 mg/g for Cd(II) at pH 6.0 and 68.2 mg/g for Co(II) at pH 6.0 (Zhao et al., 2011, 2012). Other researchers found that the adsorption capacity of Cu(II) on GO was 10 times higher than that of Cu (II) on activated carbon (Yang et al., 2010). Multi-layered graphene oxide has exceptionally high reported sorption capacity for several toxic metals including lead (842 mg/g) (Zhao et al., 2011a), cadmium (Zhao et al., 2011b) and uranium (97.5 mg/g) (Zhao et al., 2012). Results also indicate that metal adsorption to GO depends strongly on the pH and ionic strength of the system.
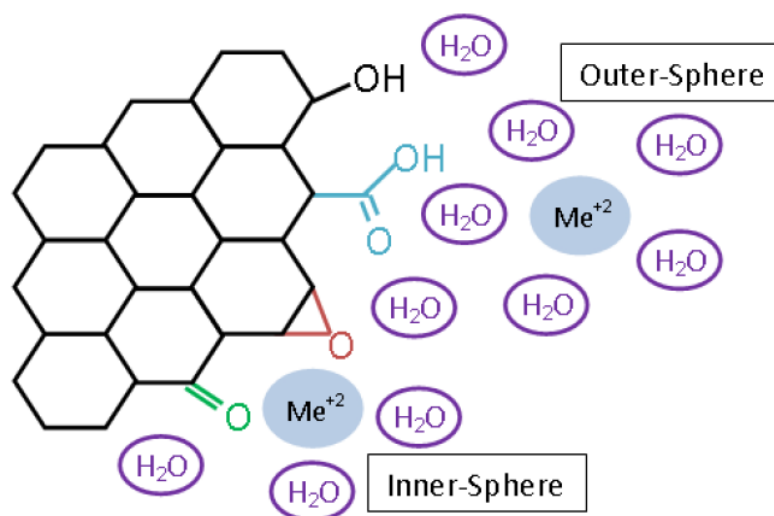
Fig. 6. Structure model of graphene oxide. Included on the edge are examples of basal epoxide (red), ketone (green), and hydroxyl (black) functional group sites and edge site ester or lactol (blue) functional groups (Showalter et al., 2016)

Reduced graphene oxide is obtained by reduction of graphene oxide, so they have some similar properties, like the large theoretical surface area (Li et al., 2012), which leads to have the great potential in the adsorption. Significantly, reduction of graphene oxide with hydrazine hydrate to obtain reduced graphene oxide can make reduced graphene oxide contain a range of -NH_2 groups (Yu et al., 2013), which can well coordinate with bivalence metal ions (Xin et al., 2012, Donia et al., 2012, Baba et al., 2006) to enhance the adsorption capacity of metal ions on graphene. Besides, the decoration of nano-materials onto graphene is also helpful to overcome the aggregation of individual graphene (Williams et al., 2008) and nanomaterials themselves.

1.1.3. Prussian blue nano-sorbent

Prussian Blue (PB, Ferric hexacyanoferrate) is a pigment of dark blue color (A dark blue color is connected with an intense intervalence charge-transfer absorption band of the compound near 700 nm, due to a transition from

the ground state to an excited state on which an electron is transferred from the Fe(III)/Fe(II) state to the Fe(II)/Fe(III) state) with idealized chemical formula $Fe^{2+}_4[Fe^{3+}(CN)_6]_3 * 14H_2O$ (in stoichiometry can sometimes be written as $Fe^{2+}[Fe^{3+}(CN)_6]_{3/2} * 7/2H_2O$). Its low-cost and high stability make its use feasible for large-scale application. PB has a simple 3D face-centered cubic lattice structure of ferrous and ferric ions occupying the corners of the cube, cyanide groups positioned on the sides and eight water molecules. It is shown in Figure 7 (Bhatt et al., 2012). The cubic unit cell dimensions are 10.2 A.

Fig. 7. Structure of Prussian blue (Bhatt et al., 2012)

In each network unit of PB, Fe(II) ions are linked by carbon atoms of cyanide ions, and Fe(III) ions are surrounded by nitrogen ends of cyanides, allowing for low-spin and high-spin electron configurations, respectively. The open framework of PB has some interstitial sites and vacancies where counter cations and other small molecules can be intercalated. One of the possible mechanism of sorption is that potassium ions can be replaced with other cations (Bhatt et al., 2012).

As mentioned before, there are three structurally distinguishable water molecules in PB: (i) coordinated water molecules at empty nitrogen sites, (ii) non-coordinated water molecules in the spherical cavities and (iii) at interstitial sites. Out of 14 water molecules, six water molecules are coordinated to Fe(II) at empty nitrogen sites 24e (x, 0, 0) site, four non-coordinated water molecules at 32f (x, x, x) site inside the spherical cavity, and

35

the remaining four non-coordinated water molecules are found at 8c (1/4, 1/4, 1/4) site of unit cell octants (Herren et al., 1980). Figure 8 shows the typical spherical cavity formed by coordinated water molecules in case of PB. The non-coordinated water molecules are omitted for clarity. The diameter of the cavity, estimated by the positions of the oxygen atoms of the coordinated water molecules, is ∼5.2 Å (Sharma et al., 2014).
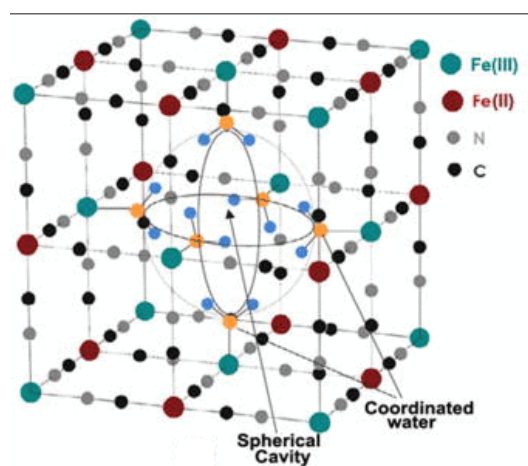

Fig. 8. The unit cell of Prussian blue (PB), The spherical cavity formed by coordinated water molecules in PB is indicated. The non-coordinated water molecules are omitted for clarity (Sharma et al., 2014)

The pharmaceutical-grade PB was used as sorbent to remove Cs from patient body after the Chemobyl disaster in 1987. After the Fukushima Daiichi nuclear disaster, Prussian blue was used as sorbent in decontamination of radioactive cesium, because of its high selectivity for cesium. This observation correlated with the hydration radio of the cations in the order of Cs(I) (3.25 Å), followed by K(I) (3.3 Å), Na(I) (3.6 Å), Ca(II) (4.1 Å), and Mg(II) (4.25 Å), with the hydrated ions of Cs just fit the cage size of the PB lattice (Thammawong et al., 2013). Ishizaki et al. (2013) revealed that the synthesized PB nanoparticles ($Fe_4(Fe(CN)_6)_3$) with many hydrophilic defect sites has supreme Cs adsorption capability and observed that the Cs(I) ions were adsorbed onto the defect sites of nanoparticles by proton-elimination reaction from the coordinated waters.

The PB nanoparticles can effectively uptake ions, however, their recovery after sorption is challenge to field applications of these adsorbents. There are many methods to immobilize Prussian blue. Some authors adopted porous silica- or glass-based nanocomposites containing PB type 10 nm nanoparticles, $Co^{2+}/[Fe(CN)_6]^{3+}$, which showed three times higher adsorption capacity of Cs than for the respective bulk materials. Kitajima et al. (2012) adopted the ion-exchange technique (Na^+ to K^+) for immobilizing PB nanoparticles onto the cotton matrices and applied the so-produced PB-matrices to adsorb Cs^+ from water at a decontamination factor (DF, defined as the ratio of Cs^+ concentration before to that after adsorption). Yasutaka et al. (2013a) applied PB impregnated non-woven fabric to remove ^{134}Cs and ^{137}Cs from water streams. These authors noted that the radioactive cesium in water samples could be concentrated within 20–60 min by passing the sample through 10–12 columns, connected in series to recover 100–108% of isotopes.

Prussian blue can be formed by several methods such as the reaction between the salt of hexacyanoferrate(II) ions and the salt of ferric ions to form the PB precipitate (Sun et al. 2007), according to the reaction:

$$FeCl_3 + K_4[Fe(CN)_6] \rightarrow 3KCl + KFe[Fe(CN)_6] \tag{8}$$

The potassium ferric hexacyanoferrate, $KFe[Fe(CN)_6]$, obtained here is known as the colloidal soluble PB. Insoluble Prussian blue could be prepared by adding excess ferric ion, resulting in the equation,

$$4FeCl_3 + 3K_4[Fe(CN)_6] \rightarrow Fe_4[Fe(CN)_6]_3 + 12KCl \tag{9}$$
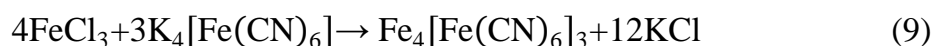
The $Fe_4[Fe(CN)_6]_3$ is prepared by the addition of ferric ions to an aqueous potassium ferrocyanide solution with a ratio of 4:3. The reaction propagates to forge a linear Fe(II)–CN–Fe(III) linkage consisting of a simple cubic lattice of alternating Fe(II) and Fe(III) ions connected through cyanide bridges. Water molecules bind the unsaturated Fe(III) ions and center each cubic octant of the unit cell (Arun et al., 2014).

It is important to notice that starting reagents are the same, but at different starting ratios. If excess potassium hexacyanoferrate in the starting reagents is used, then the colloidal soluble PB will result, while the insoluble PB is obtained if the excess ferric ion is used.

1.1.4. Magnetic Prussian blue/ Magnetic Prussian blue with graphene oxide

Prussian blue prepared by a precipitation method is usually in the form of a very fine powder, so it is unsuitable for column loading and it is difficult to separate it after sorption from aqueous solutions by filtration or centrifugation. This problem can be solved by surface coating of Fe_3O_4 magnetic nanoparticles (MNPs). Sasaki and Tanaka (2012) developed a PB modified magnetite (PB-Fe_3O_4) for decontamination of Cs(I) in water. As a result, the maximum sorption amount of Cs(I) with PB-Fe_3O_4 was 16.2 mg g/1, and the sorption ability was not greatly changed in the presence of high concentration of NaCl. Namiki et al. (2012) investigate the potential use of PB-coated magnetic nanoparticles, termed ''Prussian blueberry'', which were composed of a magnetite nanoparticle-core and a PB-shell. Under a magnetic field, Prussian blueberry (5 mg) reduced the cesium concentration of seawater (3 ml) from 150 ppm to about 50 ppm. In the large-scale study of the magnetic elimination of cesium from seawater under agitation (150 ml of seawater containing cesium (150 ppm) and mixed it with Prussian blueberry (250 mg)), Prussian blueberry eliminated similar amounts of cesium from the seawater. Under a magnetic field for 5 min, the cesium concentration was decreased by 35.0% to 35.6% of that in the non-treated groups. Thammawong et al. (2013) developed a new nano-sorbent based on the magnetic nanoparticles (MNP) functionalized with PB that possessed both high Cs adsorption capacity (96 mg Cs g/1 sorbent) and large distribution coefficient (104 ml g/1 at 0.5 ppm Cs concentration). The magnetic particles can be easily

separated from the water stream. However, the recovery of MNP in drinking water streams is not easy in practice.

Prussian blue-coated Fe_3O_4 magnetic nanocomposites have been fabricated via many kinds of methods: facile one-pot method, simple precipitation reaction, physical mixing and etc. T. Arun synthesized 10nm cubic shaped magnetic Prussian blue nanoparticles by controlling the ferric ion concentration (Arun et al., 2013). Yang fabricated magnetic Prussian blue sorbent with graphene oxide for cesium removal. Maximum adsorption capacities were 43.52 mg/g (Yang et al., 2014).

To coat PB on to the surface of MNP, it is necessary to react the hexacyanoferrate(II) ions with the ferric ions in the presence of MNP. In this case, the magnetic nanoparticles can act as nucleation sites for the precipitated Prussian blue, resulting in the coating of the PB on to the MNP surface. To improve the coating, this reaction is performed under acidic conditions. The attachment of the Prussian blue with the magnetite could be explained based on the electrostatic attraction of charges on the surface of smaller Fe_3O_4 nanoparticles with that of opposite charges in PB. The surface charge of magnetite occurred due to the presence of ferrous and ferric ions. Various possible scenarios, thus exist: (i) the positively charged magnetite surface (from protonation), gets attached to the –C≡N– bond of PB, (ii) the negatively charged surface (from deprotonation or surface metal ion hydrolysis) gets attached to the ferrous/ferric ions in PB, (iii) the ferrous/ ferric ions in the magnetite surface (in the absence of hydroxyl ions) directly replaces the ones in PB and (iv) the oxygen ions in the magnetite surface attaches to the ferrous/ferric ions in PB. The four cases described above are illustrated in Figure 9, where the top and right side of the cube represents the charges in hydrous environment. The left and bottom side of the cube in Figure 9 represents the direct attachment of PB with the ions (O^{2-} and Fe^{2+}) at the surface of the magnetite with stronger bonds compared to the other two (Namiki et al., 2012).
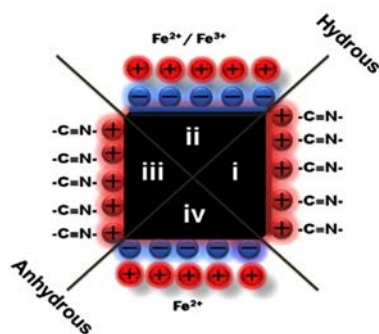
Fig. 9 Schematic diagram showing various possible mechanisms for the attachment of Prussian blue with Fe_3O_4 due to surface charges (Arun et al., 2013)

The enhancement in the fraction of PB with HCl treatment indicates that positively charged surface is more favourable. This could be understood since more negatively charged $-C\equiv N-$ sites in Prussian blue are available for attachment than positive ferrous/ferric sites. The zeta potential values for PB are found to be negative in the entire pH range (Hu et al., 2012).

The improved sorption efficiency and reduced aggregation can be achieved by synthesis of $PB/Fe_3O_4/GO$ too (Arun et al., 2013). The synthesis mechanism involves three steps (Figure 10). First, graphene oxide was dispersed in water, because of its strong hydrophilicity and electrostatic repulsion effect (Bai et al, 2010). Ferrous salt is then added to the GO suspension and stirred vigorously. The ferrous ions tend to diffuse toward the GO sheets *via* electrostatic interactions, which are then oxidized to ferric ions by oxygen containing functional groups present in the GO (Xue et al., 2011). The resultant magnetite (Fe_3O_4) nanoparticles are then deposited on the GO surface *in-situ* by the hydrolysis of ferric ions. Second, the potassium ferrocyanide solution is slowly dripped to the above solution. The solution colour changes from black to dark blue, indicating the formation of PB nanoparticles.
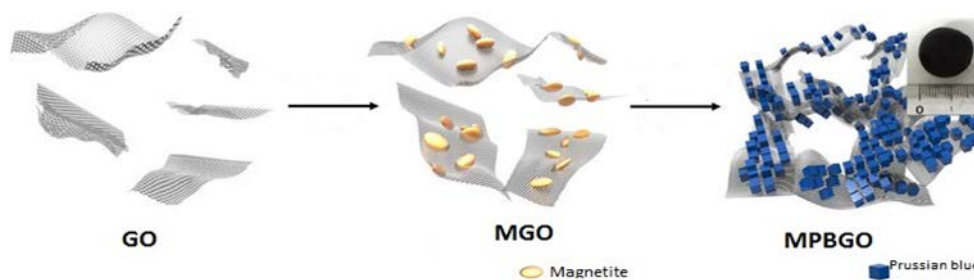
Fig. 10. Synthesis of magnetic Prussian blue sorbent based on graphene oxide (Jang et al., 2015)

To improve the deposition of PB nanoparticles on the GO surface, the reaction is carried out under acidic condition (pH 3) since Fe^{3+} sites are preferentially created on the graphene oxide surface and can react with the nearby hexacyanoferrate ions (Jang et al., 2015).

1.2. Magnetic nanoparticles stabilization

The stabilization of the iron oxide particles is crucial in obtaining magnetic ferrofluids that are stable against aggregation in both water and a magnetic field. Magnetic nanoparticles are prone to aggregates due to strong magnetic dipole–dipole attractions between particles and the high surface energy, which will limit their applications (Vayssières et al., 1998, Hong et al., 2006).

The stability of a magnetic particles results from the equilibrium between attractive and repulsive forces. In iron oxide, the surface iron atoms act as Lewis acids and coordinate with molecules that donate lone-pair electrons. Therefore, in aqueous solutions, the Fe atoms coordinate with water, which dissociates readily to leave the iron oxide surface hydroxyl functionalized. These hydroxyl groups are amphoteric and may react with acids or bases (Lefebure et al., 1998). Depending upon the pH of the solution, the surface of the magnetite will be positive or negative. The isoelectric point is observed at pH 6.8 (Bacri et al, 1990). Around this point [point of zero charge (PZC)], the surface charge density (Σ) is too small and the particles are no longer stable in water and flocculate. Playing on both electrostatic and steric stabilization is then necessary

to obtain stable iron oxide nanoparticles. Thus, it is necessary to modify these particles by functionalization and modification of the surface of magnetic nanoparticles (Fan et al., 2015).

In addition, these surface functionalities provide sites for the uptake of specific/selective metal ions and enhance the efficiency of their removal. For example, after coating Prussian blue with magnetite maximum sorption capacity for Cu^{2+} ions increase from 45.4 mg/g to 79.1 mg/g (Lujanienė et al., 2017).

1.2.1. Carbon based materials

Carbon materials as base carriers for the preparation of magnetic composites are particularly attractive because they have a variety of surface functional groups that can be tailored to specific applications, excellent mechanical strength for long-term use, and can be produced rapidly, efficiently, and with high yields. By nature, magnetic particles tend to aggregate, but will not do so in the context of a surrounding carbon material (Sun et al., 2015). There are several carbon-based materials what can be used for magnetite coating, like – activated carbon (Azari et al., 2015) or carbon nanotubes (Zhang et al., 2012).

Of all the carbon-based materials that have been tested, graphene oxide is often chosen as a base material for manufacturing magnetic materials due to its cost effectiveness, availability, versatility, low toxicity, chemical properties as well as, ultra-high specific surface area (Sun et al., 2015). Graphene oxides (GOs), produced through the chemical treatment of natural graphite through oxidation, contain a large amount of oxygen-containing functional groups such as carboxyl and carbonyl groups, which is suited to bind with metal ions. The adsorbed analytes could be easily eluted with acid according to the H^+ competing.

One of the biggest advantages of preparing magnetic composites with graphene oxide is that it is quite easy to prepare using a co-precipitation method, because the functional groups on the surface of iron oxide particles easily react

with those of graphene oxide or its derivatives (Zou et al., 2012). Synthesis scheme is shown in Figure 11.

Fig. 11. Magnetic graphene oxide synthesis

In general, magnetic nanoparticles are chemically highly active, and are easily oxidized in air, resulting in a loss of magnetism and dispersibility (Lu et al., 2007, Wu et al., 2008). When these magnetic particles are bonded with graphene oxide, they may not only be protected from oxidation, but may also have reduced toxicity, reduced aggregation, an extended surface area (Donadel et al., 2008, Zhang et al., 2012, Belessi et al., 2008) and can be easily separated via an external magnetic field.

1.2.2. Polymers

Recently, the application of biopolymers in solving environmental problems has received considerable attention. Natural polymers, especially polysaccharides that are readily available, inexpensive and biodegradable, possess numerous reactive groups able to participate in metal ion adsorption (Kekkonen et al., 2009). Typical examples of polymers used for this purpose are chitosan, alginate, dextran (Maghsoodi et al., 2009, Zhuo et al., 2009, Liu et al., 2009). However, some disadvantages related to their poor chemical resistance and weak mechanical properties still limit large-scale industrial applications with efficient sorbent regeneration. An innovative technology that gains attention in resolving these issues is the use of particulate magnetic materials

incorporated in natural polymeric matrices. This leads to good performance due to high specific surface area and to the possibility to remove the used adsorbent from the contaminated waste streams by an external magnetic field in order to regenerate it for subsequent reuse (Gregorio-Jauregui et al., 2012). Several approaches have been developed to coat iron oxide nanoparticles, including *in situ* coatings and post-synthesis coatings. In the first approach, nanoparticles are coated during the synthesis. For example, Josephson et al. have developed a coprecipitation process in the presence of dextran (Palmacci et al., 1995). The post-synthesis coating method consists of grafting the polymer on the magnetic particles was synthesized (Arshady et al., 2001, Okassa et al., 2005) (polymeric surfactants).

One of most useable polymers is chitosan. It is an alkaline, nontoxic, hydrophilic, biocompatible, and biodegradable polymer with excellent properties for the adsorption of metal ions, principally due to the presence of amino groups ($-NH_2$) in the polymer matrix, which can interact with metal ions in solution by ion exchange and complexation reactions (Giubal et al., 2004).
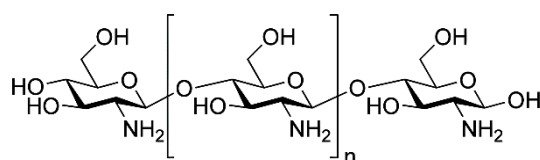
Fig. 12. Structure of chitosan

Nowadays, the preparations of magnetic nanoparticles encapsulated in chitosan are in great interest (Jia et al., 2006, Sipos et al., 2003, Bhattarai et al., 2007, Kim et al., 2006 and etc.). Hong prepared chitosan-coated magnetic nanoparticles with 28wt. % of theoretical chitosan content by coprecipitation in a solution containing Fe^{2+}, Fe^{3+}, and chitosan (Hong et al., 2007). Dung synthesized 23 nm magnetic Fe_3O_4-chitosan nanoparticles by binding chitosan on the surface of Fe_3O_4 nanoparticles (Dung et al., 2009). Liu investigated the potential application of amine-functionalized magnetite chitosan

nanocomposites as a recyclable tool for the removal of Pb^{2+}, Cu^{2+} and Cd^{2+}. They studied the adsorption/desorption mechanism of metal ions by these chitosan nanocomposites. The adsorption of Pb^{2+} onto nanocomposites was very fast (within 10 min). The removal efficiency of Pb^{2+} increased from 36.8% to 95.3% when the pH was changed from four to seven (Liu et al., 2009).

1.2.3. Organic materials

A number of research papers on toxic metal adsorption techniques evidences, that the functional groups (most are in inorganic materials) presented on the surface of magnetic nanoparticles provide a large number of active sites as well as aqueous stability, which is necessary for the successful adsorption of toxic metal from water. There are a lot of organic materials that can be used for coating magnetite, most of them are acids because of functional groups on the surface. For example, Singh reported the removal of toxic metal ions from wastewater by using carboxyl-, amine- and thiol functionalized Fe_3O_4 nanoparticles (succinic acid, ethylenediamine and 2,3-dimercaptosuccinic acid, respectively). Depending upon the surface functionality (-COOH, $-NH_2$ or -SH), these magnetic nano-adsorbents capture metal ions (Singh et al., 2013). Ozmen has used 3-aminopropyltriethoxysilane and glutaraldehyde-modified Fe_3O_4 nanoparticles for the removal of Cu^{2+} from water (Ozmen et al., 2010).

There are a couple of natural acids that can be used for this purpose. One of them is **L**-cysteine. It is a biocompatible, water-soluble, sulfur-containing amino acid with three functional groups (–SH, – NH_2, –COOH), a strong metal chelating capability, which has been widely used for adsorption of heavy metal ions (Seenivasa et al., 2015, Li et al., 2014, White et al., 2009, Uzun et al., 2008). Recently, several researches reported the preparation of the L-cysteine functionalized Fe_3O_4 magnetic nanoparticles (Cys–Fe_3O_4 MNPs) and their application for removing metal ions. Zou has reported a magnetic Fe_3O_4/Cys microspheres prepared via a solvo thermal route and their adsorption

properties for removal of Pb(II). The results revealed that the maximum adsorption capacities of Pb(II) was 459.33 mg/g (Zou et al., 2015).

Oleic acid is a commonly used surfactant to prevent the agglomeration of the iron oxide nanoparticles due to its higher affinity to magnetite. This compound is a monounsaturated fatty acid that can be found naturally in many plant or animal products. The chemical structure of oleic acid makes it a very good surfactant for magnetite nanoparticles since the oleic acid chain possesses a terminal carboxylic acid with a negative charge that has high affinity to magnetite nanoparticles surface due to their positive charge (Soares et al., 2014).

In literature we can find some articles with lauric acid coating magnetite. Lauric acid is a fatty acid with a 12-carbon atom chain, which produces a colloidal suspension of MNPs with a stable iron oxide base in the water. MNPs coated with LA present themselves as biocompatibles when used in low concentrations in vitro applications (Pradhan et al., 2007).

1.2.4. Inorganic materials

Iron oxide nanoparticles can be coated with a lot of different inorganic materials, like: oxides (Hakami et al., 2012, Zhao et al., 2010, Wang et al., 2012, Liu et al., 2008, Feng et al., 2012), silica (Zhang et al., 2007, Mulvaney et al., 2000), gold (Chen et al., 2003, Lin et al., 2001) or other. These coatings not only provide stability to the nanoparticles in solution, but also help in binding various ligands to the nanoparticle surface. These nanoparticles have an inner iron oxide core with an outer metallic shell of inorganic materials.

Among the various kinds of oxide-based nanomaterials TiO_2, ZnO are most important. These nanomaterials have various applications in many scientific and industrial fields, including wastewater purification, catalysis and magnetic devices (Yantasee et al., 2007, Xu et al., 2007). Recently, there have

been several reports on them being used as nano-adsorbents for the removal of various toxic metal ions from wastewater, such as Ni^{2+}, Cr^{3+}, Cu^{2+}, Cd^{2+}, Co^{2+}, Hg^{2+}, Pb^{2+} and As^{3+} (Hakami et al., 2012, Zhao et al., 2010, Wang et al., 2012, Liu et al., 2008, Singh et al., 2011). ZnO and TiO_2 with a high surface area and porosity exhibit higher photocatalytic activity than their bulk counterparts by minimizing the distance between the sites of photon absorption and preventing the electron–hole (e--h^+) recombination. Kumar has demonstrated the removal of Pb^{2+} and Cd^{2+} under different adsorbent concentrations, contact times, adsorbent dosages, pHs and temperature conditions, from aqueous solutions by mesoporous hierarchical ZnO nano-rods. They observed the maximum adsorption capacities of Pb^{2+} and Cd^{2+} to be 160.7 and 147.25 mg/g (Kumar et al., 2013).

Other widely used inorganic material is silica. It has been exploited as a coating material for magnetic nanoparticles too (Alcala et al., 2006, Gushikem et al., 2001, Woo et al., 2005, Ewijk et al., 1999, Bruce et al., 2004, Ma et al., 2006, Yu et al., 2003). Usually, an inert silica coating on the surface of magnetite nanoparticles prevents their aggregation in liquid, improves their chemical stability, and provides better protection against toxicity (Lesnikovich et al., 1990). This coating stabilizes the magnetite nanoparticles in two different ways (Sun et al., 2005). One is by shielding the magnetic dipole interaction with the silica shell. On the other hand, the silica nanoparticles are negatively charged. Therefore, the silica coating enhances the coulomb repulsion of the magnetic nanoparticles. Recently, Yuan prepared $Fe_3O_4@SiO_2@meso$-SiO_2 microspheres with a large pore size and a greater number of multifunctional amine groups for the adsorption of heavy metal ions. They observed that most of the metal ions such as Pb^{2+}, Cu^{2+} and Cd^{2+} can be removed within 30 min (Yuan et al., 2013). Girginova functionalized magnetite silica core shell particles with dithiocarbamate (DTC) for removal of mercury ions (Hg^{2+}) from water (Girginova et al., 2010).

Gold is another inorganic coating highly adequate to implement functionality to magnetic nanoparticles as well as to improve their stability in aqueous dispersions. Some methods exist in the literature to obtain magnetic nanoparticles coated with gold. For example, Lin has synthesized core-shell-structured Fe/Au nanoparticles by a reverse-micelle approach. The Au shell was expected to protect the Fe core and provide further organic functionalization (Lin et al., 2001). Water-soluble Au-coated magnetite nanoparticles with diameters of about 60 nm were synthesized by the reduction of Au^{3+} onto the surface via iterative hydroxylamine seeding (Lyon et al., 2004).

Sodium citrate is a common surfactant used in the synthesis of silver, gold and alumina nanoparticles due to its high solubility in several solvents and because it has a high degree of stabilization of the nanoparticles. Because its chemical structure has a negative charge it can be used for attaching nanoparticles such as Fe_3O_4, enhancing the particles dispersion and stabilization in suspensions (Soares et al., 2014).

1.3. Metal ion removal by nano-sorbents

The removal mechanism of the heavy metals by nano-sorbents can be:

- physical adsorption (Lo-Irene et al., 2005),
- surface complexation (Sigch et al., 2011),
- ion exchange (Schen et al., 2009),
- electrostatic interaction (Sigch et al., 2001)
- hard/soft acid-base interaction.

In general, the negatively-surface-charged nanoparticles form a chelate complex with metal ions above their point of zero charge (pzc) (i.e., pH > pHpzc). For example, the negatively-charged carboxylate ions (COO-) or hydroxyl ions (O-) of functionalized nanoparticles have a strong coordinating affinity in forming chelate complexes towards metal ions (Mn^+) at pH>pHpzc. The enhanced chelation tendency at higher pHs is expected, as at lower pHs the chelation sites
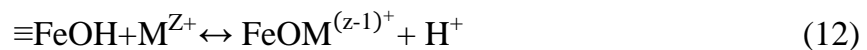
were occupied with H^+ (the chelation sites are neutral, i.e., -COOH or -OH) and were released at a higher pH, thereby originating the desired chelation. Also, at lower pHs, H^+ ions were adsorbed onto the surface of nanoparticles, leading to a net positive charge (Singh et al., 2013)

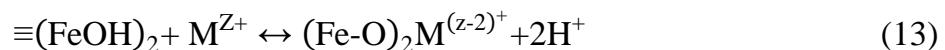### 1.3.1. Metal ion removal by magnetite

Under dry conditions, surface Fe atoms may be coordinatively unsaturated. Because they carry unoccupied atomic orbitals they are like Lewis acids and react with other Lewis acids. In aqueous systems, therefore, they coordinate with hydroxyl ions or water molecules which share their „ion "- electron pair with Fe. Upon absorption, water molecules, usually dissociate resulting in a surface covered by hydroxyl groups coordinated to the underlying Fe atoms. Hydraxylation of iron oxides is a fast reaction requiring minutes or at most hour to complete. The surface hydroxyl groups are the functional groups of magnetite, i.e. they are chemically reactive entities on the surface. Depending on pH, surface charge can change according to reactions ($\equiv$ denotes the surface):

$$\equiv FeOH_2^+ \leftrightarrow \equiv FeOH + H^+ \tag{10}$$

$$\equiv FeOH \leftrightarrow \equiv FeO^- + H^+ \tag{11}$$

Sorption of heavy metals on iron oxides may be specific or non-specific. With non-specific sorption, there is at least one water molecule between the sorbing species and the surface functional group. Specific sorption involves interaction with deprotonated surface hydroxyl groups to form mono-, and bi- nuclear, inner sphere complexes, i.e.

$$\equiv FeOH + M^{Z+} \leftrightarrow FeOM^{(z-1)^+} + H^+ \tag{12}$$

And

$$\equiv (FeOH)_2 + M^{Z+} \leftrightarrow (Fe\text{-}O)_2 M^{(z-2)^+} + 2H^+ \tag{13}$$

Heavy metal sorption is accompanied by release of protons with the number of protons released per cation being termed z. Ideally z should be one for mononuclear complexes and two for binuclear complexes, but in fact, the value often is found to be between one and two. In addition, the z value may also vary between the limits as pH rises (Cornell et al., 2003).

Heavy metal sorption may be suppressed as the ionic strength increases and this is usually considered to indicate an outer sphere (non-specific) sorption, although it may also be the result of ion pairing in solution. Porosity of magnetite is another aspect impacting sorbents efficiency. It refers to the volume of pores in a solid. It contributes to the „internal" surface area of the sample and can influence the kinetics of sorption. Diffusion into and out of the pores is often considered responsible for slow sorption and desorption processes. Pores vary in size and shape. The pores may be the result of aggregation of particles. They may also be the result of partion dehydroxylation or dissolution. In general, the solubility of magnetite is very low, except at extreme pH values. For example, the dissolution of magnetite at pH 4.5 in 0.1 mol/L $NaClO_4$, reaching equilibrium only after 20 days (Sun et al. 1998).

Since the affinity of metal ions to Fe_3O_4 is higher than that of H^+ ions, metal ions can replace the adsorbed H^+ ions from the Fe_3O_4 surface by an ion exchange mechanism (Shen et al., 2009). Liu observed the adsorption of metal ions - particularly Cd^{2+} - directly on the surface of Fe_3O_4 (Liu et al., 2008). The adsorption of metal ions by ion exchange is relatively slow when compared to surface complexation, since the organic molecules present on the surface of the nanoparticles may cause steric hindrance towards the adsorption of metal ions. In systems containing two or more sorbates, either competitive or synergistic effects may operate. The most common is a synergistic effect. Competitive behaviour may involve competition for the same surface sites, indirect effects due to the change in the electrostatic properties of the oxide/water interface and in some cases, formation of non-sorbing metal-ligand complexes in solution.

1.3.2. Metal ion removal by graphene oxide

Effective use of graphene oxide in this capacity requires knowledge of how and why sorption occurs under environmental conditions. The sorption affinity of graphene oxide for many metal ions is strong and varies from the types of heavy metal ions. For example,the affinities of GO to Cu(II), Zn(II), Cd(II) and Pb(II) followed the order of Pb(II) > Cu(II) $\gg$ Cd(II) > Zn(II) (Sitko et al., 2013). The higher electronegativity of heavy metal ions, the stronger attraction of the heavy metal ions on the negatively charged GO surface. Moreover, the standard reduction potential of the heavy metal ion is also related to the adsorption affinity. The standard reduction potentials for Pb^{2+}/Pb, Cu^{2+}/Cu, Cd^{2+}/Cd and Zn^{2+}/Zn is -0.1262 V, 0.3419 V, -0.4030 V and -0.7618 V (Haynes et al., 2014), which agreed well with the affinities order.

The mechanisms for the adsorption of heavy metal ions on the surface of GO is ascribed to electrostatic attraction, ion exchange and surface complexation (Li et al., 2015, Cao et al., 2014), e.g. Figure 13 shows the main mechanisms for the adsorption of M^{n+} on GO (Wu et al., 2012).
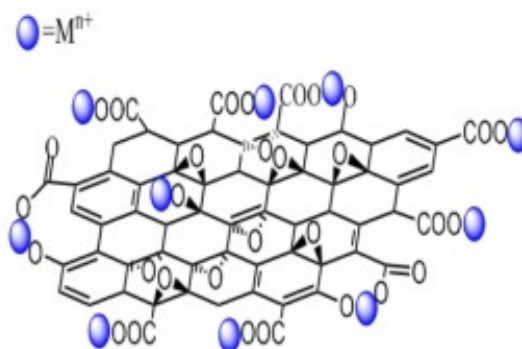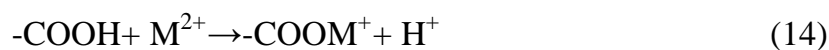

Fig. 13. Graphene oxide interactions with metal ions (Wu et al., 2012)

The electrostatic attraction shows up between the positively charged heavy metal ions and negatively charged GO sheets. The ion exchange reaction between heavy metal ions and the proton on –COOH or –OH oxygens functional groups is another mechanism for the adsorption. The proton on –COOH or –OH

was released into the solution in the adsorption process, leading to a lower equilibrium solution pH than the initial value (Madadrang et al., 2012). Reactions might be represented as (Madadrang et al., 2012, Peng et al., 2016):

$$-COOH + M^{2+} \rightarrow -COOM^+ + H^+ \qquad (14)$$

$$-OH + M^{2+} \rightarrow -OM^+ + H^+ \qquad (15)$$

$$-2COOH + M^{2+} \rightarrow -COOMOOC- + 2H^+ \qquad (16)$$

$$-2OH + M^{2+} \rightarrow -OMO- + 2H^+ \qquad (17)$$

$$-COOH + M^{2+} + -OH \rightarrow -COOMO- + 2H^+ \qquad (18)$$

1.3.3. Metal ion removal by Prussian blue

One of the most interesting abilities of Prussian blue is its excellent adsorption capacity and high selectivity to the specific alkali ion. Experiments show that the ionic selectivity depends on the size of the ions and that the selectivity sequence is $Cs^+ > K^+ > Na^+ > Li^+$ (Schneemeye et al., 1985). The adsorption mechanism between PB and cations has been hypothesized as an ion-exchange process (Vincent et al., 2011). But recently was proposed that Cs^+ ions are adsorbed into PB interstitial sites by simple physical adsorption (Ishizaki et al., 2013). Hydrated Cs^+ ions were preferably adsorbed *via* the hydrophilic defect sites and accompanied by proton-elimination from the coordination water.
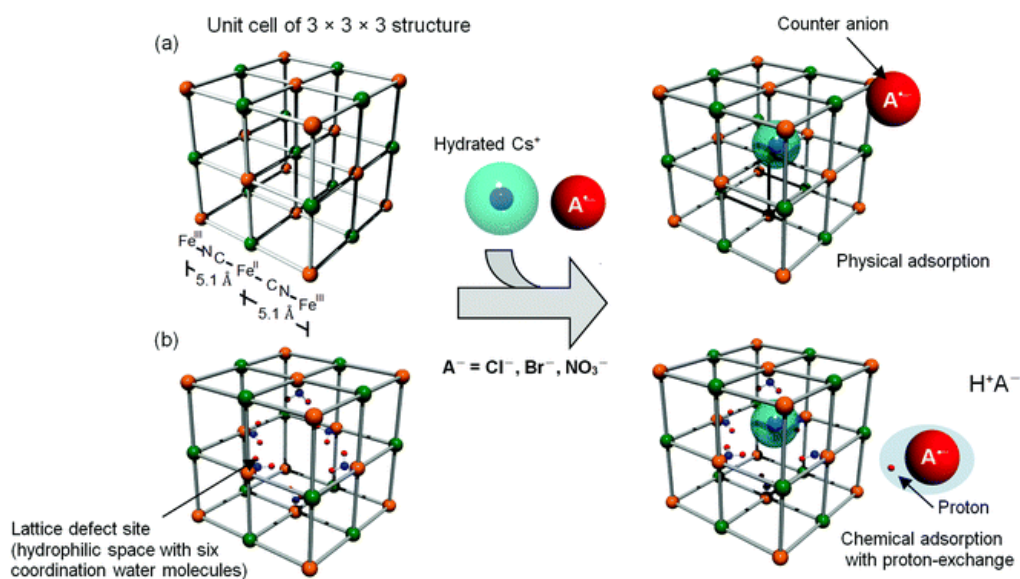
Fig. 14. Possible mechanisms of Cs^+ and Prussian blue sorbent (Ishizaki et al., 2013)

The small ions are adsorbed at the channel entrance sites without the water– ion exchange mechanism. In contrast, the large ions are adsorbed in PB by the water–ion exchange mechanism, and the adsorption site of large ions is located at the center of the cage or at the interstitial site (Ruankaew et al., 2017). Sorption mechanism is strongly dependent on ion size and lattice defect sides number. However, the basis for the ion selectivity and the intercalation mechanism between PB and alkali ions in equilibrium conditions are still unclear. The understanding of the ion selectivity in PB can be applied to designing new effective materials for removal of hazardous heavy metal from contaminated water.

1.3.4. Metal ion removal from environmental samples by nano-sorbents

There are some publications, when magnetic nano-sorbents are used for metal ions removal from environmental samples. Magnetic nanoparticles were successfully used for the separation of toxic metal ions from different sources. Wang has reported rhodamine hydrazide modifying Fe_3O_4 microspheres (Fe_3O_4-R_6G) for the selective detection and removal of mercury ions from different environmental samples, such as tap water, lake water (Linghu

Lake, Anqing, China) and river water (Changjiang River, Anqing, China). They found that 1.5×10^{-7} mol/L is the detection limit for Hg^{2+} and that 37.4 µmol/g is the maximum adsorption of Hg^{2+} in a 3 mL sample with 5 mg Fe_3O_4-R_6G (Wang et al., 2014). Warner has used surface-functionalized Fe_3O_4 nanoparticles for the separation of heavy metals in Columbia River water. They compared the removal efficiency of these surface-functionalized Fe_3O_4 nanoparticles with selected commercial sorbents with similar surface functionality, as well as bare iron oxide nanoparticles, and found that surface-functionalized particles have a higher tendency for the removal of toxic metal ions (Warner et al., 2010).

The Baltic Sea has received considerable loads of pollutants due to industrialization of Eastern Europe. Concern for the Baltic's ecological health eventually led to legislation and voluntary measures to limit pollution during the last decades of the 20th century. Man-made chemicals and heavy metals enter the Baltic Sea via waste water treatment plants, leaching off house hold materials, waste deposits, through atmospheric deposition from industrial plant emissions, and from many other sources. Once in the Baltic sea, they can cause various types of damage to the ecosystem. Some are highly visible in the form of oil-spills, for example. Many contaminants degrades slowly and their impacts can magnify as they accumulate in the aquatic food web or rapidly enter sediments. The results from the integrated assessment of hazardous substances shows that the current contamination status is elevated in all parts of the Baltic Sea. The contamination status has not changed markedly during the past six years (HELCOM et al., 2010).

By adoption of the Baltic Sea Action Plan (BSAP) the HELCOM countries decided to cooperate in order to accumulate more knowledge on selected hazardous substances, (HELCOM et al., 2007). Another important document – EU Marine Strategy Framework Directive (2008/56/EC) (MSFD) addresses hazardous substances, setting one of the qualitative descriptors for determining good environmental status as "Concentrations of contaminants are at levels not giving rise to pollution effects". According to MSFD, the progress

towards good environmental status will depend on whether pollution is progressively being phased out, i. e. whether the presence of contaminants in the marine environment and their biological effects is kept within acceptable limits, so as to ensure that there are no significant impacts on or risk to the marine environment.

Heavy metals comprise a group of elements that are potentially toxic to estuarine and marine organisms in concentrations above the threshold level. Their natural concentration plays an essential role in many biochemical processes in organisms. Such concentration is called the background concentration. Any concentration lower or higher than this background can be toxic. Two subgroups are recognized: (1) transitional metals (e. g. copper, zinc) which are essential to metabolism at low concentration but may be toxic at higher concentration, and (2) metalloids (e. g. arsenic, cadmium, lead, mercury, tin) which generally are not required for metabolic function and are toxic at low concentration (Kennish et al., 1997). Heavy metal levels in aquatic environment vary with a lot of factors, including the type of bedrock and sediment, mineralogy, organic content, redox conditions in water and sediments, water currents, salinity, etc. (Swedish EPA et al., 2000). Upon entering into the water, they tend to accumulate in sediments through complex physical and chemical adsorption mechanisms. They can also release them back into the ecosystem when changes occur in environmental conditions such as pH, redox potential, the presence of organic chelators, resuspension, desorption or (bio) degradation of the sorptive substances, resulting in a secondary contamination source affecting the ecosystem (Zubenko et al., 2000). The most important and commonly studied heavy metals are lead, chromium, cadmium, copper, zinc, mercury, nickel and arsenic (Leivuori et al., 2000, Swedish EPA et al., 2000, HELCOM et al., 2010).

The results of the previous studies showed a higher marine and riverine sediment contaminated with mercury, cadmium, lead, zinc and copper

and a lower content of nickel and chromium. The sediments in different areas of the Baltic Sea differed in metal concentrations (Table 3)

Table 3 Metal concentrations (mg/kg d.w., variability (from-to) or average (±sd when given)) in surficial sediments (0 – 5 cm) of the Baltic Sea measured during the previous studies

	Pb	Cu	Cd	Ni	Cr	Zn	Sampling year	Reference
The Curonian Lagoon (sand)	7.6	3.9	0.12	3.3	7	15.1	2013–2014	Jokšas et al., 2016
The Curonian Lagoon (silt)	28	28.9	0.64	19.8	28.7	76.4	2013–2014	Jokšas et al., 2016
Klaipėda Strait (sand)	8	3-29	-	-	37-74	16-140	1990–2004	Pustelnikovas et al., 2007
Klaipėda Strait (coarse silt, mud)	10	10-757	-	-	46-119	38-287	1990–2004	Pustelnikovas et al., 2007
Gulf of Finland	25.3-54.2	21.6-48.8	0.14-2.04	33.2-40.7	50.2-95.2	131-201	2007–2009	Vallius, 2012
	51	43	1.2	-	-	199	1992–1996	Vallius and Leivouri, 2003
Eastern Gotland Basin	45.6	99.3	6.97	72.9	37.6	448	1997	Kunzendorf and Vallius, 2004
	45-139	63-205	-	-	-	195-892	2003	Hille, 2005, 2006
Gulf of Gdansk	11.9–27.5*	6.0–25.1*	0.19–1.97*	-	-	33.5–167.9*	2010	Dabrowska et al., 2013
	11-80	27-79	0.7-6.0	-	-	80-429	-	Glasby and Szefer, 1998
Gdansk Deep	77**	-	2.04**	-	-	230**	-	Zalewska et al., 2015
Port of Gdansk	2-93	1-131	0.14-2.0	1.7-11	1.7-38	9-334	1990–2004	Pustelnikovas et al., 2007
Vistula Lagoon	33-36	18-23	0.8-0.9	-	-	103-111	-	Glasby and Szefer, 1998
Bornholm Basin	56.7	38.5	1.09	38.7	56.4	167	1998–1999	Kuznezof and Vallius, 2004
	41	67	0.34	64	92	193	1997–2008	Emelyanov et al., 2010

*the range of the average concentrations, ** maximal values

1.3.5. Various factors affecting heavy metals sorption efficiency

Various factors like pH, foreign ions, ionic strength, sorbent dosage, contact time, temperature etc. can affect sorption efficiency.

Solution pH is one of the vital parameters that affect the solubility of metal ions, degree of ionization, and the surface characteristics. Thus, most of the studies involved in metal ions adsorption have extensively investigated the pH effect. Optimum pH values are dependent on the type of sorbent and target metal ion. The optimum pH value for the removal of the most of cationic metal ions by magnetic materials was observed at pH 5.0 and pH 5.5. In case of cationic metal ions, it was observed that with an increase in pH, metal removal was increased, but at higher pH values removal was either decreased or increased. At low pH, most of these functional groups present are protonated and presented in the positively charged form. In addition, the presence of a large number of H^+ and H_3O^+ ions in the aqueous solution may compete with the metal ions for adsorption sites available on nano-sorbents. This electrostatic repulsion will occur between metal ions and positively charged surface, thus a lower adsorption was observed at low pH in most of the studies. At higher pH range H^+ ions concentration decrease and the surface become negatively charged. This favours the metal ion removal due to electrostatic interaction. In addition, with increase in the pH deprotonation of functional groups is possible resulting in a free lone pair of electrons suitable for coordination with metal ions. At very high pH values adsorption of metal cation is attributed to the formation of metal hydroxide species such as soluble $M(OH)^+$ and/or insoluble precipitate of $M(OH)_2$ (Reddy et al., 2013).

Foreign ions could remarkably affect the electrical double layer structure of hydrated particulate, which would then impact the binding of adsorbing species (Wang et al., 2013). The effects of foreign ions and ionic strength on the adsorption of heavy metal ions are mainly ascribed to: (1) foreign ions would compete with heavy metal ions for the limited reactive sites on the adsorbent surface according to their affinities between the ionic species and adsorbents, which would reduce the adsorption capacities of the adsorbates; (2) ionic strength can impact particle aggregation by influencing electrostatic interactions; and (3) ionic strength would affect the activity coefficient of the

heavy metal ions and thus limit the heavy metal ions transfer from the solution to the surface of adsorbent (Zhao et al., 2011).

Temperature affects the sorption rate by alternating the molecular interactions and solubility. Increasing temperature may lead to the increase either in the amount of the available adsorption sites on the sorbents surface or in the diffusion rate of heavy metal ions, and thus accelerating the adsorption rate.

1.4. Sorption isotherm

Adsorption isotherm is a functional expression that correlates the amount of solute adsorbed per unit weight of the adsorbent and the concentration of an adsorbate in bulk solution at a given temperature under equilibrium conditions. It is important to establish the appropriate relationship for the batch equilibrium data using empirical or theoretical equations as it may help in modelling, analysis and design of adsorption systems. The adsorption isotherms are one of the most subjects in understanding the mechanism of the adsorption and the characteristics of isotherms, which are needed before the interpretation of the kinetics of the adsorption process. Many models have been proposed to explain adsorption equilibrium like Langmuir, Freudlich and others. These are useful for summarizing sorption data and for comparison reasons.

The Langmuir isotherm assumes that monolayer adsorption takes place on an adsorbent with a structurally homogenous surface, on which the binding sites have the same affinity for the adsorption, and no interaction occurs between adsorbates (Peng et al., 2010).

Langmuir isotherm equation applies to a reaction of a surface Fe (≡Fe) atom with an adsorbate molecule X. e.g.,

$$\equiv Fe + X \leftrightarrow \equiv FeX \tag{19}$$

The equilibrium constant K_{ads} is then:

$$K_{ads} = \frac{[\equiv FeX]}{[\equiv FeX][X]} * \exp \frac{(-\Delta G_{ads})}{RT} \qquad (20)$$

With $-\Delta G_{ads}$ being the free energy of sorption.

The Langmuir equation is written as:

$$\Gamma_X = \Gamma_{max} \left(\frac{K_{ads} * X_{aq}}{1 + K_{ads} * X_{aq}} \right) \qquad (21)$$

Where X_{aq} is the equilibrium concentration of the sorbate and $\Gamma_x =$ mass sorbate/mass sorbent. Γ_{mzx} corresponds to the level of sorbate required to saturate all available surface sites (at $X_{aq} \geq 1$) and provide a monolayer coverage. This equation relates the amount sorbed to the equilibrium concentration X_{aq} of the sorbate in the bulk solution. Overall, sorption increases with rising sorbate concentration until a plateu corresponding to saturation of all surface sites is reached. To determine whether the adsorption is favourable, a dimensionless constant separation factor or equilibrium parameter R_L is defined based on the following equation:

$$R_L = \frac{1}{1 + K_L C_0} \qquad (22)$$

Where K_L is (L/mg) is the Langmuir isotherm constant. The R_L value can indicate whether the type of the isotherm is favourable ($0 < R_L < 1$), unfavourable ($R_L > 1$), linear ($R_L = 1$), or irreversible ($R_L = 0$).

The Freundlich model is commonly used to predict that the adsorption occurs on the heterogeneous surface, on which the adsorbed molecules are interactive and the amount of solute adsorbed raises infinitely with the increase of the concentration. This model does not estimate surface saturation, thus infinite surface coverage is predicted, suggesting physical sorption on the surface. It can be linearly expressed as follows:

$$\log q_e = \log K_F + \left(1/n \right) \log C_e \qquad (23)$$

where, K_F and n are the Freundlich parameters related to adsorption capacity and adsorption intensity, respectively. If the value of 1/n is lower than 1, it indicates

a normal Langmuir isotherm; otherwise, it is indicative of cooperative adsorption. The constant k can be defined as a sorption coefficient, which represents the quantity of adsorbed metal ions for a unit equilibrium concentration (i.e., $C_e = 1$). The Freundlich constants can be obtained from the plot of log qe versus log C_e.

Dubinin–Radushkevich isotherm is generally applied to express the adsorption mechanism with a Gaussian energy distribution onto a heterogeneous surface. This isotherm model is another empirical model which was initially formulated for the adsorption process following a pore filling mechanism. It is generally applied to express the adsorption process occurring on both homogeneous and heterogeneous surfaces. The non-linear expression of Dubinin-Radushkevich isotherm model can be illustrated as Equations Nr. 24 and Nr. 25:

$$q_e = q_s \exp(-K_{DR}\varepsilon^2) \tag{24}$$

$$\varepsilon = RT\ln\left(1+\frac{1}{C_e}\right) \tag{25}$$

where q_s (mg P/g) is a constant in the Dubinin-Radushkevich isotherm model which is related to adsorption capacity; K_{DR} (mol^2/kJ^2) is a constant in related to the mean free energy of adsorption; R (J/mol K) is the gas constant equal to 8,314; and T (K) is the absolute temperature.

The value of mean sorption energy, E (kJ/mol), is described as:

$$E = \frac{1}{(2B_D)^{1/2}} \tag{26}$$

The constant, B_D, is related to the mean free energy of sorption per mole of the sorbate. The value of mean sorption energy gives information about the chemical and physical sorption.

Temkin isotherm contains a factor that is explicitly taking into the account adsorbent–adsorbate interactions. By ignoring the extremely low and large value of concentrations, the model assumes that the heat of adsorption

(function of temperature) of all molecules in the layer would decrease linearly rather than logarithmic with coverage. As implied in the equation, its derivation is characterized by a uniform distribution of binding energies (up to some maximum binding energy) which was carried out by plotting the quantity sorbed qe against $\ln C_e$ and the constants were determined from the slope and intercept. The model is given by the following equation:

$$q_e = \frac{RT}{b} \ln(A_T C_e) \tag{27}$$

$$q_e = \frac{RT}{B_T} \ln A_T + \left(\frac{RT}{b}\right) \ln C_e \tag{28}$$

$$B = \frac{RT}{B_T} \tag{29}$$

A_T = Temkin isotherm equilibrium binding constant (L/g)

B_T = Temkin isotherm constant R= universal gas constant (8.314J/mol/K)

T= Temperature at 298K.

B = Constant related to the heat of sorption (J/mol)

Conclusions

Environmental pollution by heavy metal ions is a global threat. Its magnitude is increasing very fast. The recent development of nanotechnology offers great opportunity for the fabrication of new nanomaterials with unique surface functionalities and large surface-to-volume ratios for removing these pollutants. Specifically, oxide-based nanomaterials, such as magnetite Fe_3O_4, as well as their nanocomposites. These magnetic nanomaterials can be modified with different functional groups to improve their lifetime, catalytic efficiency and sorptive properties. Further, the use of magnetic nanomaterials or their nanocomposites gives the posibility of magnetic separation and reusability (not

possible with non-magnetic nanomaterials), which are significant for practical application.

But in many cases, the removal efficiency of sorbents is evaluated by many parameters, like sorption capacity, sorbent dosage, time, solutions pH, other ions in solution. Usually the sorption capacity is calculated for a single-metal system, which is opposite with the common observation of the industrial wastewater or other polluted water sources containing a mixture of different heavy metals. It is desirable for the full applications in practice to examine these sorption parameters, as well as the behaviour of the individual metals in multi metal systems, in which more than two types of metals exist together and might compete for the same adsorption sites.

2. MATERIALS AND METHODS

2.1 Magnetic nanosorbents synthesis

The magnetite nanoparticles (M) were prepared by the conventional co-precipitation method, corresponding to the following reaction path:

$$2FeCl_3+FeCl_2+8NH_3+4H_2O \rightarrow Fe_3O_4+8NH_4Cl \qquad (30)$$

$FeCl_3*6H_2O$ (11.68 g) and $FeCl_2*4H_2O$ (4.30 g) were dissolved in 200 mL of deionized water under nitrogen atmosphere with vigorous stirring. The pH of the solution was increased by adding dropwise 12.5 mL of NH_4OH solution (28%) into the above mixture under continuous stirring. The colour of the solution turned black immediately. The reaction mixture was heated to 80^oC for 2 h at 300 rpm. After cooling the solution to room temperature, the resulting Fe_3O_4 nanoparticles were separated using a magnet and then washed with deionized water to remove the base excess until the pH became neutral. The black precipitate was then washed three times with ethanol (3*50 mL) and dried in a vacuum.

The graphene oxide (GO) was synthesized via the oxidation of expanded graphite by the modified Hummers method. Generally, 4.0 g of flake graphite and 3.0 g of $NaNO_3$ were added into 300 mL of concentrated H_2SO_4 under vigorous stirring and ice-water bath conditions. Then 18.0 g of $KMnO_4$ was slowly added into the mixture for ~2 h. The suspension was continuously stirred for 48 hours, and then 560 mL of 5.0 wt% H_2SO_4 was added into the suspension for ~2 h with vigorous stirring at 98 ± 1 °C. After the suspension temperature decreased to 60 °C, 24 mL of H_2O_2 (30 wt%) was added into the system to eliminate the excess $KMnO_4$, and the suspension was continuously stirred for 2 h at a room temperature. At last, the colour of the mixture changed from dark brown to yellow. After centrifugation at 20000 r/min for 60 min, the

solid phase was dispersed by using a vigorous stir and ultrasonic water bath and rinsed with Milli-Q water until the solution pH was near to that of Milli-Q water.

Magnetic graphene oxide was prepared by co-precipitation of Fe(II) and Fe(III) in the presence of GO in alkaline solution according to the following procedure. 0.1 g of graphene oxide was exfoliated into 200 mL of deionized water via ultrasonication for 2 h. 20 mL of iron source solution containing 0.324 g (1.2 mmol) of $FeCl_3*6H_2O$, 0.167 g (0.6 mmol) of $FeCl_2*4H_2O$ and 2.5 mL of HCl (2 mol/L) solution were added slowly to the above suspension of GO at 30°C with vigorous stirring under nitrogen atmosphere. Then, 10 mL of ammonia solution was added drop wise to alter the mixture pH to a value of 10. Afterwards, the mixture was heated to 90°C and 3 mL of hydrazine hydrate was added with constant stirring to result a black solution. This solution was cooled to room temperature after being rapidly stirred for 4 h. Finally, the precipitate was isolated by a permanent magnet, washed with deionized water and ethanol for several times, and dried under vacuum at 60°C for 12 h.

Magnetic Prussian blue nanosorbent (MPB) was synthesized according by the following procedure. Magnetite particles were synthesized by a method described earlier. 0.3 g of magnetite was redispersed in 300 mL water, 100 mL 56.8 mmol/L $FeCl_3$ was added to the magnetite suspension under stirring, and then 50 mL 42.6 mmol/L $K_4[Fe(CN)_6]$ was slowly dropped in. The colour of the mixture gradually changed from brown to dark cyan, and the precipitate was harvested by a magnet after stirring for 1 h, followed by washing with water several times until the solution became colourless. Finally, the powder was dried in an oven at 50°C.

Magnetic Prussian blue with graphene oxide nanosorbent (MPBGO) was synthesized in two stages. First, 30 mg GO and 0.3 g magnetite were dispersed in 50 mL and 300 mL of water by ultrasound, respectively. These two suspensions were then mixed together and stirred vigorously for 10 min. The brown precipitate was collected with a magnet and washed with water. Second, the precipitate was re-dispersed in 300 mL water under stirring for the

following experiment. Next, 100 mL 56.8 mmol/L $FeCl_3$ was added to the above precipitate suspension under stirring, and then 50 mL 42.6 mmol/L $K_4[Fe(CN)_6]$ was slowly dropped in. The colour of the mixture gradually changed from brown to dark cyan, suggesting the formation of a MPBGO nanocomposite. The mixture was stirred for another hour. The precipitate was recovered with a magnet and then washed with a lot of water repeatedly until the solution became colourless. Finally, the powder was dried in an oven at 50°C (Yang et al., 2014).

2.2. Characterization of nanosorbent structural, morphological and magnetic properties

M, MGO, MPB and MPBGO were characterized by Mössbauer spectroscopy, X-ray diffraction (XRD), Fourier transform infrared spectroscopy (FTIR), Raman spectroscopy, Transmission electron microscopy (TEM) and Scanning electron microscopy (SEM).

The Mössbauer spectra was acquired at room temperature applying the Mössbauer spectrometer in the transmission geometry using the ^{57}Co (Rh) source. Normos Dist software was used for analysis of spectra. The X-ray diffraction (XRD) analyses were conducted by means of a D8 (Bruker AXS) X-ray diffractometer. TEM/SEM was used to observe the surface state and the structure of the samples using the Transmission electron microscope (Tecnai G2 F20 X-TWIN, resolution 0.25-0.102 nm) and scanning electron microscope (High resolution FESEM Su-70 Hitachi). The Fourier transform infrared (FTIR) spectra were recorded with a Vertex70v vacuum spectrometer with the 2 cm^{-1} spectral resolution using a KBr pellet for the sample preparation. Raman spectra was recorded using a RAM II system (180° backscattering configuration) with the 1064 nm laser.

2.3. Heavy metal removal by synthesized nanosorbents (Sorption study)

Batch experiments were performed to measure sorption capacities. For the preparation of aqueous metal solutions $Pb(NO_3)_2$, $Cu(NO_3)_2$ * $6H_2O$,

Co(NO$_3$)$_2$*6H$_2$O and Ni(NO$_3$)$_2$*6H$_2$O were used. A stock solution of 1000 µmol/L of Pb(II), Cu(II), Co(II) and Ni(II) metal ions was prepared by dissolving the required amounts of Pb(II), Cu(II), Co(VI) and Ni(II) in 1000 mL deionized water. Solutions of desired concentration were prepared by diluting the stock solution using deionized water. However, the blank check was always performed to ensure conformity. All sorption experiments were carried out in batch conditions using 10 mL of metal ion solution and 0.01 g of magnetic nanosorbent. The shaker was used to mix the suspensions at 250 rpm and 25.0°C for all tested conditions. Samples were pipetted at certain intervals and the sorbent was separated using a magnet. (Figure Nr 15)
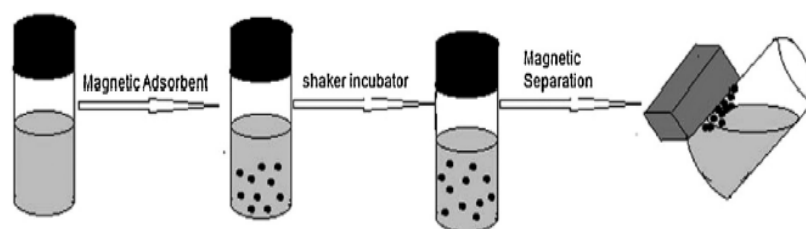

Fig. 15. Schematic illustration of magnetic separation (Anbia et al., 2015)

The amounts of analyte sorbed by sorbents (Q_e, mg/g) and the removal efficiency (%) were calculated using Eqs. 31-32

$$Q_e = \frac{(C_0-C_e)V}{m} \tag{31}$$

$$\text{Removal efficiency } (\%) = \frac{C_0-C_e}{C_0}*100 \tag{32}$$

where Q_e is the equilibrium adsorption capacity of the adsorbent in mg/g, C_0 is the initial concentration in mg/L and C_e is the concentration at equilibrium of metal ions in mg/L, V is the volume in L of metal ions solution and m is the weight in g of the sorbent.

The pH dependence data was obtained by taking 10 mL 200 µmol/L of Cu(II)/or Co(II)/or Pb(II)/or Ni(II) solutions into different polyethylene bottles with pH ranging from 3 to 9 and it was monitored with the WTW pH-

electrode SenTix 41, calibrated with standard buffers DIN 19266 and a WTW inoLab Multi Level 1 m. The pH of suspensions was adjusted by adding 0.001 mol/L solutions of HCl and NaOH. The centrifuge bottles were shaken to reach equilibrium until the pH remained stable over the desirable range (±0. 1 pH unit) for 24 h. The pH in solution was measured before and after sorption.

Concentration dependence data was obtained by taking solutions with concentrations ranging from 25 µmol/L to 1000 µmol/L for heavy metals. The solution pH was kept constant as 7±0.1 and sorption process was conducted at constant temperature 25°C, for 24 h. Further, the concentration dependence data was presented graphically. The equilibrium state concentration dependence data was employed for the adsorption isotherm modelling using the known Freundlich, Langmuir and Dubinin–Radushkevich isotherms models.

The kinetics of the adsorption process were investigated to determine the effect of the initial concentration of metal ions on the Q_e with respect to time and the time required to achieve equilibrium adsorption. The kinetics study was carried out using 0.01 g of M, MGO, MPB and MPBGO in 10 mL of 200µmol/L Pb(II), Cu(II), Co(II) and Ni(II) metal ion solutions at pH 7.0. Two simple kinetic models, namely the pseudo-first-order and the pseudo-second-order, are the most often used to analyse the rate of sorption. The pseudo-first-order kinetic and the pseudo-second-order kinetic are expressed by Eqs. (33) and (34),

$$\ln\left(Q_e - Q_t\right) = \ln Q_e - k_1 t \tag{33}$$

$$\frac{t}{Q_t} = \frac{1}{k_2 Q_e^2} + \frac{1}{Q_e} t \tag{34}$$

The sorption experiments in multi-metal solutions (when Cu(II), Co(II), Ni(II) and Pb(II) are in one solution) were performed too. Heavy metals concentration was 200 µmol/L, dosage – 100 mg, time – 2 h and pH – 7.

For desorption study, the metal ion-loaded sorbent was collected from the sorption experiments and washed with water to remove the unsorbed metal ions. Then, solid nanoparticles were mixed with HNO_3 solution at pH 4.0.

The amount of heavy metal released from the sorbent into the supernatant was quantified. The recovery efficiency *(R)* from the solid phase can be defined as:

$$R(\%) = \frac{C_{des}}{C_{ads}} * 100 \qquad (35)$$

where C_{des} and C_{ads} are the amount of metal released into the aqueous solution and the amount of metal sorbed onto the particles (mol/L).

The sorbents then were washed with 0.1 mol/L disodium hydrogen phosphate and water for several times prior to reuse. To test the reusability of the sorbent, this sorption–desorption cycle was repeated 3 times by using the same sorbent.

To test the effect of sorbent dosage the sorption was carried out by using M, MGO, MPB and MPBGO (100, 200 and 300 mg) in a 10 mL aqueous heavy metal solution (200 µmol/L). The batch adsorption experiments were carried out under continuous shaking at 150 rpm for 120 min at the room temperature of 25 °C. After that, the samples were separated by a magnet.

Sea water samples were collected from 4th, 6th, 7th and 64th stations in the Baltic Sea. (Figure 16). One litre of each water sample was spiked with 200 µmol/L of the selected metal ions, viz. Cu(II), Co(II), Ni(II) and Pb(II). Batch sorption procedure with 0.01 g sorbent was used to test M, MGO, MPB and MPBGO usability to remove heavy metals from sea water.
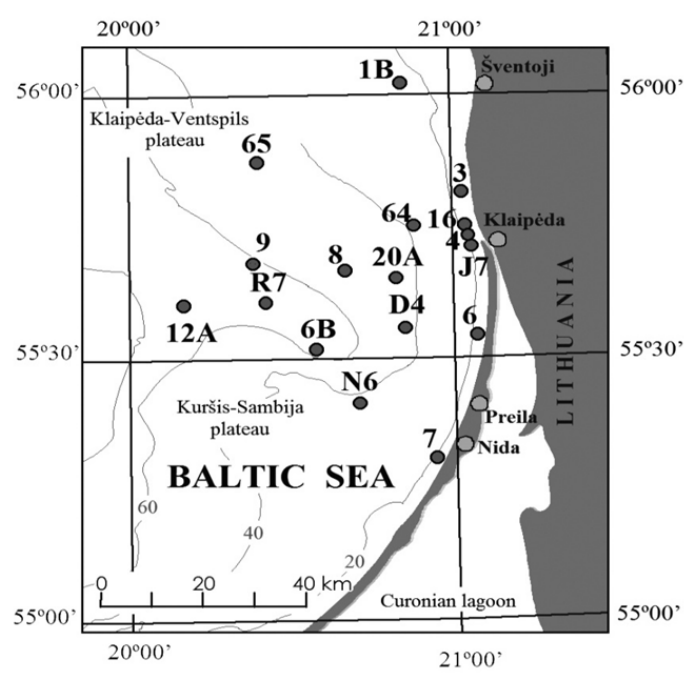
Fig. 16. The map of sampling stations in Baltic sea

Heavy metals concentration in all experiments was measured using Inductively coupled plasma mass spectrometry (ICP-MS) (ELEMENT-2, Thermo Fischer Scientific). The ACS reagent grade or higher-grade chemicals were used. All solutions were prepared using deionized (Elix, Milipore) or Milli-Q (Millipore Milli-Q Synthesis A-10) water.

2.4.   Assessment of the reliability of the analysis

In any research, it is important to ensure quality and properly assess the accuracy of the used methods. The uncertainty was used to evaluate the accuracy of tests and measurements. Concept of uncertainty: "... when all known or expected constituents of the evaluation are evaluated and corrections are made accordingly to them, the uncertainty of the established results remains uncertain, it is a doubt, how accurated measurement results represents the measured value" (ISO 1993). The accuracy of the obtained results is influenced by all the research steps: preparation of the sample, analysis, measurements and calculations. Each of these steps could be a source of uncertainty.

The standard uncertainty was calculated according to the formula:

$$u(A) = (u_1^2 + \cdots + u_n^2)^{1/2} \qquad (36)$$

there: u_1, ..., and u_n sources of uncertainty: sample preparation, measurement and others.

According to the Law of Gauss, a general standard uncertainty was calculated:

$$u_{c(y(x_1....x_n))} = \sqrt{\sum_{i=1}^{n} \left(\frac{\delta y}{\delta x_i}\right) (u(x_i))^2} \qquad (37)$$

where y (x_1, x_2, x_n) corresponds to the function of x_1, x_2, x_n.

Correlation coefficient (R^2) was used to evaluate the experimental and theoretical data of the sorption isotherms and kinetic models. It was defined by the equation:

$$R^2 = \frac{\sum\left(q_{ecal} - q_{mexp}\right)^2}{\sum\left(q_{ecal} - q_{mexp}\right)^2 + \left(q_{cal} - q_{mexp}\right)^2} \qquad (38)$$

where q_{exp} is the amount of metal sorbed during the experiment (mg / g), q_{cal} - the amount of metal calculated using the kinetic or isothermal model (mg / g), q_{mexp} is the average q_{exp} value (mg / g).

The influence of three variables (initial concentration of metal ions, time and sorbent content) on the sorption efficiency was estimated using a dispersion analysis (ANOVA). The F-test was used to determine the statistical significance of the model. It was made using Design-Expert software (Stat-Ease).

3.   RESULTS AND DISCUSSION

3.1. Magnetic nanosorbents characterization

Figure 17 shows the room temperature magnetization curves of the magnetite (M), magnetic graphene oxide (MGO), magnetic Prussian blue (MPB) and magnetic Prussian blue with graphene oxide (MPBGO). All curves display virtually no hysteresis or remnant magnetization, and thus show superparamagnetism. Superparamagnetic sorbents are particularly useful, especially for environmental applications, since the sorbents can be easily collected when the magnetic field is on, and easily flushed from the filtration system when the magnetic field is off, as the sorbents have no remnant magnetization. The saturation magnetization (M_s) of the magnetite is about 53 emu/g, magnetic graphene oxide – about 38emu/g, magnetic Prussian blue – about 48 emu/g and magnetic Prussian blue with graphene oxide – 22emu/g. It drops, when sorbent is coated with material which hasn't magnetization on their own. The saturation magnetization (Ms) of the GO and PB-coated magnetite (is about half that of the pure magnetite. This is equivalent to having 56 % of PB in the MPBGO sorbent.
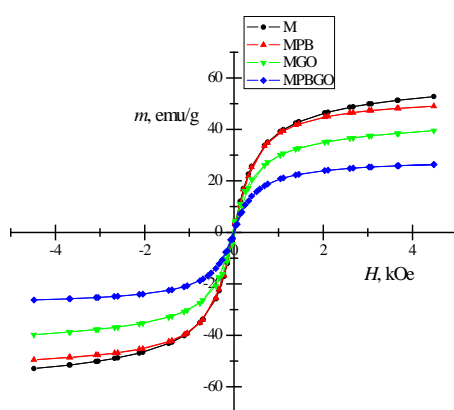

Fig. 17. Magnetization measurements of the synthesized sorbents

Mössbauer spectra was fitted to two hyperfine field distributions having a different isomer shift (δ= 0.25 ± 0.01 and δ= 0.65 ± 0.05 mm/s) which

can be attributed to sublattices A and B of magnetite (Figure 18). The area ratio was Fe(II)/Fe(III) = 1.36. The average hyperfine fields were lower by approximately 20 % compared with those of bulk magnetite ($B_0(A) = 49.3$ and $B_0(B) = 46$ T), because of collective excitations and superparamagnetic relaxation of the magnetic moment of small magnetite nanoparticles of ≈12 nm size. The size was evaluated according to a decrease in the hyperfine field due to collective excitations as given by

$$B=B_0(1-kT/KV) \qquad (38)$$

where k is the Boltzmann constant, T is temperature, K is the magnetic anisotropy of magnetite and V is the volume of nanoparticles. The ratio of the areas of MGO Mössbauer spectra corrected according to the mass thickness of the samples (25 mg/cm^2) 1.9:1, respectively.
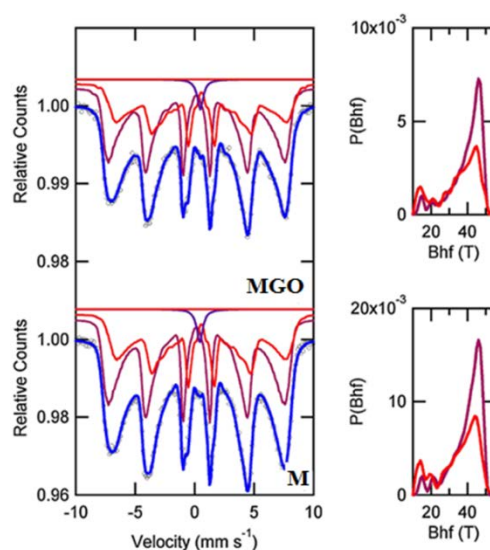

Fig. 18. Mössbauer spectra of nanocrystalline magnetite and magnetic graphene oxide. Hyperfine field distributions are shown on the right

The Mössbauer spectrum of the MPB corresponds to the typical spectrum of the Prussian blue $Fe_4[Fe(CN)_6]_3$. The Fe(II)/Fe(III) ratio in the sample was found to be close to 3:4. The recorded MPBGO spectrum showed the presence of nano-crystalline magnetic compound (25%), which was close to the maghemite structure, and PB with some changes in its structure (Fig. 19).
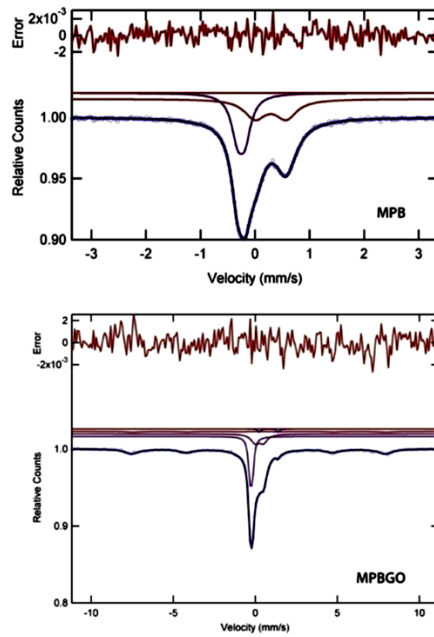
Fig. 19. Mössbauer spectra of nano-crystalline magnetic Prussian blue (MPB) and magnetic Prussian blue with graphene oxide (MPBGO) composites

The XRD pattern confirmed the same size of magnetite crystalline nanoparticles (~11.2 nm) in the MGO as obtained from Mössbauer spectra. (Figure 20)
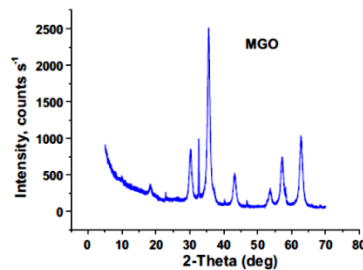

Fig. 20. XRD pattern of MGO composite

In the XRD pattern of MGO nanocomposite, many characteristic diffraction peaks of the pure cubic spinel crystal structure of Fe_3O_4 were found ($2\theta = 30.2°$, $2\theta = 35.6°$, $2\theta= 43.3°$, $2\theta= 53.7°$, $2\theta= 57.1°$, $2\theta= 62.8°$). The disappearance of the typical GO peak ($\approx 2\theta= 10°$), in the XRD pattern of MGO is assigned to the GO reduction and suppression of weak carbon peaks by magnetite (Si et al., 2008). In the XRD pattern of MPB and MPBGO nano-

composites four additional diffraction peaks at 17.4°, 24.8°, 35.3°, 39.5°, which agree well with the specific Prussian blue peaks, were observed (Fig. 21).

The XRD analyses confirmed the same order for crystalline magnetite of 9.5 nm and for crystalline PB of 8.14 nm in the magnetic PB- based composites as obtained from Mössbauer spectra.
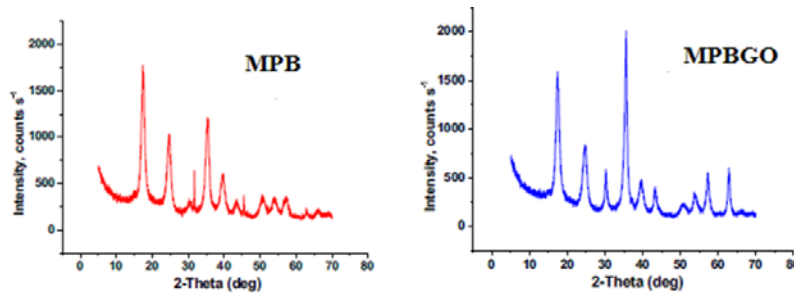

Fig. 21. Typical XRD patterns of MPB and MPBGO composites

The FTIR spectrum of GO indicated a wide absorption band at about 3300–3500 cm^{-1} (Figure 22), which is associated with the hydroxyl groups O–H on the GO sheets (Si et al., 2008). The typical peaks confirm the presence of the oxygen-containing functional moieties in carbon frameworks, which include bands at 1066 cm^{-1} (C–O is stretching vibration of epoxide) and 1732 cm^{-1} (C=O is stretching of carbonyl and carboxyl groups; Fig. 22). The band at 1532 cm^{-1} could be linked to formation of –COO– after coating of GO with Fe$_3$O$_4$ nanoparticles. The peak at 1734 cm^{-1} corresponding to –COOH groups on the GO shifts to 1594 cm^{-1} due to the formation of –COO–after coating with Fe$_3$O$_4$. Characteristic stretching vibration peak at 580 cm^{-1} observed in the FTIR spectra also indicated oxidation of graphite and Fe$_3$O$_4$ bonded to the GO sheets. The typical absorption band at 2072 cm^{-1} observed for PB is due to the stretching vibration of the C≡N group. The absorption band of Fe^{2+}-CN-Fe^{2+} at 500 cm^{-1} and 600 cm^{-1} can be attributed to the formation of PB. The specific adsorption band peaks of PB (2072 cm^{-1}, 600 cm^{-1} and 500 cm^{-1}) and of the magnetite (640 cm^{-1} and 570 cm^{-1}) can be found in the recorded spectrum of the MPB and

MPBGO, indicating that magnetic nano-particles were successfully coated with PB.
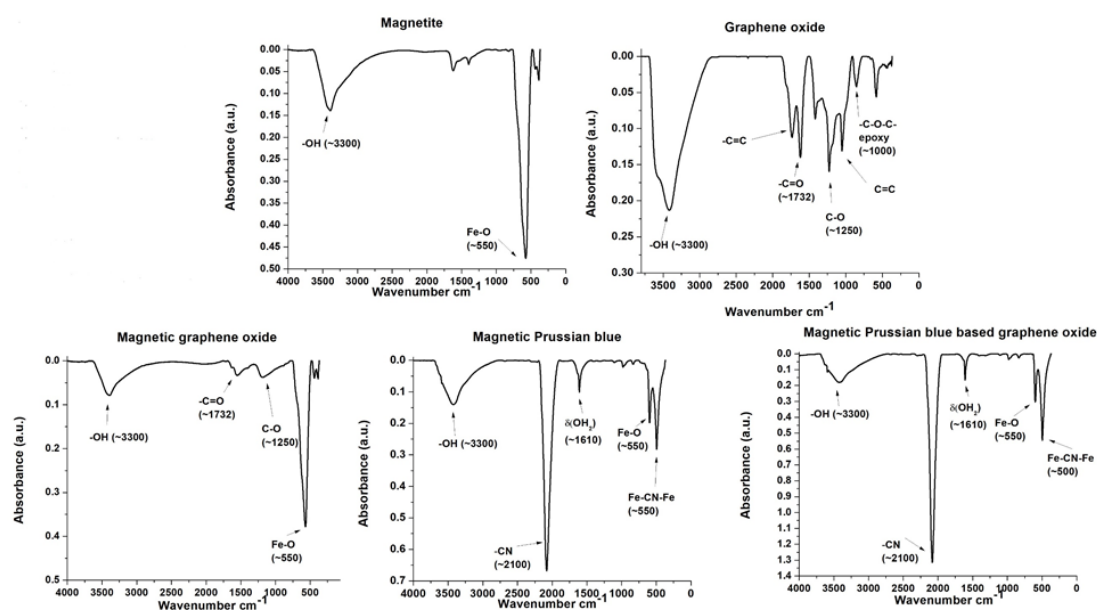

Fig. 22. Typical FTIR spectra of M, MGO, MPB and MPBGO composites

The Raman spectrum of MGO demonstrated two main bands of GO, the prominent D peak at ~1293 cm^{-1} and the G peak at ~1592 cm^{-1}. Spectra of MPB and MPBGO showed typical peaks of PB at about 217 cm^{-1}, 280 cm^{-1}, 500 cm^{-1}, 1295 cm^{-1} and 2157 cm^{-1}, while no characteristic GO peaks were found in the MPBGO spectrum (Fig. 23). This fact can be explained by the presence of PB particles not only on the surface of magnetite but also on the sheets of GO. This is an indication of a different synthesized composite structure as compared with that described in previous publications where only magnetic particles were covered with PB (Yang et al., 2014).
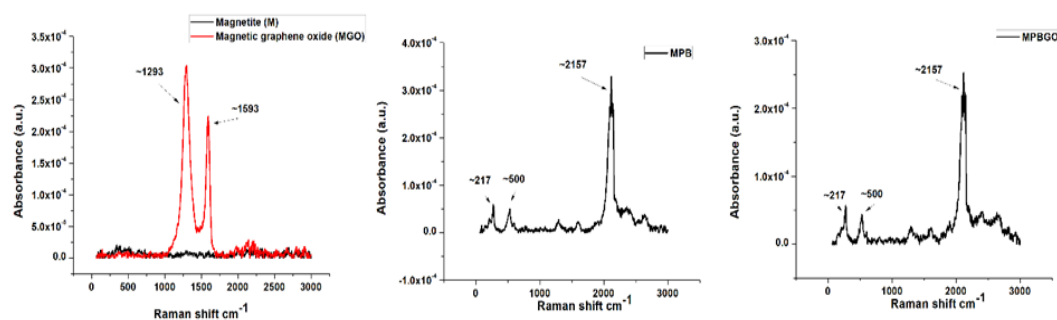

Fig. 23. Raman spectra of M, MGO, MPB and MPBGO sorbents

Morphology and particle size of the magnetite nanoparticles, magnetic graphene oxide, magnetic Prussian blue and magnetic Prussian blue based on graphene oxide sorbents were investigated by SEM (a, b) and TEM (c, d, e, f), and the images are shown in Fig. 24. SEM images of MGO showed that, the iron oxide nanoparticles of about 12 nm randomly and loosely entangled together are dispersed on the surface of GO (Figure 24 A, B). The characterization of MPB (Figure 24 C, D) and MPBGO (Figure 24 E, F) structures by transmission electron microscopy (TEM) indicated that the cores of magnetic nanoparticles had a typical size of about 10 nm or smaller. It can be seen, that many nanoparticles were in-homogeneously attached to the surface of the GO sheets.
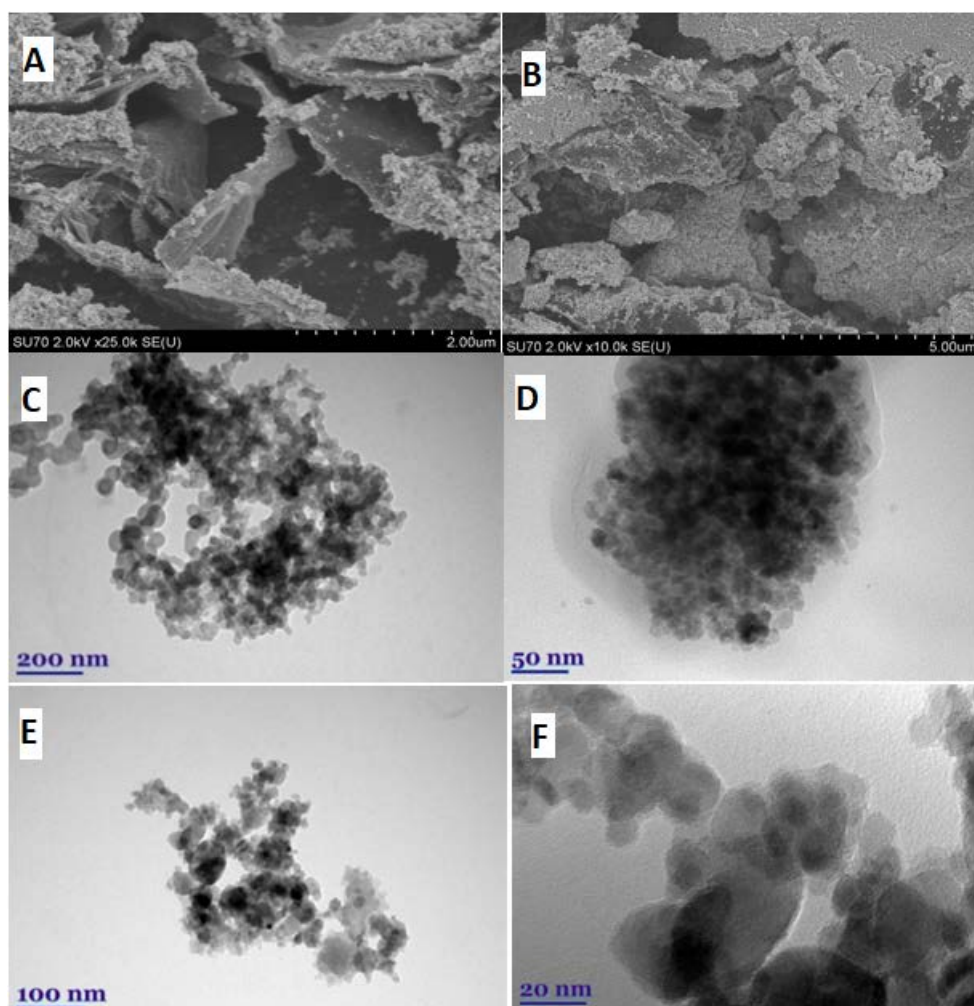

Fig. 24. SEM images of magnetic graphene oxide (A, B), TEM images of MPB and MPBGO sorbents (C, D, E, F)

3.2. Sorption experiments

3.2.1. Equilibrium sorption isotherms

Adsorption isotherms provide important information about sorption mechanisms of Cu(II), Co(II), Ni (II) and Pb(II) on magnetic nanosorbents. Distribution of metal ions between the liquid-phase and solid-phase was described by Langmuir, Freundlich and Dubinin–Radushkevich models.

The effect of the initial concentration of heavy metals on magnetite (M) was investigated in the range 0,25–2 mmol/L with a pH value fixed at 7 (Figure 25 A).
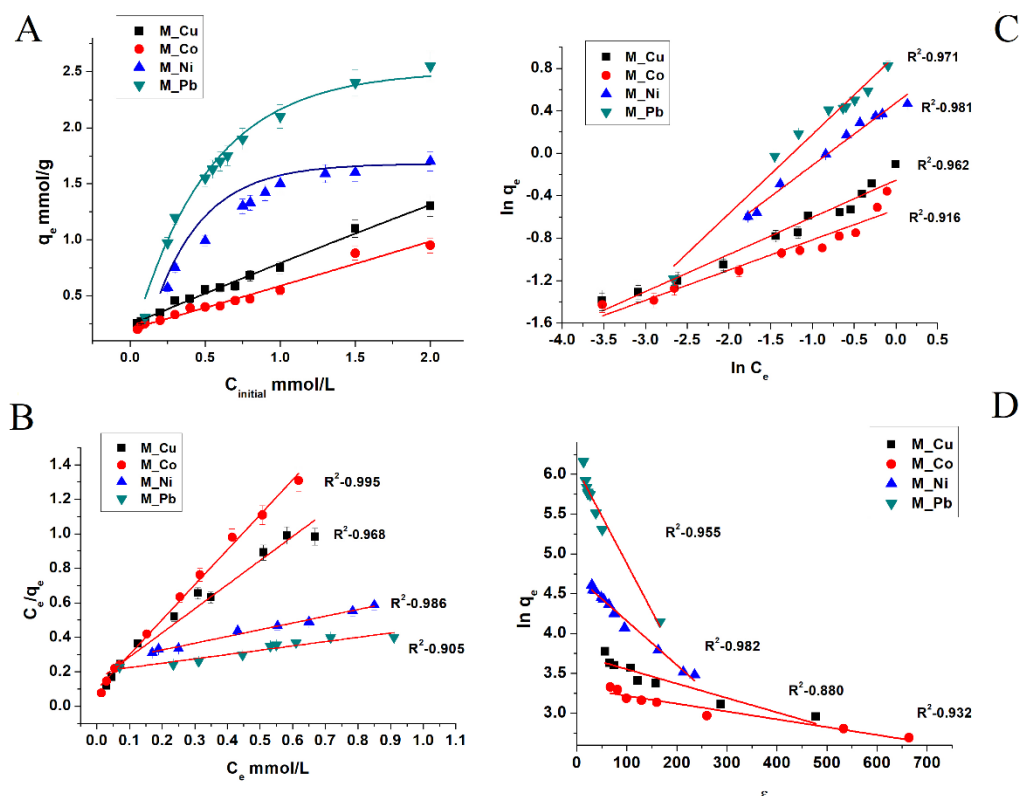

Fig. 25. Initial concentration of heavy metals versus q_e (A), Langmuir isotherms (B), Freudlish isotherms (C) and Dubinin–Radushkevich (D) for sorption on magnetite

Sorption of heavy metals on magnetite increased with increasing initial concentration. Q_e values for Cu(II) was observed – 1.3 mmol/g, Co(II) –

0.95mmol/g, Ni(II) – 1.7mmol/g and Pb(II) – 2.55mmol/g. The fitted isotherms a result of metals sorption on magnetite are shown in Fig. 25 B, C, D and Table 4.

Table 4. Parameters for Langmuir, Freundlich and Dubinin–Radushkevich models of Cu(II), Co(II), Ni(II) and Pb(II) sorption on magnetite

	Cu	Co	Ni	Pb
Langmuir* R^2	0.968	0.995	0.986	0.905
Q_{Max}, mg/g	45.7	29.1	150	827
B	0.03	0.36	0.03	0.01
R_L	0.956	0.736	0.970	0.994
Freudlich** R^2	0.962	0.916	0.981	0.971
K	1.79	3.39	2.98	8.37
1/n	0.349	0.284	0.587	0.746
Dubinin–Radushkevich*** R^2	0.881	0.932	0.983	0.955
Q_s, mg/g	41.3	27.2	109	424
K_{ad}, mol²/kJ²	0.002	0.001	0.006	0.011
E, kJ/mol	16.6	12.7	9.6	6.49

*Qmax – maximum sorption capacity, B, R_L – Langmuir isotherm constant.

**K, 1/n – Freudlich isotherm constant

***Q_s – theoretical monolayer sorption capacity (mg/g), K_{ad}- Dubinin-Radushkevich constant, E – sorption energy.

As listed in Table 4, the sorption of Cu(II) and Ni(II) on magnetite can be fitted to both models (R^2 – 0.96 for Cu(II) and 0.98 for (Ni(II)). Co (II) sorption better fitted by the Langmuir model (R^2 - 0.995) compared to Freundlich model (R^2 - 0.916). Pb (II) sorption contrary better fitted to Freudlich (R^2 – 0.971), then Langmuir (R^2 – 0.905). The maximum adsorption capacities of magnetite calculated from a Langmuir model at pH 7.0 were 45.7 mg/g. 29.1 mg/g, 150 mg/g and 827 mg/g for Cu(II), Co(II), Ni(II) and Pb(II) respectively.

The Freundlich constant (1/n) is related to the sorption intensity of the sorbent. When, 0.1 < 1/n < 0.5, it is easy to adsorb; 0.5 < 1/n < 1, there is some difficulty with the absorption; 1/n > 1, there is quite a lot of difficulty with the absorption as stated by Treybal (Treybal et al., 1981). Our results showed that Cu(II) and Co(II) can be easy sorbed on magnetite (1/n – 0.349 and 0.284).

Ni(II) and Pb(II) sorption has some difficulties (1/n – 0.587 and 0.746 respectively).

The Dubinin–Radushkevich isotherm parameters are listed in Table 4 too. The magnitude of E is useful for estimating the mechanism of the sorption reaction. Sorption is dominated by chemical ion exchange if E is in the range of 8–16 kJ/mol, where as physical forces may affect the adsorption in the case of E < 8 kJ/mol [27]. The calculated E values are 16.6, 12.7, 9.6 and 6.49 for Cu(II), Co(II), Ni(II) and Pb(II) respectively using nano-magnetite. Values are in the sorption energy range of chemical ion exchange reactions, except for Pb(II). This suggests that Cu(II), Co(II) and Ni(II) sorption onto magnetite is attributed to chemical sorption and Pb(II) to physical sorption. This can be explained by the fact, that Pb(II) ions are heavier as compared to other metal ions in this work (M(Pb)- 207, M(Co, Ni) – 59) .

The effect of the initial concentration of heavy metals on magnetic graphene oxide (MGO) was investigated in the range 0,25–2 mmol/L with a pH value fixed at 7 (Figure 26 A). Sorption of heavy metals on magnetic graphene oxide increased with increasing initial concentration. Q_e values for Cu(II) was observed – 0.86 mmol/g, Co(II) – 0.84 mmol/g, Ni(II) – 1.78 mmol/g and Pb(II) – 2.30 mmol/g. The fitted isotherms result of metals sorption on magnetite are shown in Fig. 26 B, C, D and Table 5.
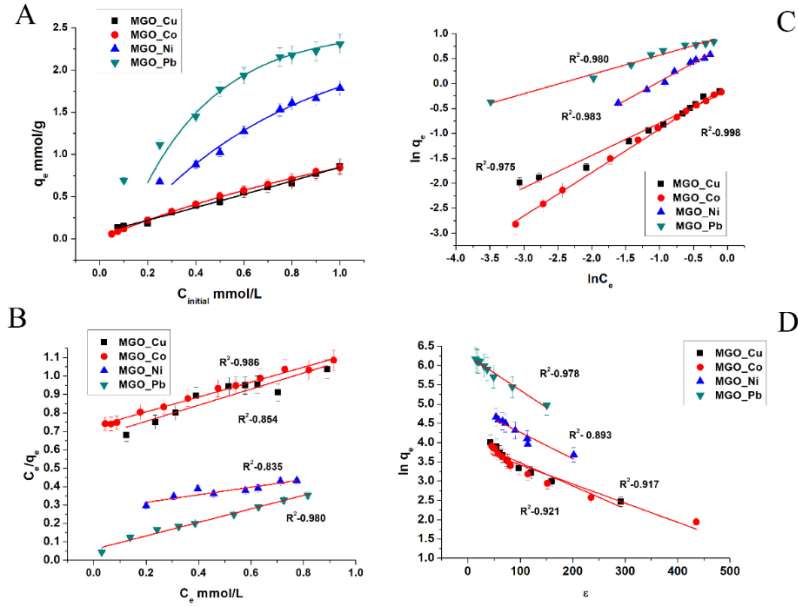
Fig. 26. Initial concentration of heavy metals versus q_e (A), Langmuir isotherms(B), Freudlish isotherms (C) and Dubinin–Radushkevich (D) for sorption on magnetic graphene oxide.

Table 5. Parameters for Langmuir, Freundlich and Dubinin–Radushkevich models of Cu(II), Co(II), Ni(II) and Pb(II) sorption on magnetic graphene oxide.

	Cu	Co	Ni	Pb
Langmuir*				
R^2	0.854	0.986	0.835	0.980
Q_{Max}, mg/g	146	145	286	564
B	0.01	0.01	0.01	0.03
R_L	0.990	0.991	0.988	0.971
Freudlich**				
R^2	0.975	0.998	0.983	0.980
K	1.40	1.10	6.16	9.05
1/n	0.648	0.871	0.750	0.386
Dubinin–Radushkevich***				
R^2	0.917	0.921	0.893	0.750
Q_s, mg/g	57.9	49.7	139	512
K_{ad}, mol²/kJ²	0.006	0.005	0.007	0.009
E, kJ/mol	9.2	10.2	8.57	7.46

*Qmax – maximum sorption capacity, B, R_L – Langmuir isotherm constant.

**K, 1/n – Freudlich isotherm constant

***Q_s – theoretical monolayer sorption capacity (mg/g), K_{ad}- Dubinin-Radushkevich constant,

E – sorption energy.

It can be noticed that the sorption isotherms were fitted better by the Freudlich model (R^2 – 0.975 for Cu(II) and R^2 – 0.983 for Ni(II)) than by the Langmuir model (R^2 – 0.854 for Cu(II) and R^2 – 0.835 for Ni(II)) or to the both models (R^2 – 0.99 for Co(II) and R^2 – 0.98 for Pb(II)), suggesting that sorption of metal ions on MGO is a multi-layer coverage. The Q_{max} values of Cu(II), Co (II), Ni(II) and Pb(II) sorption were 146, 145, 286, 564 mg/g, respectively. The Q_{max} expressed in mmol/g were 2.36 ± 0.3, 2.47 ± 0.4, 4.89 ± 0.2, 2.72 ± 0.2 for Cu(II), Co(II), Ni(II) and Pb(II), respectively, suggesting that 1 g of MGO can adsorb ca. about 2.5 mmol of Cu(II), Co(II), Pb(II) and about 5mmol Ni(II).

1/n values obtained from Freudlich isotherm varied between 0 and 1 (0.648, 0.871, 0.750 and 0.368) suggesting a high affinity between adsorbate and adsorbent. The ratio 1/n above one is typical for cooperative sorption (Foo et al., 2010).

The Dubinin-Radushkevish isotherm model was applied to find the nature of sorption on magnetic graphene oxide too. R^2 values were found to be in the range of 0.750 to 0.917. E values were found to be 7.46, 8.57, 9.2 and 10.2 kJ mol/1 for Pb (II), Ni(II), Cu(II) and Co(II), respectively. These results demonstrated that sorption of Cu(II), Co(II) and Ni(II) was ion-exchange, and of Pb(II) was physisorption.

The heavy metals sorption isotherms on magnetic Prussian blue are presented in Fig. 27. The results demonstrated that the sorption capacity increased with the increasing of initial concentration of the metal ion. Maximum equilibrium concentration of Cu(II) was found to be 1.9 mmol/g, of Co(II) – 1.35 mmol/g, of Ni(II) – 1.18 mmol/g and of Pb(II) – 1.77 mmol/g. Linear fits of isotherms are shown in Figure 27 B, C, D. Parameters calculated from isotherms are summarized in Table 6.
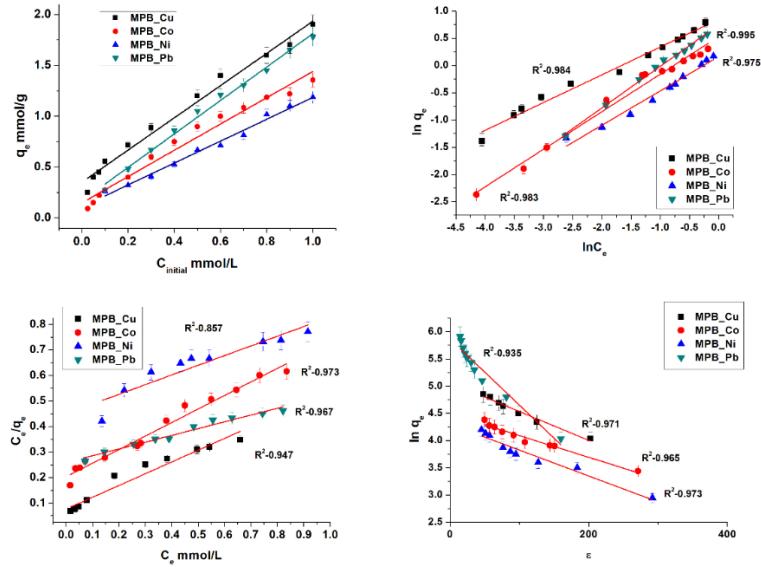
Fig. 27. Initial concentration of heavy metals versus qe (A), Langmuir isotherms (B), Freudlish isotherms (C) and Dubinin–Radushkevich (D) for sorption on magnetic Prussian blue composite

Table 6. Parameters for Langmuir, Freundlich and Dubinin–Radushkevich models of Cu(II), Co(II), Ni(II) and Pb(II) sorption on magnetic Prussian blue

	Cu	Co	Ni	Pb
Langmuir*				
R^2	0.947	0.973	0.857	0.967
Q_{Max}, mg/g	138	111	155	778
B	0.09	0.04	0.01	0.01
R_L	0.914	0.957	0.986	0.995
Freudlich**				
R^2	0.984	0.983	0.975	0.995
K	7.05	3.38	1.46	5.56
1/n	0.509	0.689	0.630	0.763
Dubinin–Radushkevich***				
R^2	0.942	0.943	0.868	0.914
Q_s, mg/g	159	86.5	73.1	364
K_{ad}, mol^2/kJ^2	0.006	0.004	0.005	0.012
E, kJ/mol	9.47	11.3	9.7	6.32

*Qmax – maximum sorption capacity, B, R_L – Langmuir isotherm constant.

**K, 1/n – Freudlich isotherm constant

***Q_s – theoretical monolayer sorption capacity (mg/g), K_{ad}- Dubinin-Radushkevich constant, E – sorption energy.

The effect of initial metal ion concentration on the adsorbed ions at equilibrium (Q_e) on magnetic Prussian blue with graphene oxide (MPBGO) are shown in Fig. 28 A.
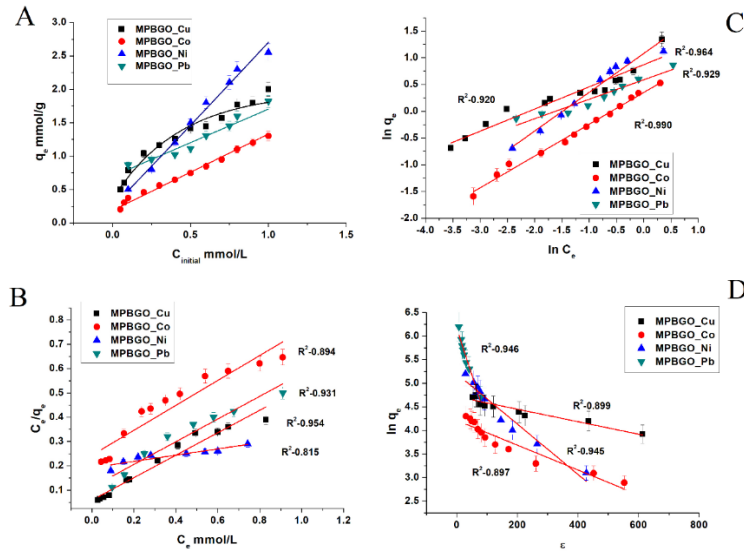
Fig. 28. The initial concentration of heavy metals versus qe (A), Langmuir isotherms (B), Freudlish isotherms (C) and Dubinin–Radushkevich (D) for sorption with magnetic Prussian blue with graphene oxide

As illustrated in Fig. 28 A, all the metal ions (Cu(II), Co(II), Ni(II) and Pb(II)) adsorption capacity depends on the initial metal ion concentration. Sorption capacity relatively rapidly increased with the increase of the initial metal ion concentration. Equilibrium sorption capacity of MPBGO for different ions was in the following order: Ni(II)>Cu(II)>Pb(II)>Co(II), with the values of: 2.55 mmol/g, 2.12 mmol/g, 1.81 mmol/g and 1.40 mmol/g respectively. The maximum adsorption capacities of the MPBGO sorbent for heavy metal ions were evaluated using the adsorption isotherms. The calculated correlation coefficients (b, Q_{max}, 1/n, and K_L) and linear regression coefficient (R^2) values for each model are summarized in Table 7.

Table 7. Parameters for Langmuir, Freundlich and Dubinin–Radushkevich models of Cu(II), Co(II), Ni(II) and Pb(II) sorption on magnetic Prussian blue with graphene oxide

	Cu	Co	Ni	Pb
Langmuir*				
R^2	0.954	0.894	0.815	0.931
Q_{Max}, mg/g	138	115	460	443
B	0.12	0.04	0.01	0.02
R_L	0.889	0.966	0.989	0.980

Freudlich**				
R²	0.920	0.990	0.964	0.929
K	2.38	1.42	2.93	1.79
1/n	0.414	0.594	0.794	0.364
Dubinin–Radushkevich***				
R²	0.899	0.897	0.945	0.946
Qₛ, mg/g	110	66.7	178	466
Kₐd, mol²/kJ²	0.001	0.003	0.005	0.019
E, kJ/mol	9.6	13.8	9.7	5.05

*Q_{max} – maximum sorption capacity, B, R_L – Langmuir isotherm constant.

**K, 1/n – Freudlich isotherm constant

***Q_s – theoretical monolayer sorption capacity (mg/g), K_{ad}- Dubinin-Radushkevich constant,

E – sorption energy.

3.2.2. The influence of pH on heavy metal sorption efficiency

The pH dependence data was obtained for the studied metal cations using magnetite (M) and the results are presented graphically in Fig. 29. The uptake was greatly affected with the change in solution pH. It was noted that during lower range of pH, the uptake of Cu(II) and Pb(II) has increased rapidly. However, at the latter stage of pH i.e., beyond pH 6, it was attained with almost a constant value of sorption. Uptake of Co (II) and Ni (II) increased with increasing pH value. Quantitatively, increasing the pH from 3 to 6, the respective increase of Cu(II) was from 2.03% to 89.84%. The Pb(II) has increased from 11.58% to 92,63%. Co(II) increased from 14.37% to 89.76% respectively for the increase in pH from 3 to 9. Similarly, the Ni(II) sorption has increased from 8.23% to 94.55%.
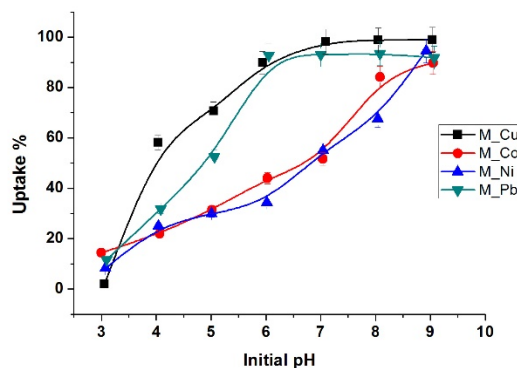

Fig. 29. Effect of initial pH on the percent sorption of Cu(II), Co(II), Ni(II) and Pb(II) from aqueous solutions by the magnetite (M)

The pH dependence data obtained for these metal ions using magnetite can be explained by the surface properties of magnetite (Figure 30). In aqueous systems, the surface of iron oxides is covered with FeOH groups. Surface hydroxyl groups protonate or deprotonate to generate surface charge $FeOH_2^+$ or FeO^- functions at pH values below or above the pH_{ZPC}, respectively.
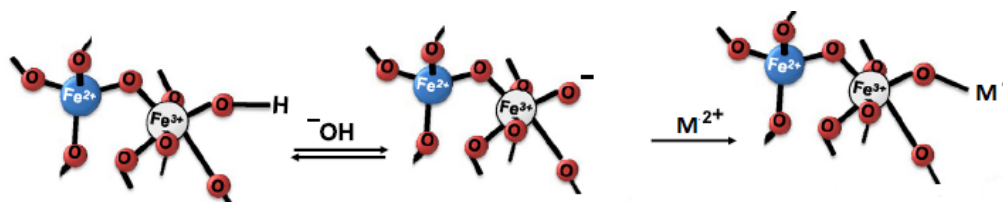

Fig. 30. Heavy metal sorption on magnetite surfaces

At low pH region i.e., pH between 2 and 4 both solid surface of the sorbent and sorbing species were possessed with an enhanced positive charge which has caused strong electrostatic repulsion. Therefore, it seems low uptake of these metal cations may occur. This may be due to the ion exchange of heavy metal in aqueous solution with Fe^{2+} ions in the Fe_3O_4 lattice structure. Similar observation has been reported by Cheong and Lee (Cheong et al., 1996). The further increase in pH i.e., beyond 4.0 the partial acidic dissociation of solid magnetite surface may perhaps cause for some electrostatic attraction of these metal cations which showed a gradual increase in metal uptake. Beyond pH 8.0 there could be a mixed effect of sorption with co-precipitation or even coagulation of these metal cations (Tiwari et al., 2009, Hui et al., 2005, Tiwari et al., 2007), which would cause almost 100% removal.

The initial pH dependent sorption of Cu(II), Co(II), Ni(II) and Pb(II) on magnetic graphene oxide was shown in Fig. 31. The sorption of Cu(II) and Pb(II) on magnetic graphene oxide was minimal at pH ~ 3.0 and significantly increased with increasing pH from 4.0 to 8.0. The high-level adsorption was observed at pH ~ 7. Approximately 95% of Cu(II) and Pb(II) was removed by magnetic graphene oxides. The sorption behaviour of Co(II)

and Ni(II) on magnetic graphene oxides was slower over a wide range of pH from 3.0 to 7.0. About 20% uptake was observed at pH 7. Above pH 7 uptake started to increase and at pH 9 uptake reached about 75%.
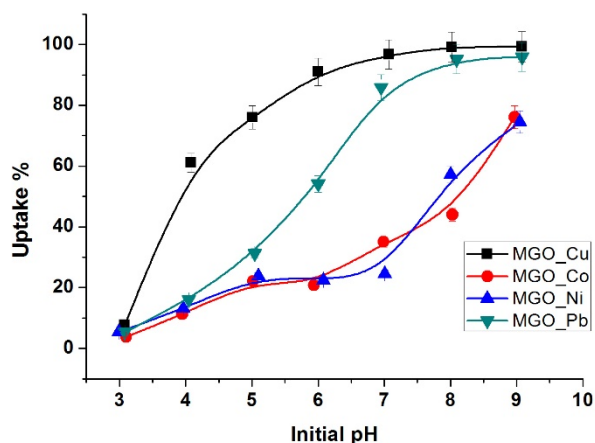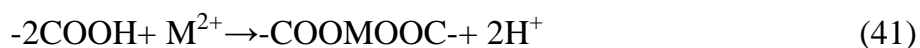

Fig. 31. The effect of initial pH of heavy metals on magnetic graphene oxide

The lower sorption capacity at pH 2-3 might be ascribed to the competition of M^{2+} with H^+. In other words, an excess of H^+ tended to occupy the surface-active sites and compete effectively with M^{2+} due to electrostatic forces at low pH, which leaded to fewer available binding sites for M^{2+}. With the increase of pH, the –COOH and –OH groups converted to –COO- and –O-, and surface charge was more negative to sorb the positively charged metal ions. The following reactions can occur:

$$-COOH + M^{2+} \rightarrow -COOM^+ + H^+ \tag{39}$$

$$-OH + M^{2+} \rightarrow -OM^+ + H^+ \tag{40}$$

$$-2COOH + M^{2+} \rightarrow -COOMOOC- + 2H^+ \tag{41}$$

$$-2OH + M^{2+} \rightarrow -OMO- + 2H^+ \tag{42}$$

$$-COOH + M^{2+} + -OH \rightarrow -COOMO- + 2H^+ \tag{43}$$

In addition, the relative high sorption percentages at high pH (>8) were attributed to the precipitation between M^{2+} and OH^-.

Figure 32 shows the amount of heavy metal sorbed at various pH values on magnetic Prussian blue sorbent. These results showed that uptake gradually increased as the pH increased from 3 to 5-6, later remaining constant. For Cu(II), Co (II) and Ni(II) maximum pH was at about 5 (uptake – 96%), for Pb(II) – about 7 (uptake 90%) respectively. This occurred because part of the Prussian blue may dissolve in acidic conditions.

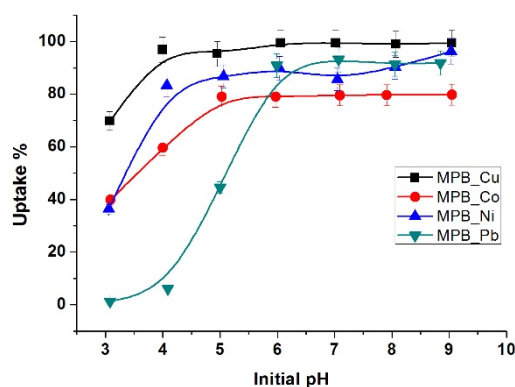**Fig. 32**. The effect of initial pH of heavy metals on magnetic Prussian blue

The sorption of metal ions on magnetic Prussian Blue with graphene oxide was investigated at a pH from 3 to 9 too. As shown in Figure 33 the sorption of Cu(II) increases quickly at pH 3–4 and remains constant at pH 5–9 with uptake 95-98%.
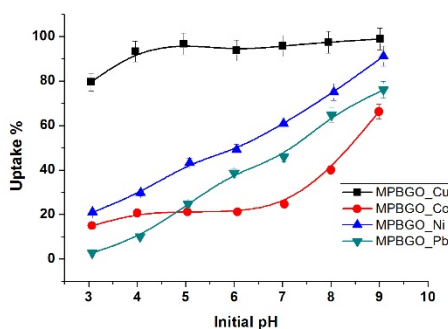

Fig. 33. The effect of initial pH of heavy metals on magnetic Prussian blue with graphene oxide

The sorption of Ni(II) and Pb(II) increases at all pH ranges. As for the Co (II) sorption, it increases in pH range 3-4, then remain constant in pH range 4-7. Above pH 7 sorption increases rapidly. It should be noted that in case of Cu(II), the high adsorption is also observed in acidic solution, i.e. 80% of metal ions are removed from the solution at pH = 3. A pH higher than 3–4 is beneficial for the ionization of the oxygen-containing functional groups on the surface of GO that play a significant role in the uptake of Co(II), Ni(II) and Pb(II). The negative charges generated on the GO surface enlarged the cation exchange capacity of GO and, simultaneously, the electrostatic attraction became more important. The adsorption of metal ions decreases in pH lower than 3–4 due to the low dissociation of the functional groups and competition between H^+ and metal ions for the same sorption site. The fast uptake in Co(II) sorption can be explained by the formation of hydroxides complexes.

3.2.2.1. Contour response surface plots

Contour plot is the map of the response surface as a two-dimensional design. This analysis gives a better understanding of the influence of parameters and their interaction on the response. To investigate the interactive effect of two factors on the uptake of Cu(II), Co(II), Ni(II) and Pb(II), the response surface methodology-central composite design was used, and contour plots were created. Figures 34 – 37 shows the combined effect of initial pH and final pH with different sorbents (magnetite, magnetic graphene oxide, magnetic Prussian blue and magnetic Prussian blue with graphene oxide). The initial pH value was determined at the beginning of the sorption experiment, when the aqueous solution of Cu (II), Co (II), Ni (II) or Pb (II) ions was mixed with the sorbent. The final pH value was measured after sorption, when, with the help of magnet, sorbent was separated from the solution. It is clear, that increasing initial pH and decreasing final pH give us higher uptake value. The dependence of metal sorption on pH is related to both the metal chemistry in solution and the ionization state of the functional groups of the sorbent, which affects the availability of binding sites. In initial solution with pH lower than 4.0, the uptake

capacity was lower due to competition between hydrogen and metal ions on the binding sites of sorbent (Pavan et al., 2008). As the solution initial pH increased over pH 8.0, precipitation of ions can lower the sorption efficiency (Yan et al., 2003). From all contour response surface plots, we can calculate uptake values from different initial and final pH values.

Fig. 34. Contour response surface plots of pH effects on sorption efficiency by magnetite

Fig. 35. Contour response surface plots of pH effects on sorption efficiency by magnetic graphene oxide
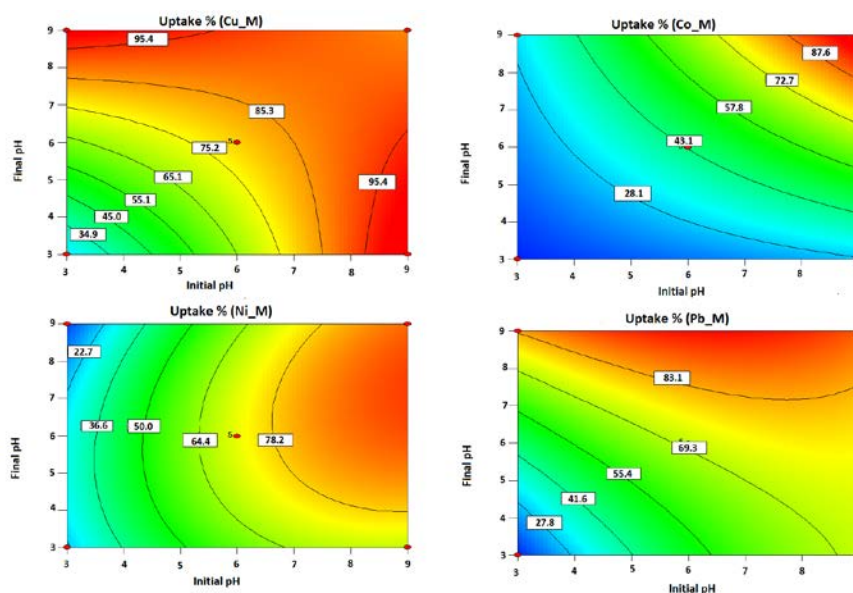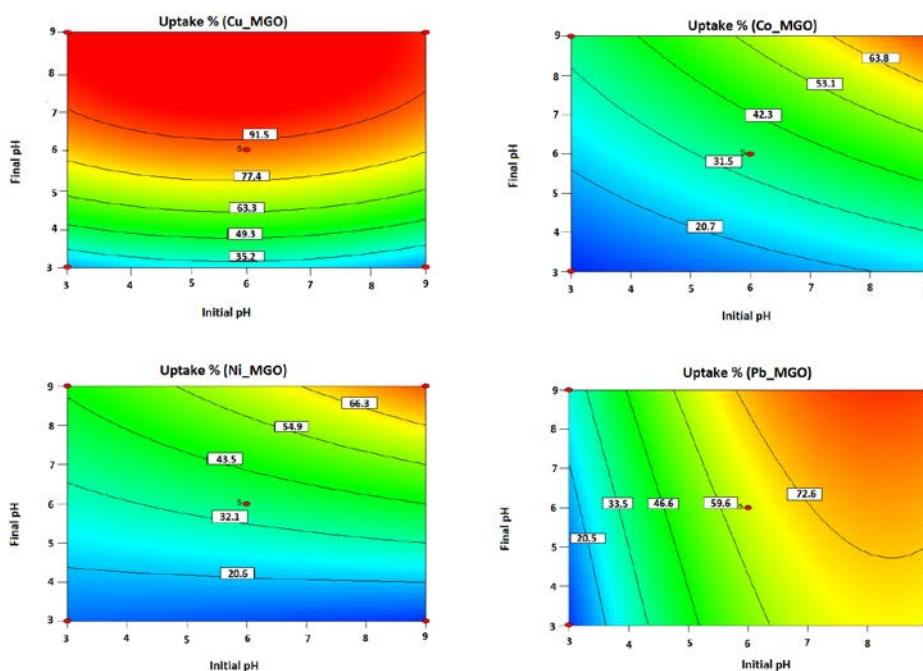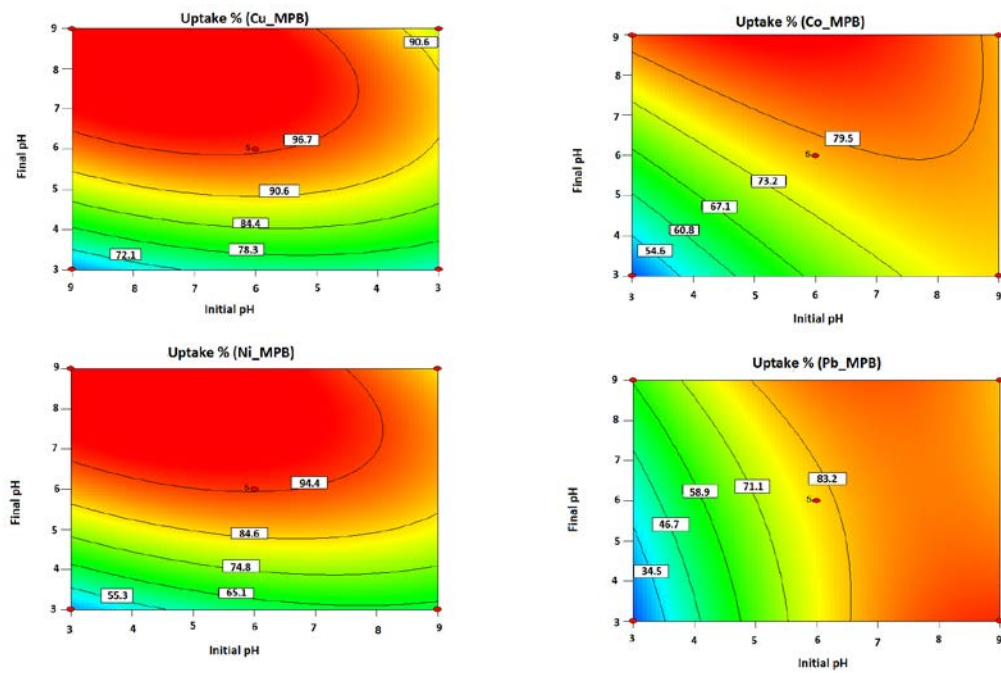
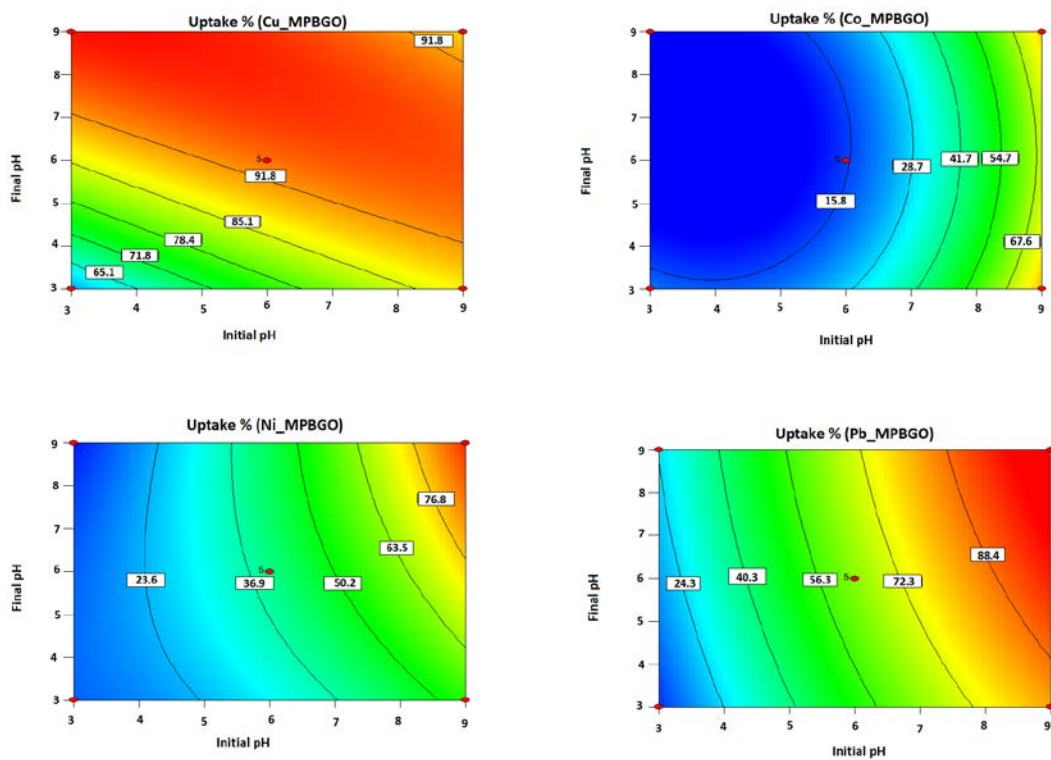**Fig. 36**. Contour response surface plots of pH effects on sorption efficiency by magnetic Prussian blue

Fig. 37. Contour response surface plots of pH effects on sorption efficiency by magnetic Prussian blue with graphene oxide

3.2.3. Sorption kinetics

The results of sorption studies carried out as a function of contact time, for Cu(II), Co(II), Ni(II) and Pb(II) are presented in Figure 38. The results showed that the sorption of the studied heavy metals shows a fast increase with the contact time and reaches equilibrium at 60 and 120 min using all four nano sorbents. The removal percentages were 89.94 %, 61 %, 64.3 %, and 97.65 % for Cu(II), Co(II), Ni(II) and Pb(II) metal ions, respectively, using nano magnetite. The percentages decreased to 78.28 %, 58.2 %, 60.24% and 93.3 % for Cu(II), Co(II), Ni(II) and Pb(II) ions respectively using magnetic graphene oxide nanocomposite. The data showed similar observations with Prussian blue nanocomposites. The removal percentages were 88.2 %, 72.4 %, 72.2 %, and 95.57 % for Cu(II), Co(II), Ni(II) and Pb(II) metal ions, respectively, using magnetic Prussian blue composite. The percentages decreased to 83.9 %, 59.1 %, 62.7% and 82.41 % for Cu(II), Co(II), Ni(II) and Pb(II) ions respectively using magnetic Prussian blue with graphene oxide nanocomposite.
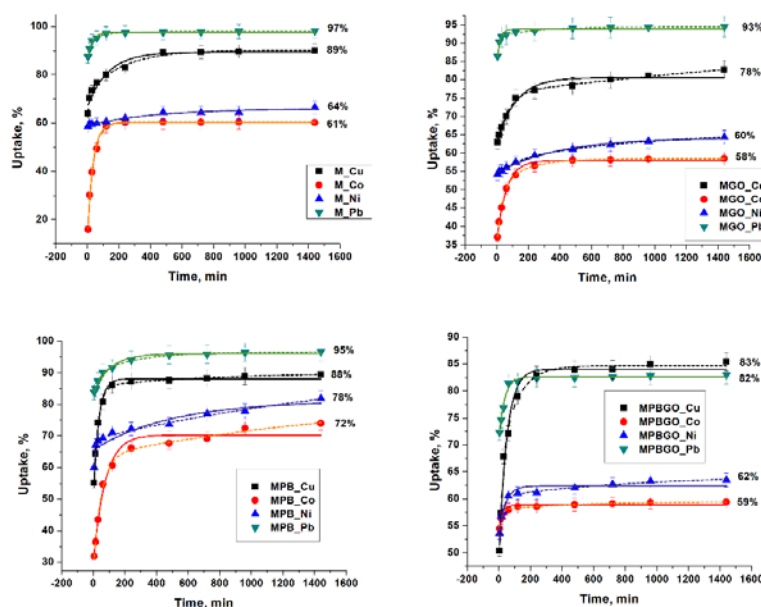
Fig. 38. Effect of contact time on the heavy metal ions removal efficiency

In order, to determine the rate constants, pseudo-first order and pseudo-second order were employed to model the sorption data. The linearized

pseudo-first-order equation can be represented by the following equation (Lagergren 1898):

$$\ln\left(q_e\text{-}q_t\right)=\ln q_e\text{-}k_1t \tag{44}$$

where k_1 (in minute) is the pseudo-first-order sorption rate constant and q_e and q_t are the values of the mass sorbed per unit mass of sorbent at equilibrium (capacity) and at time t, respectively. Plot of ln (qe−qt) versus t for a sorbent would yield a straight line if the sorption process follows a pseudo-first order kinetic behaviour.

The linearized Lagergren second-order kinetic equation may be represented by the following equation:

$$\frac{t}{q_t}=\frac{1}{k_2q_e^2}+\frac{1}{q_e}*t \tag{45}$$

where k_2 (in grams per milligram per minute) is the pseudo second- order rate constant. The value of k_2 depends on the operating conditions, such as initial pH and solution concentration, temperature, agitation rate, etc. The validity of pseudo second-order model was checked by the fitted straight line too (Figure 39).
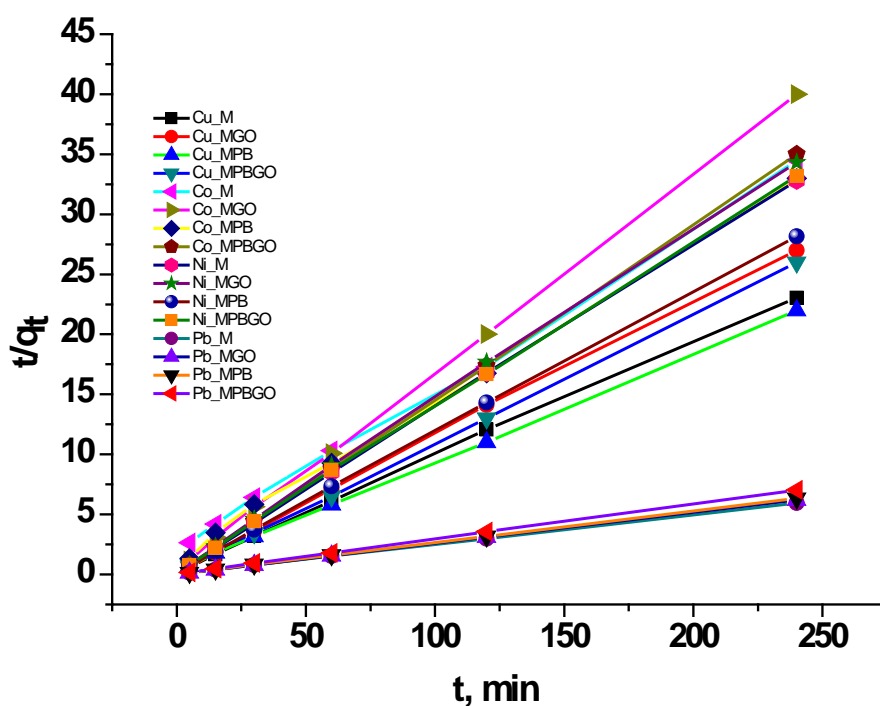
Fig. 39. Pseudo second order model

The corresponding kinetic parameters and the determination coefficients are summarized in Table 8.

Table 8. Parameters of the pseudo first-order, pseudo second-order models for heavy metals sorbed by magnetic nanocomposites

Composite	Metal	Pseudo first order				Pseudo second order		
		R^2	k_1	Qexp	Qt	R^2	k_2	Qt
M	Cu	0,801	0,009	11,4	8,62	0,999	0,029	10,4
	Co	0,991	0,064	7,13	4,4	0,996	0,006	7,91
	Ni	0,961	0,007	7,6	5,4	0,999	0,104	7,33
	Pb	0,895	0,035	40,4	11,8	0,999	0,022	40,5
MGO	Cu	0,627	0,004	10,0	4,59	0,999	0,023	8,52
	Co	0,996	0,041	6,85	9,42	0,995	0,046	6,2
	Ni	0,971	0,024	7,05	5,7	0,999	0,068	7,21
	Pb	0,707	0,019	38,9	32,8	0,999	0,022	40,5
MPB	Cu	0,977	0,064	11,2	12,5	0,997	0,023	10,9
	Co	0,969	0,014	7,99	4,35	0,991	0,012	7,68

	Ni	0,812	0,017	8,69	7,3	0,999	0,068	8,56
	Pb	0,656	0,010	39,5	23,8	0,997	0,024	38,0
MPBGO	Cu	0,938	0,058	10,1	10,7	0,997	0,028	9,75
	Co	0,922	0,047	6,95	7,37	0,999	0,023	6,94
	Ni	0,946	0,036	7,32	6,8	0,999	0,089	7,25
	Pb	0,925	0,047	34,1	17,4	0,999	0,020	34,2

The high coefficients of determination (R^2), the similarity between the experimental capacities at equilibrium and the calculated capacities of the models indicate that the pseudo second-order model fits the experimental data better than pseudo first-order. The rate constants ranged from 0.0067 min^{-1} to 0.1 min^{-1} depending on metal and sorbents. It increased in following order:

- Co>Pb>Cu>Ni with magnetite (0.0067 min^{-1}, 0.0227 min^{-1}, 0.0297 min^{-1} and 0.1047 min^{-1} respectively);
- Pb>Cu>Co>Ni with magnetic graphene oxide (0.0227 min^{-1}, 0.0238 min^{-1}, 0.0466 min^{-1}, 0.0685 min^{-1});
- Co>Pb>Cu>Ni with magnetic Prussian blue (0.0124 min^{-1}, 0.0236 min^{-1}, 0.0245 min^{-1}, 0.0685 min^{-1});
- Pb>Co>Cu>Ni with magnetic Prussian blue with graphene oxide (0.02 min^{-1}, 0.0236 min^{-1}, 0.0281 min^{-1}, 0.0891 min^{-1}).

To analyse the rate controlling steps such as mass transport and chemical reaction processes is very beneficial to specify the sorption mechanism. The sorption reaction is usually divided into the following steps (Sarkar et al., 2003): (1) transport of ions from the boundary film to the external surface of the sorbent (film diffusion); (2) transfer of ions from the surface of the intraparticular active sites (particle diffusion); (3) sorption of ions by the active sites of sorbent. Weber and Morris model is a widely used intraparticle diffusion model (IDM) to predict the rate controlling step (Weber et al., 1963). The rate constants of intraparticle diffusion (K_{id}) at the stage *i* were determined using the following equation:

$$q_t = K_{id}t^{1/2} + C_i \qquad (44)$$

where q_t is the amount sorbed at time t, $t^{1/2}$ is the square root of the time, C_i is the intercept at stage i. The value of C_i is related to the thickness of the boundary layer. The larger C_i represents the greater effect of the boundary layer on ion diffusion. The plots of q_t versus $t^{1/2}$ show two different linearity profiles (Figure 40-41).
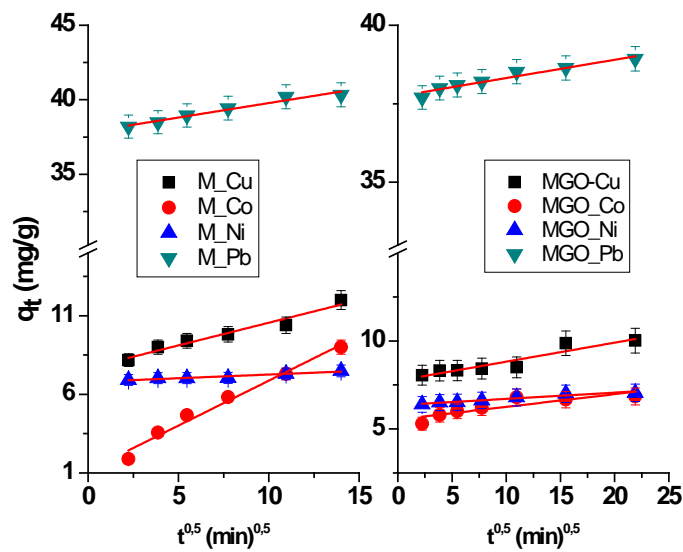
Fig. 40. Intraparticle diffusion model for magnetite and magnetic graphene oxide

Magnetite and magnetic graphene oxide demonstrated one linear characterization indicating that one step occurred in the sorption process (ions are sorbed on sorbent surface, complexation may occur). Magnetic Prussian blue and magnetic Prussian blue with graphene oxide showed multilinearity characterizations, indicating that two steps occurred in the sorption process.
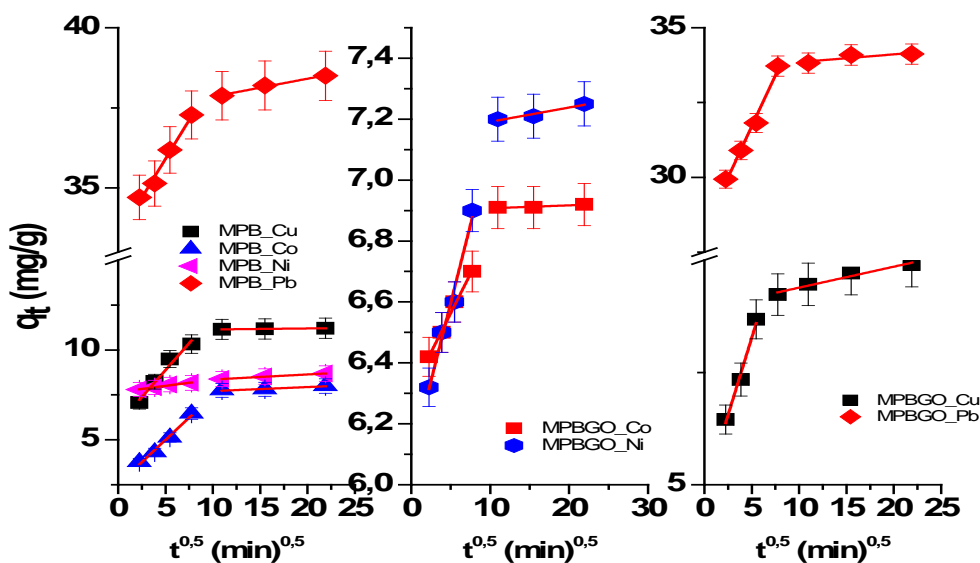
Fig. 41. Intraparticle diffusion model for MPB and MPGO

The first sharp section can be attributed to the diffusion of sorbate through the solution to the external surface of the sorbent, or the boundary layer diffusion of the sorbate molecules. The second subdued portion is the gradual sorption stage, where intraparticle diffusion is rate-controlled (Cheung et al., 2007). This kind of multi-linearity in the shape of the intraparticle diffusion plot has also been observed by Ofomaja in the sorption of lead(II) onto mansonia wood sawdust (Ofomaja et al., 2010). The intraparticle diffusion parameters and the determination coefficients are summarized in Table 9. The larger slopes of the first sharp sections indicate that the rate of heavy metal removal is higher in the beginning stage due to the instantaneous availability of large surface area and active adsorption sites. The lower slopes of the second subdued portion are due to decreased concentration gradients that make heavy metal diffusion in the micropores of sorbent take a long time, thus leading to a low removal rate.

Table 9. The intraparticle diffusion parameters and the determination coefficients

Composite	Metal	R^2	K_{id}	I_{id}			R^2	K_{id}	I_{id}
M	Cu	0,964	0,288	7,67	**MGO**	Cu	0,862	0,108	7,74
	Co	0,978	0,571	1,16		Co	0,719	0,072	5,53

	Ni	0,905	0,047	6,79		Ni	0,936	0,035	6,35
	Pb	0,957	0,193	37,8		Pb	0,923	0,058	37,7

		$1\text{-}R^2$	$2\text{-}R^2$	$1\text{-}K_{id}$	$2\text{-}K_{id}$	$1\text{-}I_{id}$	$2\text{-}I_{id}$
MPB	Cu	0,958	0,983	0,599	0,006	5,88	11,0
	Co	0,978	0,934	0,495	0,022	2,53	7,49
	Ni	0,951	0,996	0,069	0,028	7,66	8,07
	Pb	0,972	0,972	0,485	0,055	33,4	37,9
MPBGO	Cu	0,970	0,942	0,688	0,046	4,83	8,92
	Co	0,993	0,960	0,052	0,009	6,31	6,89
	Ni	0,974	0,891	0,102	0,005	6,08	7,14
	Pb	0,984	0,986	0,682	0,026	28,2	33,5

3.2.4. The influence of sorbent dosage on the sorption efficiency

The effect of sorbent (M, MGO, MPB and MPBGO) dosage on the removal efficiencies of heavy metal was investigated and the results are listed in Figure 42. It was found that the adsorption efficiency of the metal ions increased with increasing initial amount of sorbent. Metal removal increased with larger sorbent dosages because more active sites to bind metal ions were available. Uptake increased 3, 4 and 5 times with MPB, M and MGO respectively, when sorbent dose increased from 10 mg to 20 mg. Magnetite sorption increased from 15.3% to 66.1%, magnetic graphene oxide – from 11.2% to 55.3%, magnetic Prussian blue – from 32.2% to 90.5%. Increasing sorbent dose from 20 mg to 30 mg did not have as big of an impact as increasing it from 10 mg to 20 mg. Uptake increased about 1.5 times. Different impact was noticed with MPBGO sorbent. Uptake has increased about 1.5 times, upon increasing sorbent dosage: 40.6%, 67.7% and 97.4% for 10 mg, 20 mg and 30 mg respectively.
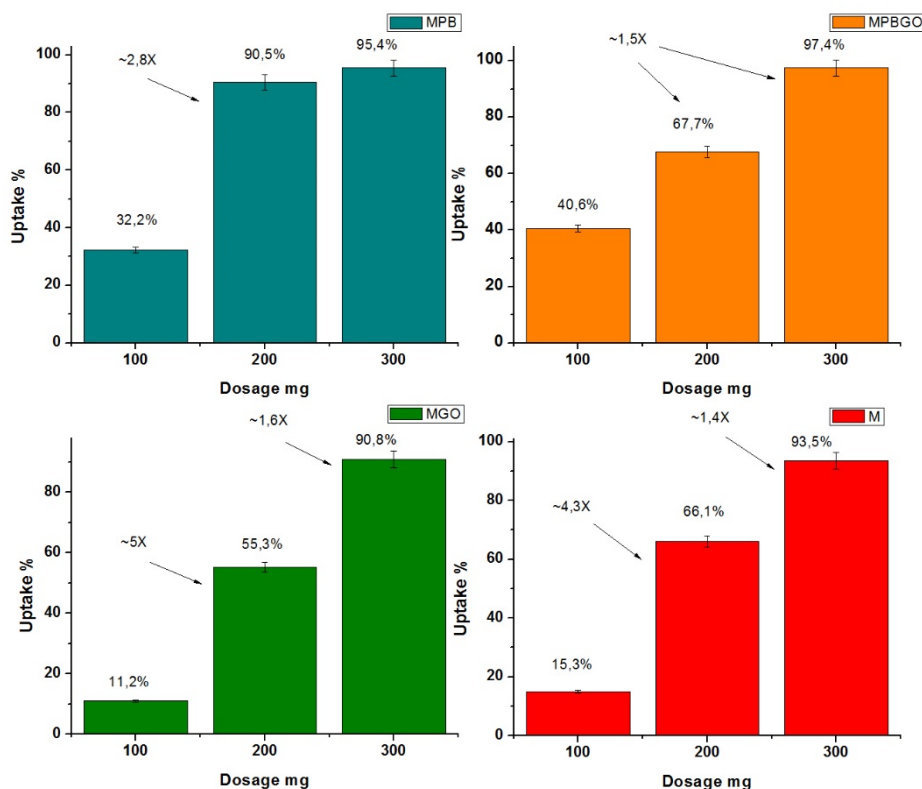
Fig. 42. The effect of sorbent dosage on heavy metal removal efficiency

3.2.5. Heavy metal sorption-desorption cycles (reuse study)

The recovery of heavy metals from magnetite (M) nanoparticles was studied at pH = 4 using nitric acid as eluting solution. Figure 43 indicates that after one circle about 80% of heavy metals were removed from sorbent. Desorption rate has decreased in circle 2 and 3 – 40% and 15.6% respectively. This can be explained by sorption- desorption rates in the first circle. Also, it was reported that divalent metal ions such as Mn(II), Co(II), Ni(II) and Cu(II) can become incorporated with spinel structures (Ainsworth et al., 1994). It was suggested that the difficulty of desorbing cations from iron oxides can be attributed to the formation of inert surface complexes too (Uheida et al., 2006).
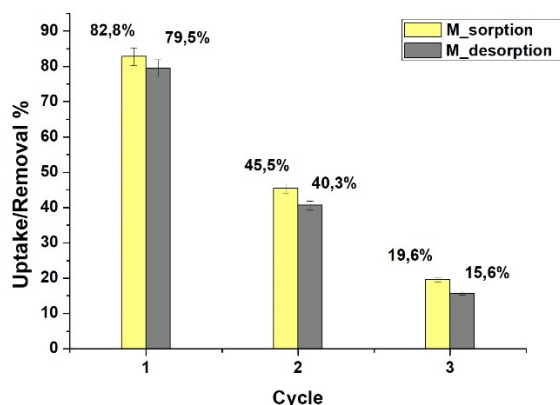
Fig. 43. Sorption-desorption cycles on magnetite (M)

To investigate the regeneration and reusability of prepared MGO nanoparticles, the MGO was used 3 times in consecutive sorption–desorption cycles too. The sorption efficiency of the regenerative MGO was used to evaluate the reusability. As shown in Figure 44, 86.8% of heavy metals were sorbed and 81.1% were desorbed with magnetic graphene oxide in first cycle. Uptake decreased in second and third cycle to 66.9 % and 46.7% for sorption and 63.6 % and 41.8 % for desorption process. The results might be attributed to the loss of sorbent during the multiple washing after one sorption– desorption cycle finished. In addition, the active sites on sorption occupied by heavy metal ions could not be completely recovered by desorption.

Fig. 44. Sorption-desorption cycles on magnetic graphene oxide (MGO)

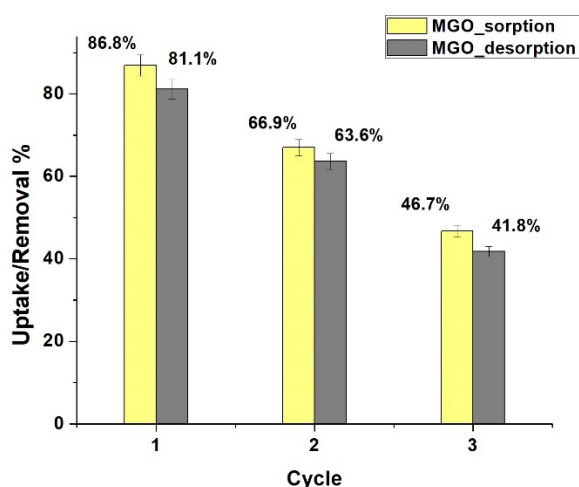The re-cycling of magnetic Prussian blue sorbent in the removal of Cu(II), Co(II), Ni(II) and Pb(II) was investigated too. Figure 45 shows the effects of three consecutive sorption–desorption cycles. As we can see after the first cycle, sorption-desorption efficiency was 85.7% and 80.4%, after the second – 76.7% and 68.2%, after third – 67.8% and 55.3% respectively. In each cycle efficiency decreased about 10%. This can happen, because strong acid and low pH values in the desorption cycle was used, under which conditions Prussian Blue dissolution can happen.
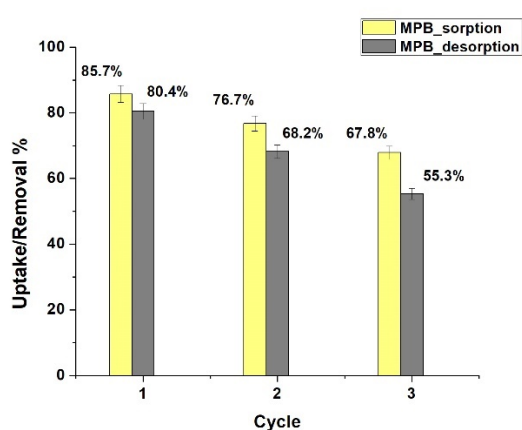
Fig. 45. Sorption-desorption cycles on magnetic Prussian blue (MPB)

The regeneration of heavy metal-retained magnetic Prussian blue with graphene oxide sorbent was conducted for three sequential cycles (Fig. 46). Results were found to be similar like with MPB sorbent. After the first cycle, sorption-desorption efficiency was 84.4% and 79.7%, after the second – 71.7% and 65.2%, after third – 59.8% and 52.9% respectively.
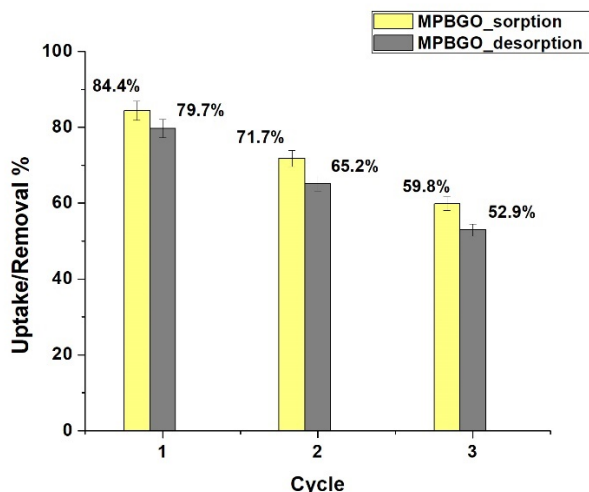
Fig. 46. Sorption-desorption cycles on magnetic Prussian blue with graphene oxide (MPBGO)

3.2.6. Competitive effects of heavy metals in sorption experiments

To examine the competitive effects the metals effect on each other in multi-metal solutions, the removal efficiencies of M, MGO, MPB and MPBGO for each metal in single and multi-solutions were compared and are shown in Figure 47.
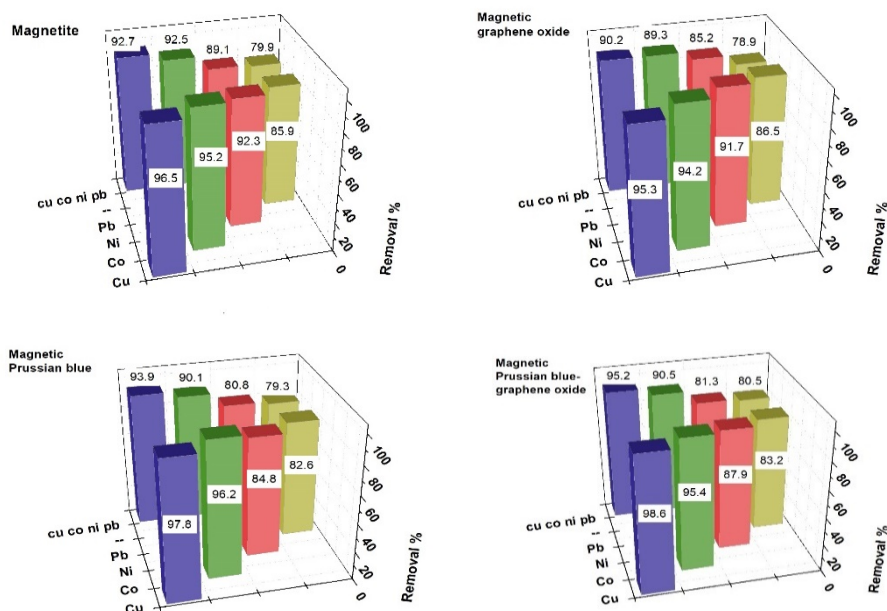
Fig. 47. Percentage removal of Cu(II), Co(II), Ni(II) and Pb(II) from single and multi-metal solutions

It can be seen that the percentage removal of Cu (II), Co (II), Ni (II) and Pb (II) ions from a single-metal system (non-competitive) were 96.5%, 95.2%, 92.3% and 85.9% on magnetite, 95.3%, 94.2%, 91.7% and 86.5% on the magnetic graphene oxide, 97.8%, 96.2%, 84.8% and 82.8% on magnetic Prussian blue, 98.6%, 95.4%, 87.9% and 83.2% on magnetic Prussian blue-graphene oxide, respectively. In multi-metal solutions all heavy metal sorption was slightly reduced (for example, Cu(II) from 96.5% to 92.7% on M, Co(II) from 94.2% to 89.3% on MGO, Ni(II) from 84.8% to 80.8% on MPB, Pb(II) from 83.2% to 80.5% on MPBGO) by the presence of other metal ions. The removal percentage dropped about max 5-6% with all four sorbents. The decrease in sorption capacity of same adsorbent in multimetal solution than that of single metal ion may be ascribed to the lesser availability of binding sites. In case of the multi - metal solution, when metals compete for the same sorption sites of a sorbent, metals with a greater affinity could displace others with weaker affinity (Qin et al., 2006). The higher sorption of Pb(II) on different adsorbents containing -COOH and -OH functional groups in multimetal solutions was reported in other studies (Ducoroyt et al., 2008, Qin et al., 2006). The extent to which a metal ion will bind depends strongly on the chemistry of the metal ion and its preference to form covalent or ionic bonding (Wang et al., 2006). Metal ions act as Lewis acids of accepting electron pairs from ligands. Pearson divided metal ions into class A 'hard' ions, class B 'soft' ions and borderline ions. The theory was further refined by Nieboer and Richardson (1980), and Nieboer and McBryde (1973) who described class A metal ions as nonpolarizable hard metals that prefer to bind to nonpolarizable hard bases by bonds that are principally ionic, and class B metal ions as polarizable soft metals that prefer to bind to polarizable soft bases by bonds that are mainly covalent. Cu(II), Co(II), Ni(II) and Pb(II) are classified as borderline ions (intermediate between class A and B, but with properties nearer that of class B metal ions). Based on this, the competition effects observed in our study could be explained. Due to all heavy metals used in my study belonging to the same borderline class, they did not have much effect on each other.

3.2.7. Competitive sorption of heavy metals in Baltic Sea water samples

To develop sorbents for water treatment in natural aqueous systems, sorption experiments were carried out in seawater (SW) collected from the Baltic Sea. Spiked samples (mixture of Cu(II), Co(II), Ni (II) and Pb(II)) were analyzed to confirm, that heavy metal can be removed from sea water using magnetic nanosorbents. Results are listed in Figure 48.
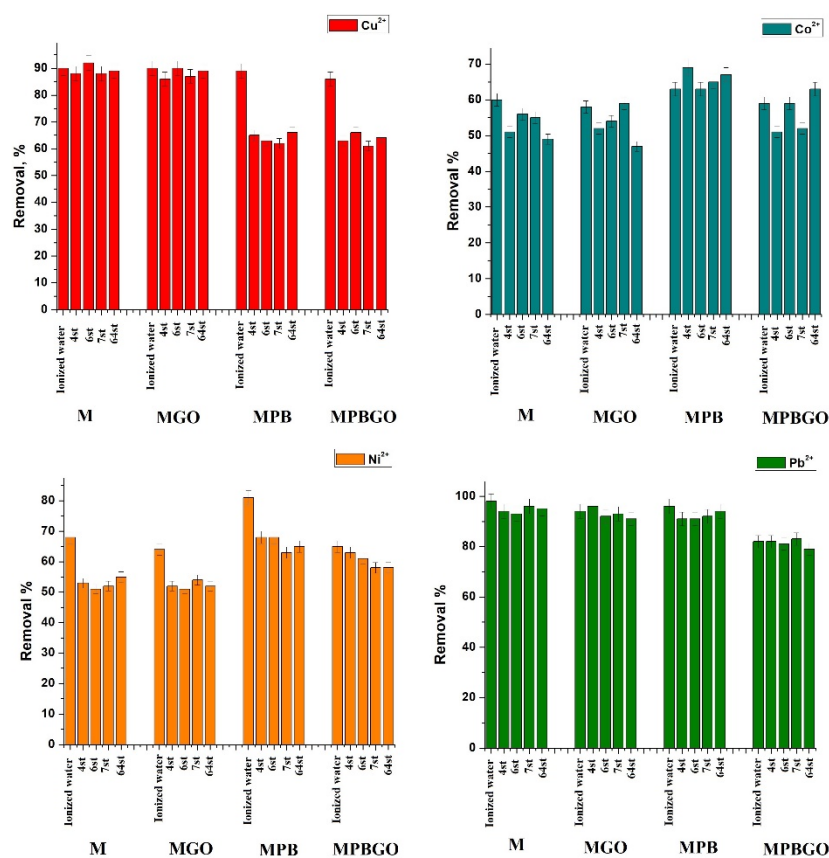
Fig. 48 Sorption of heavy metals (%) in Baltic Sea water samples

The removal percentage values of Pb (II) using M, MGO, MPB and MPBGO as sorbents were identified to reach 82 – 95 % in all water samples. For Co(II) removal percentage was identified to be around 50-60% using all water samples too. Cu(II) removal percentage was about 90% with magnetite, and magnetic graphene oxide. With sorbents, which contain Prussian blue (MPB and MPBGO) removal decreased by about 10 – 20 %. The same phenomena discovered for Ni(II) too, when the removal percentage dropped from 80% to

60% using magnetic Prussian blue sorbent. This behaviour is related to the interfering of dissolved ions in seawater. High concentrations of K^+, Na^+ and other ions naturally occur in seawater. It is very well known that due to similar hydration radii, potassium ions in MPB and MPBGO nanosorbents can compete with heavy metals for sorption sites on the PB surface. The effect of coexisting ions was usually related to the hydration radii of cations and it decreased in the order as follows: K^+ (3.3 Å) Na^+ (3.6 Å) Pb^{2+} (4.02 Å) Ni^{2+} (4.04 Å) Ca^{2+} (4.1 Å) Cu^{2+} (4.19 Å) Co^{2+} (4.23 Å) Mg^{2+} (4.25 Å). Removal efficiency can be increased to 100% by increasing the dose of sorbents. Thus, magnetic nanosorbents work well to remove heavy metals in the presence of other ions and dissolved solids.

3.3. Modelling of heavy metals sorption process

3.3.1. Central composite Rotatable Design (CCRD)

The Central Composite Rotatable Design (CCRD) was used to establish the influence of experimental parameters and the interactions on the heavy metal ion removal with magnetic Prussian blue. The CCRD had eight factorial points, six axial points, and six center points - total of 20 runs used to set optimum points. All experiments were made in neutral pH to prevent metal ion precipitation. The quantity of metal ion removal (Y) was chosen as the response of the design experiments. The relationship between the removal of heavy metal ions and the parameters was acquired with coded variables as the following for Cu(II), Co (II), Ni(II), and Pb(II), respectively:

$$Cu(II)uptake=-0,52+0,73*A+5,78*B+5,58*C+4,57*AB+0,01*AC+2,51*BC-0,96*A^2-3,95*B^2-1,51*C^2$$

$$Co(II)uptake=-0,41+2,28*A+0,01*B-9,94*C+0,01*AB-2,63*AC-3,17*BC-1,02*A^2-2,67*B^2+7,99*C^2$$

$$Ni(II)uptake=1,22-1,42*A+2,85*B-0,01*C+6,18*AB+0,01*AC+4,77*BC+$$
$$0,51*A^2-1,07*B^2+6,60*C^2$$

$$Pb(II)uptake=1,41-2,77*A+3,83*B-0,01*C+1,32*AB+0,02*AC+9*BC+$$
$$1,03*A^2-1,59*B^2+5,78*C^2$$

Figure 48 represents the assessment of predicted and actual results. It is clearly recognized that the predicted values fitted well with the actual values. The coefficients of determination for Cu(II), Co(II), Ni(II) and Pb(II) removal were obtained as 0.974, 0.873, 0.952 and 0.880, respectively.

Fig. 48. Actual results versus predicted results on heavy metal uptake
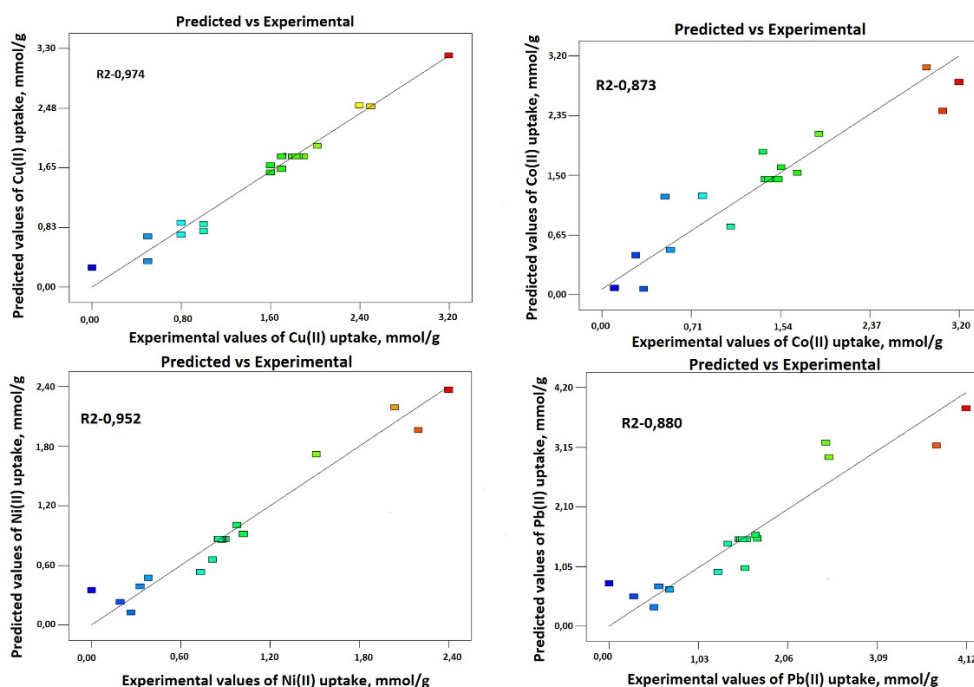
To determine the three variables (time, initial concentration of heavy metal and amount of sorbent) influence to the Cu (II), Co (II), Ni (II) and Pb (II) sorption efficiency, ANOVA variation analysis was applied. In the analysis model: A is the initial concentration of metal ions, B is the time, and C is the amount of sorbent. Results are shown in Table 10.

Table 10. The analysis of variance (ANOVA) for Cu(II), Co(II), Ni(II) and Pb(II) removal

Source	Cu(II) removal			Co(II) removal			Ni(II) removal			Pb(II) removal		
	Sum of Squares	F value	P value	Sum of Squares	F value	P value	Sum of Squares	F value	P value	Sum of Squares	F value	P value
Model	1,23	46,16	<0,0001	1,51	8,33	0,0013	0,84	23,44	<0,0001	2,01	8,82	0,0011
A	3,88	145,48	<0,0001	3,60	19,91	0,0012	2,67	74,53	<0,0001	7,24	31,84	0,0002
B	2,25	84,14	<0,0001	4,56	25,22	0,0005	0,38	10,65	0,0085	0,89	3,92	0,0760
C	3,20	119,85	<0,0001	3,23	17,86	0,0018	3,56	99,21	<0,0001	8,05	35,38	0,0001
AB	0,097	3,63	0,0861	0,60	3,32	0,0986	1,77	0,0049	0,8287	8,12	0,036	0,8538
AC	0,22	8,16	0,0171	0,011	0,058	0,8143	0,40	11,15	0,0075	1,19	5,23	0,0452
BC	0,097	3,63	0,0861	0,15	0,85	0,3778	3,48	0,097	0,7617	0,012	0,055	0,8200
A^2	0,077	2,89	0,1202	0,087	0,48	0,5032	0,022	0,61	0,4538	0,089	0,39	0,5456
B^2	1,32	49,53	<0,0001	0,61	3,35	0,0973	0,097	2,70	0,1312	0,22	0,95	0,3527
C^2	0,021	0,77	0,4009	0,58	3,19	0,1046	0,39	10,95	0,0079	0,30	1,32	0,2767
Residual	0,027	-	-	0,18	-	-	0,036	-	-	0,23	-	-
Lack of fit	0,049	1,96	0,01	0,36	1,37	0,0532	0,071	1,79	0,0483	0,45	1,43	0,0681
Pure error	4,46	-	-	2,11	-	-	3,01	-	-	1,07	-	-
Standard deviation	0,16			0,43			0,19			0,48		
PRESS	1,90			13,96			2,71			17,19		
R^2	0,9765			0,8823			0,9547			0,8881		
Adjected, R^2	0,9553			0,7763			0,9140			0,7874		
Predicted R^2	0,8326			0,9120			0,9083			0,8694		
Adeq Precision	25,385			10,49			16,72			10,38		

The *F* values of the design for Cu(II), Co(II) Ni(II) and Pb(II) removal were 46.16, 8.33, 23.44 and 8.82, respectively, and demonstrate that the models were statistically significant and there was only a 0.04% chance in Cu(II), 0.02% in Co(II), 0.05% in Ni(II) and 0.01% in Pb(II) removal that the model *F* values could incur due to noise. The lack of fit *F* value of Cu(II) removal is 1.96 and suggested that it was not significant relative to the pure error. A non-significant lack of fit was considered good and was desired for the model to fit. Also, for the Co(II) Ni(II) and Pb(II) removal, the lack of fit *F* values of 1.37, 1.79 and 1.43 suggested that they were not significant relative to the pure error for these metal ions removals and that the quadratic models were valid for the present study. Values of "p-value" less than 0.0500 means that model terms are significant. Values greater than 0.1000 indicate the model terms are not significant.

3.3.2. 3D response surface plots

Figure 49 demonstrates the response surface 3D plots for the effect of interaction between time, initial ion concentration and amount of sorbent for Cu(II), Co(II), Ni(II) and Pb(II) ion uptake, respectively. The effect of removal time was not particularly significant in improving the sorption capacity of nanocomposite, while the concentration of the heavy metal ions confirmed a stronger effect on the sorption uptake. It was mentioned in earlier section what max sorption of heavy metals on magnetic Prussian blue sorbent was reached in 60min (about 70-80 % after 5 min). The same behaviour was determined with all four heavy metals. Uptake increased when increasing initial concentration and/or time.
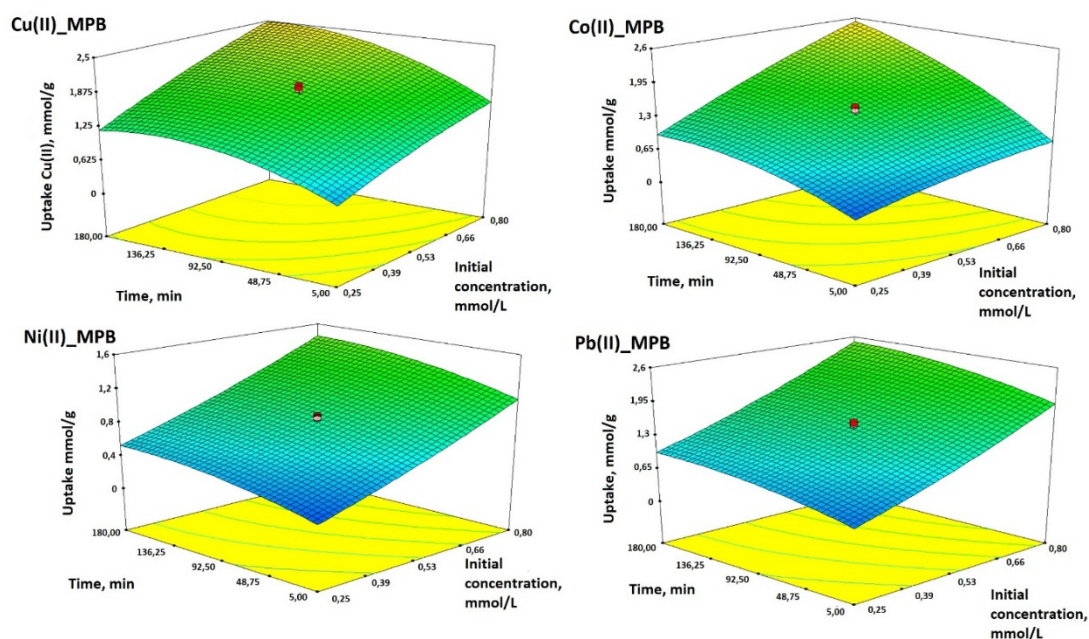
Fig. 49. Response surface 3D plots indicating the effect of interaction between heavy metal ion concentration and removal time for Cu(II), Co(II), Ni(II) and Pb(II)

As shown in Figure 50, the sorbent dosage is significant parameter for the uptake efficiency and clearly demonstrates that with increased sorbent dosage, uptake efficiency improves.
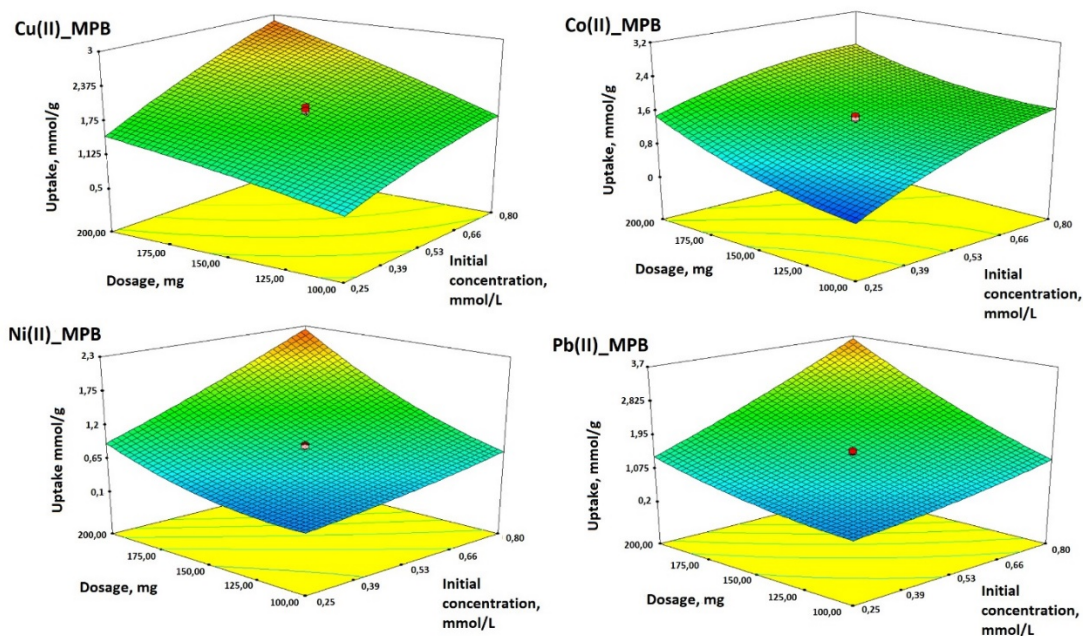
Fig. 50. Response surface 3D plots indicating the effect of interaction between heavy metal ion concentration and sorbent dosage for Cu(II), Co(II), Ni(II) and Pb(II)

This could be explained that when there are higher amounts of sorbent, there are more sites where heavy metal ion can sorb in the adsorbing surface too. The fast sorption is probably attributed to the exterior surface sorption by magnetite and Prussian blue nanoparticles.

Conclusions

1. Maximum sorption capacities of nanocomposites for studied elements estimated by Langmuir isotherm were as follows: Ni (II) adsorbed on magnetite (150 mg / g), Co (II) – magnetic graphene oxide (145 mg / g), Pb (II) - magnetic Prussian blue (778 mg / g) and Cu (II) - magnetic Prussian blue with graphene oxide (138 mg / g).

2. Fast sorption kinetics of studied elements have been found in experiments with magnetic nanosorbents. Maximum uptake is reached within 60min. Sorption corresponds to the pseudo-second-order reactions.

3. It has been found, that the optimal pH range for sorption experiments with magnetic nanosorbents is at pH 5 – 7.

4. Sorption of heavy metals with magnetite and magnetic graphene oxide corresponds to ion-exchange reactions. Two stages process: 1 - ion exchange, 2 - particle diffusion in the interior of the sorbent was found to be characteristic of element sorption to porous sorbents (MPB, MPBGO).

5. Synthesized magnetic nanosorbents can be used several times – MPB sorption efficiency reached 60%, while MPBGO - 50%, after third sorption cycle.

6. Magnetic nanosorbents can be used for heavy metals removal from natural water samples with complex chemical composition.

REFERENCES

1. Ahmaruzzaman, M. 2011. Industrial water as low-cost potential adsorbents for the treatment of wastewater laden with heavy metals. Advances in Colloid and Interface Science 166, 36-59.

2. Ainsworth, C.C., Pilon, J.L., Gassman, P.L., Van Der Sluys, W.G. 1994. Cobalt, cadmium, and lead sorption to hydrous iron oxide: Residence time effect. Soil Science Society of America Journal. 58, 1615-1623.

3. Akiko, K., Hisashi, T., Nobutsugu, M., Kazunori, Y., Tohru, K. 2012. Efficient Cesium Adsorbent Using Prussian Blue Nanoparticles Immobilized on Cotton Matrices. Chemistry letters 41, 1473-1474.

4. Alcala, M. D., Real, C. 2006. Synthesis based on the wet impregnation method and characterization of iron and iron oxide-silica nanocomposites. Solid State Ionics 177, 955-960.

5. Anbiaa, M., Kargosha, K., Khoshbooe, S. 2015. Heavy metal ions removal from aqueous media bymodified magnetic mesoporous silica MCM-48. Chemical engineering research and design 93, 779–788.

6. Arshady, R. 2001. Radiolabeled and Magnetic Particles in Medicine and Biology. Critrus Books London U.K. 3.

7. Arun, T., Joseyphus, R.J. 2014. Prussian blue modified Fe_3O_4 nanoparticles for Cs detoxification. Journal of Materials Science 49, 7014–7022.

8. Arun, T., Prakash, K., Kuppusamy, R., Joseyphus, R.J. 2013. Magnetic properties of Prussian blue modified Fe_3O_4 nanocubes. Journal of Physics and Chemistry of Solids. 74, 1761–1768.

9. Azari, A., Kakavandi, B., Kalantary, R.R., Ahmadi, E. 2015. Rapid and efficient magnetically removal of heavy metals by magnetite-activated carbon composite: a statistical design approach Journal of Porous Materials 22, 1083–1096.

10. Baba, Y., Ohe, K., Kawasaki, Y., Kolev, S.D. 2006. Adsorption of mercury(II) from hydrochloric acid solutions on glycidylmethacrylate–divinylbenzene microspheres containing amino groups. Reactive and Functional Polymers 66, 1158-1164.

11. Bacri, J.-C., Perzynski, R., Salin, D. J. 1990. Ionic ferrofluids: A crossing of chemistry and physics. Journal of Magnetism and Magnetic Materials 85, 27-32

12. Bai, H., Li, C., Wang, X., Sh,i G. 2010. A pH-sensitive graphene oxide composite hydrogel. Chemical Communications 46, 2376–2378.

13. Bakhshayesh, S., Dehghani, H. 2013. Synthesis of magnetite-porphyrin nanocomposite and its application as a novel magnetic adsorbent for removing heavy cations. Materials research Bulletin. 48, 2614-2624.

14. Barquist, K, Larsen, SC. 2010. Chromate adsorption on bifunctional, magnetic zeolite composites. Microporous Mesoporous Mater 130, 197-202.

15. Bee, A., Massart, R., Neveu, S. J. 1995. Synthesis of very fine maghemite particles. Journal of Magnetism and Magnetic Materials. 149, 6-9.

16. Belessi, V., Zboril, R., Tucek, J., Mashlan, M., Tzitzios, V., Petridis, D. 2008. Ferrofluids from Magnetic−Chitosan Hybrids. Chemistry of Materials. 20, 3298–3305.

17. Bhatt, P., Yusuf, S.M., Bhatt, R., Schütz, G. 2012. Magnetic properties of nanoparticles of Prussian blue-based molecular magnets $M_3[Cr(CN)_6]_2 \cdot zH_2O$ (M = Fe, Co, and Ni). Applied Physics A: Materials Science and Processing. 109, 459 – 469.

18. Bhattarai, S. R., Bahadur, K. C., Arya,l S., Khill, M. S., Kim, H. Y. 2007. N-Acylated chitosan stabilized iron oxide nanoparticles as a novel nano-matrix and ceramic modification. Carbohydrate polymers. 63, 467-477.

19. Bruce, I. J., Taylor, J., Todd, M., Davies, M. J., Borioni, E., Sangregorio, C., Sen, T. J. 2004. Synthesis, characterisation and application of silica-magnetite nanocomposites. The Journal of Magnetism and Magnetic Materials. 284, 145-160.

20. Calvin, S., Carpenter, E. E., Harris, V. G. 2003. Characterization of passivated iron nanoparticles by x-ray absorption spectroscopy. Physical Review B. covering condensed matter and materials physics 68, 3411-3415.

21. Cao, Y., Li, X. 2014. Adsorption of graphene for the removal of inorganic pollutants in water purification: A review. Adsorption 20, 713-727.

22. Chang, L., Chang, S., Chen, W., Han, W., Li, Z., Zhang, Z., Dai, Y., Chen, D. 2016. Facile one-pot synthesis of magnetic Prussian blue core/shell nanoparticles for radioactive cesium removal. RSC Advances. 6, 96223-96228.

23. Chem, J., Yuan, T.J. 2015. Effects of citrate on preparation and properties of nano-Fe_3O_4. Journal of Materials Engineering and Performance. 43, 85-89.

24. Chen, C. 1986. Magnetism and metallurgy of soft magneticmaterials. New York: Dover Publications, Inc.

25. Chen, M., Yamamuro, S., Farrell, D., Majetich, S. A. J. 2003. Gold-coated iron nanoparticles for biomedical applications. Journal of Applied Physics. 93, 7551-7556.

26. Cheong, J.H., Lee, K.J. 1996. Removal of Co^{2+} Ions from Aqueous Solution by Ferrite Process. Separation Science and Technology. 31, 1137-1143.

27. Cheung, W.H., YSzeto, Y.S., McKay, G. 2007. Intraparticle diffusion processes during acid dye adsorption onto chitosan. Bioresource Technology. 98, 2897–2904.

28. Cornell, R.M., Schwertmann, U. 2000. Iron oxides in the Laboratory. Wiley-VNH, Weinheim.

29. Cornell, R.M., Schwertmann, U. 2003. Iron oxides. Wiley-VNH, Weinheim.

30. Crini, G. 2006. Non-converntional low-cost adsorbents for dye removal: a review. Bioresource Technology. 97, 1061-1085.

31. Donia, A.M., Atia, A.A., Abouzayed, F.I. 2012. Preparation and characterization of nano-magnetic cellulose with fast kinetic properties towards the adsorption of some metal ions. Chemical Engineering Journal 191, 22-30.

32. Ducoroy, L., Bacquet, M., Martel, B., Morcellet, M. 2008. Removal of heavy metals from aqueous media by cation exchange nonwoven PET coated with _-cyclodextrin-polycarboxylic moieties. Reactive and Functional Polymers. 68, 594–600.

33. Dung, D.T.K., Hai, T.H., Phuc, L.H., Long, B.D., Vinh, L.K., Truc, P.N. 2009. Preparation and characterization of magnetic nanoparticles with chitosan coating. Journal of Physics: Conference Series 187.

34. E.Guibal, 2004. Metal ion interactions with chitosan—A review. Separation and Purification Technology. 38, 43-74.

35. Elliott SR. 1998. The physics and chemistry of solids. New York: Wiley.

36. El-Reasha, Y.G. Abou. 2016. Magnetic chitosan modified with cysteine-glutaraldehyde as adsorbent for removal of heavy metals from water. Journal of enviromental Chemical Engineering 4, 2835-2847.

37. Fan, C., Li, K., Li, J.,Ying, D., Wang, Y., Jia, J. 2017. Comparative and competitive adsorption of Pb(II) and Cu(II) using tetraethylenepentamine modified chitosan/$CoFe_2O_4$ particles. Journal of Hazardous Materials. 326, 211-220.

38. Fan, H.L., Li, L., Zhou, S.F., Liu, Y.Z. 2016. Continuous preparation of Fe_3O_4 nanoparticles combined with surface modification by L-cysteine and their application in heavy metal adsorption. Ceramics International 42, 4228-4237.

39. Feng, L., Cao, M., Ma, X., Zhu, Y. Hu, C. 2012. Superparamagnetic high-surface-area Fe_3O_4 nanoparticles as adsorbents for arsenic removal. Journal of Hazardous Materials. 217, 439–446.

40. Foo, K.Y., Hameed, B.J. 2010. Insights into the modeling of adsorption isotherm systems. The Chemical Engineering Journal. 156, 2–10.

41. Fratila, R.M., Mitchell, S.G., del Pino, P., Grazu, V., de la Fuente, J.M. 2014. Strategies for the biofunctionalization of gold and iron oxide nanoparticles. Langmuir 30, 15057-15071.

42. Fu, F., Wang, Q. 2011. Removal of heavy metal ions from wastewaters: A review. Journal of Environmental Management. 92, 407-418.

43. Fu, L., Dravid, V.P., Johnson, D.L., 2001. Self-assembled (SA) bilayer molecular coating on magnetic nanoparticles. Applied Surface Science. 181, 173–178.

44. Gao, W., Alemany, L. B., Ci, L. J., Ajayan, P. M. 2009. New insights into the structure and reduction of graphite oxide. Nature Chemistry. 1, 403-408.

45. Ge, F, Li, Meng-Meng, Ye, H., Zhao, Bao-Xiang. 2011. Effective removal of heavy metal ions Cd^{2+}, Zn^{2+}, Pb^{2+}, Cu^{2+} from aqueous solution by polymermodified magnetic nanoparticles. Journal of Hazardous Materials. 211, 366–372.

46. Girginova, P.I., Daniel-da-Silva, A.L., Lopes, C.B., Figueira, P., Otero, M., Amara, V.S., Pereira, E., Trindade, T. 2010. Silica coated magnetite nanoparticles for magnetic removal of Hg^{2+} from water. Journal of Colloid and Interface Science. 345, 234–240.

47. Gupta, A.K., Curtis, A.S.G. 2004. Lactoferrin and ceruloplasmin derivatized superparamagnetic iron oxide nanoparticles for targeting cell surface receptors. Biomaterials. 25, 3029–3040.

48. Gupta, A.K., Gupta, M. 2005. Synthesis and surface engineering of iron oxide nanoparticles for biomedical applications. Biomaterials 26, 3995–4021.

49. Gushikem, Y., Rosatto, S. S. 2001. Metal Oxide Thin Films Grafted on Silica Gel Surfaces: Recent Advances on the Analytical Application of these Materials. Journal of the Brazilian Chemical Society. 12, 693-694.

50. Hakami, O., Zhang, Y., Banks, C. J. 2012. Thiol functionalised mesoporous silica-coated magnetite nanoparticles for high efficiency removal and recovery of Hg from water. Water Research. 46, 3913–3922.

51. Harikishore, D., Reddy, K., Lee, S.M. 2013. Application of magnetic chitosan composites for the removal of toxic metal and dyes from aqueous solutions. Advances in Colloid and Interface Science 201, 68–93.

52. Haynes, W.M. 2014. CRC Handbook of Chemistry and Physics, CRC press.

53. HELCOM. 2007a. 2007. HELCOM Baltic Sea Action Plan. HELCOM Ministerial meeting. Krakow, Poland, 15 November, 101.

54. HELCOM. 2010. Hazardous substances in the Baltic Sea – An integrated thematic assessment of hazardous substances in the Baltic Sea. Baltic Sea Environment Proceedings, 120B, 116.

55. Herren, P., Fischer, P., Ludi, A., Halg, W. 1980. Neutron diffraction study of Prussian Blue, $Fe_4[Fe(CN)_6]_3$ xH_2O. Location of water molecules and long-range magnetic order. Inorganic Chemistry. 19, 956-959.

56. Hong, R.Y., Feng, B., Liu, G., Wang, S., Li, H.Z., Ding, J.M., Zheng, Y., Wei, D.G. 2009. Preparation and characterization of Fe_3O_4/polystyrene composite particles via inverse emulsion polymerizatio. Journal of Alloys and Compounds. 476, 612–618.

57. Hong, S., Rhee, I. 2007. Relaxivity of hydrogen protons of water molecules in the aqueous solutions of dextran and chitosan coated ferrite nanoparticles. International Journal of Magnetic Resonance Imaging. 1, 15–20.

58. Hu, M., Belik, A.A., Imura, M., Mibu, K., Tsujimoto, Y., Yamauchi, Y. 2012. Synthesis of superparamagnetic nano porous iron oxide particles with hollow interiors by using Prussian blue coordination polymers. Chemistry of Materials. 24, 2698–2707.

59. Huang, Y.H., Hsueh, C.L., Cheng, H.P., Su, L.C., Chen, C.Y. 2007. Thermodynamics and kinetics of adsorption of Cu(II) onto waste iron oxide Journal of Hazardous Materials 144, 406-411

60. Hui, K.S., Chao, C.Y.H., Kot, S.C. 2005. Removal of mixed heavy metal ions in wastewater by zeolite 4A and residual products from recycled coal fly ash. Journal of Hazardous Materials. 127, 89–101.

61. Hur, J., Shin, J., Yoo, J., Seo, Y.S. 2015. Competitive Adsorption of Metals onto Magnetic Graphene Oxide: Comparison with Other Carbonaceous Adsorbents. The Scientific World Journal 11-18.

62. Ishizaki, M., Akiba, A., Ohtani, A., Hoshi, Y., Ono, K. 2013. Proton-exchange mechanism of specific Cs+ adsorption via lattice defect sites of Prussian blue filled with coordination and crystallization water molecules Dalton Transaction 43, 16049-16055.

63. ISO Guide to the Expression of Uncertainty in Measurement. ISO 1993, ISBN 92-67-10188-9.

64. Jang, S.C., Haldorai, Y., Lee, G.W., Hwang, S.K., Han, Y.K., Roh, C., Huh, Y.S. 2015. Porous three-dimensional graphene foam/Prussian blue composite for efficient removal of radioactive ^{137}Cs. Scienfitic reports.

65. Jia, Z., Yujun, W., Yangcheng, L., Jingyu, M., Guangsheng, L. 2006. In situ preparation of magnetic chitosan/Fe_3O_4 composite nanoparticles in tiny pools of water-in-oil microemulsion. Reactive and Functional Polymers 66, 1552-1558.

66. Jiang, W., Yang, H.-C., Yang, S. Y., Horng, H. E., Hung, J. C., Chen, Y. C., Hong, C.-Y. J. 2004. Preparation and properties of superparamagnetic nanoparticles with narrow size distribution and biocompatible. Journal of Magnetism and Magnetic Materials. 283, 210-214.

67. Jolivet, J. P. 2000. Metal Oxide Chemistry and Synthesis. From Solution to Solid State; Wiley: Chichester, U.K.

68. Jolivet, J. P., Belleville, P., Tronc, E., Livage, J. 1992. Influence of Fe(II) on the formation of the spinel iron oxide in alkaline media. Clays and Clay Minerals. 40, 531-539.

69. Jolivet, J. P., Chaeneac, C. 2002. Synthesis of iron oxide-based magnetic nanomaterials and composites. Comptes Rendus Chimie. 5, 659-664.

70. Jolivet, J. P., Froidefond, C., Pottier, A., Chaenea,c C., Cassaignon, S., Tronc, E., Euzen, P. J. 2004. Size tailoring of oxide nanoparticles by precipitation in aqueous medium. A semi-quantitative modelling. Journal of Materials Chemistry. 14, 3281-3288.

71. Jusoh, A., Shiung, L.S., Ali, N., Noor, M.J.M.M. 2007. A simulation study of the removal efficiency of granular activated carbon on cadmium and lead. Desalination 206, 9-16.

72. Kabbashi, N.A., Atieh, M.A., Al-Mamun, A., Mirghami, M.E.S., Alam, M.D.Z., Yahya, N. 2009. Kinetic adsorption of application of carbon nanotubes for Pb(II) removal from aqueous solution. Journal of Enviromental Sciences. 21, 539-544.

73. Kalantari, K., Ahmad, M.B., Masoumi, H.R.F., Shameli, K., Basri, M., Khandanlou, R. 2015. Rapid and high capacity adsorption of heavy metals by Fe_3O_4/montmorillonite nanocomposite using response surface methodology: Preparation, characterization, optimization, equilibrium isotherms, and adsorption kinetics study. Journal of the Taiwan Institute of Chemical Engineers 49, 192-198.

74. Kalantari, K., Ahmad, M.B., Masoumi, R.H.F., Shameli, K., Basri, M., Khandanlou, R. 2014. Rapid Adsorption of Heavy Metals by Fe_3O_4/Talc Nanocomposite and Optimization Study Using Response Surface Methodology. International Journal of Molecular Sciences. 15, 12913-12927.

75. Kandah, M.I., Meunier, J.L. 2007. Removal of nickel ions from water by multi-walled carbon nanotubes. Journal of Hazardous Materials. 146, 283-288.

76. Kang, K.C., Kim, S.S., Choi, J.W., Kwon, S.H. 2008. Sorption of Cu^{2+} and Cd^{2+} onto acid- and base-pretreated granular activated carbon and activated carbon fiber samples. Journal of Industrial and Engineering Chemistry. 14, 131-135.

77. Karami, H. 2013. Heavy metal removal from water by magnetite nanorods. Chemical Engineering Journal. 209-216.

78. Kekkonen, V., Lafreniere, N., Ebara, M., Saito, A., Sawa, Y., R. Narain, R. 2009. Synthesis and characterization of biocompatible magnetic glyconanoparticles, Journal of Magnetism and Magnetic Materials. 321, 1393–1396.

79. Kennish, M. J. 1997. Practical handbook of estuarine and marine pollution. CRC Press marine science series, United States of America. 524.

80. Khani, R., Sobhani, S., Beyki, M.H. 2016. Highly selective and efficient removal of lead with magnetic nano-adsorbent: Multivariate optimization, isotherm and thermodynamic studies. Journal of Colloid and Interface Science. 466, 198-205.

81. Kim, D.K., Zhang, Y., Voit, W., Rao, K.V., Muhammed, M. 2001. Synthesis and characterization of surfactant-coated superparamagnetic monodispersed iron oxide nanoparticles. Journal of Magnetism and Magnetic Materials. 225, 30–36.

82. Kim, E. H., Ah, Y., Lee, H. S. J. 2006. Antibiofouling polymer-coated superparamagnetic iron oxide nanoparticles as potential magnetic resonance contrast agents for in vivo cancer. Journal of American Chemical society. 128, 7383-7389.

83. Klotz, S., Steinle-Neumann, G., Strassle, T., Philippe, J., Hansen, T., Wenzel, M.J. 2008. Magnetism and Verwey transition in Fe_3O_4 under preasure. Physical Review B. 77.

84. Kong, L., Lu, C., Bian, X., Zhang, W., Wang, C. 2011. Constructing Carbon-Coated Fe_3O_4 Microspheres as Antiacid and Magnetic Support for Palladium Nanoparticles for Catalytic Applications. Applied Materials & Interfaces 3, 35-42.

85. Krishna, R.H., Swamy, A.V.V.S. 2012. Physico-Chemical Key Parameters, Langmuir and Freundlich isotherm and Lagergren Rate Constant Studies on the removal of divalent nickel from the aqueous solutions onto powder of calcined brick. International Journal of Engineering Research and Development. 4 (1), 29-38.

86. Kumar, K Y, Muralidhara, H B, Arthoba, Nayaka Y, Balasubramanyam, J., Hanumanthappa, H. 2013. Hierarchically assembled mesoporous ZnO nanorods for the removal of lead and cadmium by using differential pulse anodic stripping voltammetric method. Powder Technology. 239, 208–216.

87. Kuo, C.Y., Lin, H.Y. 2009. Adsorption of aqueous cadmium (II) onto modified multiwalled carbon nanotubes following microwave/chemical treatment. Desalination 249, 792-796.

88. Lakouraj, M.M., Mojerlou, F., Zare, E.N. 2014. Nanogel and superparamagnetic nanocomposite based on sodium alginate for sorption of heavy metal ions. Carbohydrate Polymers 106, 34-41.

89. Lanf, A.R. 2009. Dyes and pigments: new research. Nova Science Publishers, Inc, New York.

90. Lasheen, M.R., El-Sherif, I.Y., Sabry, D.Y., El-Wakeel, S.T., El-Shahat, M.F. 2015. Adsorption of heavy metals from aqueous solution by magnetite nanoparticles and

magnetite-kaolinite nanocomposite: equilibrium, isotherm and kinetic study. Desalination and Water Treatment. 1–10.

91. Laurent, S., Forge, D., Port, M., Roch, A., Robic, C., Elst, L.V.,Robert, N. Muller, R.N. 2008. Magnetic Iron Oxide Nanoparticles: Synthesis, Stabilization, Vectorization, Physicochemical Characterizations, and Biological Applications. Chemical Reviews. 108, 2064–2110.

92. Lee, S.J., Jeong, J.R., Shin, S.C., Kim, J.C., Kim, J.D. 2004. Synthesis and characterization of superparamagnetic maghemite nanoparticles prepared by co-precipitation technique. Journal of Magnetism and Magnetic Materials 282, 147-150.

93. Lee, S.M., Laldawngliana, C., Tiwari, D. 2012. Iron oxide nano-particles-immobilized-sand material in the treatment of Cu(II), Cd(II) and Pb(II) contaminated waste waters. Chemical Engineering Journal 195-196, 103-111.

94. Lefebure, S., Dubois, E., Cabuil, V., Neveu, S., Massart, R. 1998. Monodisperse magnetic nanoparticles: preparation and dispersion in several media. Journal of Materials Research and Technology. 13, 2975-2984.

95. Leivuori, M. 2000. Distribution and accumulation of metals in sediments of the northern Baltic Sea. Finnish Institute of Marine Research, PhD thesis, Contributions. 9–43.

96. Lesnikovich, A. E., Shunkevich, T. M., Naumenko, V. N., Vorobyova, S. A., Baykov, M. W. J. 1990. Dispersity of magnetite in magnetic liquids and the interaction with a surfactant. Journal of Magnetism and Magnetic Materials. 17, 7907-7916.

97. Li, D., Zhang, B., Xuan, F. 2015. The sequestration of Sr(II) and Cs(I) from aqueous solutions bymagnetic graphene oxides. Journal of Molecular Liquids 209, 508-514.

98. Li, F., X. Jiang, X., Zhao, J., Zhang, S. 2015. Graphene oxide: a promising nanomaterial for energy and environmental applications. Nano Energy 16, 488-515.

99. Li, J., Zeng, X., Rem, T., Heide, E. 2014. The Preparation of Graphene Oxide and Its Derivatives and Their Application in Bio-Tribological Systems. Lubricants 2, 137-161.

100. Li, J., Zhang, S., Chen, C., Zhao, G., Yang, X., Li, J., Wang, X. 2012. Removal of Cu(II) and Fulvic Acid by Graphene Oxide Nanosheets Decorated with Fe_3O_4 Nanoparticles. Applied Materials & Interfaces, 4, 4991–5000.

101. Li, Q., Wang, Z., Fang, D.M., Qu, H.Y., Zhu, Y., Zou, H.J., Chen, Y.R., D,u Y.P., Hu, H.L. 2014. Preparation, characterization, and highly effective mercury adsorption of L-cysteine-functionalized mesoporous silica. New Journal of Chemistry.38, 248–254.

102. Li, Y.H., Liu, F.Q., Xia, B., Du, Q.J., Zhang, P., Wang, D.C., Wang, Z.H., Xia, Y.Z. 2010. Removal of copper from aqueous solution by carbon nanotube/calcium alginate composites. Journal of Hazardous Materials. 177, 876-880.

103. Lin, J., Zhou, W., Kumbhar, A., Fang, J., Carpenter, E. E., O'Connor, C. J. J. 2001. Gold-Coated Iron (Fe@Au) Nanoparticles: Synthesis, Characterization, and Magnetic Field-Induced Self-Assembly. Journal of Solid State Chemistry. 159, 26-31.

104. Liu, J F., Zhao, Z S., Jiang, G B. 2008. Coating Fe_3O_4 Magnetic nanoparticles with humic acid for high efficient removal of heavy metals in water. Environmental Science & Technology. 42, 6949–6954.

105. Liu, X., Hu, Q., Fang, Z., Zhang, X., Zhang, B. 2009. Magnetic chitosan nanocomposites: a useful recyclable tool for heavy metal ion removal. Langmuir 25, 3–8.

106. Liu, Y., Chen, L., Li, Y., Wang, P., Dong, Y. 2016. Synthesis of magnetic polyaniline/graphene oxide composites and their application in the efficient removal of Cu(II) from aqueous solutions. Journal of environmental Chemical engineering. 4, 825-834.

107. Lo-Irene, H. M. C., Chen, G. H. 2005. Fast removal and recovery of Cr(VI) using surface-modified jacobsite nanoparticles. Langmuir. 21, 11173–11179.

108. Lu, A.H., Salabas, E.L., Shuth, F. 2007. Magnetic nanoparticles: synthesis protection, functionalization, and application. Angewandte Chemie. 46, 1222-1244.

109. Lujanienė, G., Šemčuk, S., Leščinskytė, A., Kulakauskaitė, I., Mažeika, K., Valiulis, D. Pakštas, V., Skapas, M., Tumėnas, S. 2017. Magnetic graphene oxide based nano-composites for removal of radionuclides and metals from contaminated solutions. Journal of Environmental Radioactivity 166, 166-174.

110. Lyon, J. L., Fleming, D. A., Stone, B., Schiffer, P., Willians, M. E. 2004. Synthesis of Fe oxide core/au shell nanoparticles by iterative hydroxylamine seeding. Nano Letters. 4, 719-723.

111. Ma, D., Guan, J., Normandin, F., Denommee, S., Enright, G., Veres, T., Simard, B. 2006. Multifunctional nano-architecture for biomedical applications. Chemistry of Materials. 18, 1920-1927.

112. Madadrang, C.J., Kim, H.Y., Gao, G., Wang, N., Hu, J., Fenf, H., Gorring, M., Kasner, M.L., Hou, S. 2012. Adsorption behavior of EDTA-graphene oxide for Pb(II) removal. ACS Applied Materials & Interfaces 4, 1186-1193.

113. Maghsoodi, V., Razavi, J., Yaghmaei, S. 2009. Production of chitosan by submerged fermentation from Aspergillus niger. Scientia Iranica, 16, 145–148.

114. Mahmeda, N., Heczko, O., Lancok, A., Hannula, S.P. 2014. The magnetic and oxidation behavior of bare and silica-coated iron oxide nanoparticles synthesized by reverse co-precipitation of ferrous ion (Fe^{2+}) in ambient atmosphere. Journal of Magnetism and Magnetic Materials. 353, 15-25.

115. Majewski, P., Thierry, B. 2007. Functionalized magnetite nanoparticles—synthesis, properties, and bio-applications. Critical Reviews in Solid State and Material Sciences 32, 203-215.

116. Martinez-Mera, I., Espinosa-Pesqueira, M.E., Perez-Hernandez, R., Arenas-Alatorre. 2007. Synthesis of magnetite (Fe_3O_4) nanoparticles without surfactants at room temperature. Journal of Material Letters. 61, 4447-4451.

117. Massart, R., Cabuil V. 1987. Magnetic colloidal properties of ionic ferrofluids. Journal de Chimie Physique. 84.

118. Mauter, M.S. 2008. Enviromental applications of carbon-based nanomaterials. Environmental Science & Technology. 42, 5843-5859.

119. Mayo, J. T., Yavuz, C., Yean, S., Cong, L., Shipley, H., Yu, W., Falkner, J., Kan, A., Tomson, M., Colvin, V. L. 2007. The effect of nanocrystalline magnetite size on arsenic removal. Science and Technology of Advanced Materials. 8, 71–75.

120. Mi, X., Huang, G., Xie, W., Wang, W., Liu, Y., Gao, J. 2012. Preparation of graphene oxide aerogel and its adsorption for Cu^{2+} ions. Carbon 50, 4856-4864.

121. Morales, M. P., Veintemillas-Verdaguer, S., Montero, M., Serna, C. J., Roig, A., Casas, L., Martınez, B., Sadiumenge, F. 1999. Surface and Internal Spin Canting in γ-Fe_2O_3 Nanoparticles. Chemistry of Materials. 11, 3058-3064.

122. Mulvaney, P., Liz-Marzan, L. M., Giersig, M., Ung, T. 2000. Silica encapsulation of quantum dots and metal clusters. Journal of Materials Chemistry. 10, 1259-1270.

123. Muzzarelli, R.A.A. 2011. Potential of chitin/chitosan-bearing materials for uranium recovery: An interdisciplinary review. Carbohydrate Polymers. 84, 54-63.

124. Namasivayam, C., Ranganathan, K. 1994. Recycling of waste Fe(III)/Cr(III) hydroxide for the removal of nickel from waste water adsorption and equilibrium studies. Waste Management. 14, 709-716.

125. Namiki, Y., Namiki, T., Ishii, Y., Koido, S., Nagase, Y., Tsubota, A., Tada, N., Kitamot,o Y. 2012. Inorganic-Organic Magnetic Nanocomposites for use in Preventive Medicine: A Rapid and Reliable Elimination System for Cesium. Pharmaceutical Research 29, 1404–1418.

126. Naseem, R., Tahir, S.S. 2001. Removal of Pb(II) from aqueous solution by using bentonite as an adsorbent. Water Research. 35, 3982-3986.

127. Novoselov, K.S., Geim, A.K., Morozov, S.V., Jiang, D., Zhang, Y., Dubonos, S.V., Grigorieva, I.V., Firsov, A.A. 2004. Electric Field Effect in Atomically Thin Carbon Films. Science 306, 666-669.

128. Ofomaja, A.E. 2010. Intraparticle diffusion process for lead(II) biosorption onto mansonia wood sawdust. Bioresource Technology. 101, 5868–5876.

129. Okassa, L. N., Marchais, H., Douziech-Eyrolles, L., Cohen-Jonathan, S., Souce, M., Dubois, P., Chourpa, I. 2005. Development and characterization of sub-micron poly (D, L-lactide-co-glycolide) particles loaded with magnetite/maghemite nanoparticles. The International Journal of Pharmaceutics. 302, 187-196.

130. Oliveira, LCA, Petkowicz, Di, Smaniotto, A, Pergher, SBC. 2004. Magnetic zeolites: a new adsorbent for the removal of metallic contaminants from water. Water Research. 38, 3699-704.

131. Ortega, E.P., Ramos, R.L., Cano, J.V.F. 2013. Binary adsorption of heavy metals from aqueous solutions onto natural clays. The Journal of Chemical & Engineering Data. 225, 535-546.

132. Ozmen, M, Can, K, Arslan, G, Tor, A, Cengeloglu, Y., Ersoz, M. 2010. Adsorption of Cu(II) from aqueous solution by using modified Fe3O4 magnetic nanoparticles. Desalination. 254, 162–169.

133. Parker, P., 1980. Encyclopedia of Environmental Sciences (2nd edn), McGraw Hill, New York, 354-358.

134. Pavan, F.A., Mazzocato, A.C., Jacques, R.A., Dias Silvio, L.P. 2008. Ponkan peel: a potential biosorbent for removal of Pb(II)ions from aqueous solution. Biochemical Engineering. 40, 357–362.

135. Peng, W., L,i H., Liu, Y., Song, S. 2016. Comparison of Pb(II) adsorption onto graphene oxide prepared from natural graphites: Diagramming the Pb(II) adsorption sites. Applied Surface Science. 364, 620-627.

136. Pillay, K., Cukrowska, E.M., Coville, N.J., 2009. Multi-walled carbon nanotubes as adsorbents for the removal of parts per billion levels of hexavalent chromium from aqueous solution. The Journal of Hazardous Materials. 166, 1067-1075.

137. Pradhan, P., Giri, J., Banerjee, R., Bellare, J., Bahadur, D. 2007. Cellular interactions of lauric acid and dextran-coated magnetite nanoparticles. The Journal of Magnetism and Magnetic Materials. 311, 282–287.

138. Qin, F., Wen, B., Shan, X. Q., Xie, Y. N., Liu, T., Zhang, S. Z., et al. 2006. Mechanisms of competitive adsorption of Pb, Cu, and Cd on peat. Environmental Pollution. 144, 669–680.

139. Qiu, J., Yang, R., Li, M., Jianf, N. 2008. Preparation and characterization of porous ultrafine Fe_2O_3 particles. Materials Research Bulletin. 40, 1968–1975.

140. Rao, M.M., Reddy, D.H.K.K., Venkateswarlu, P., Seshaiah, K. 2009. Removal of mercury from aqueous solutions using activated carbon prepared from agricultural by-product/waste. J. environ Manage. 90, 634-43

141. Ren, X., LI, J., Tan, X., Shi, W., Chen, C., Shao, D., Wen, T., Wang, L., Zhao, G., Sheng, G., Wang, X. 2014. Impact of Al_2O_3 on the aggregation and deposition of graphene oxide. Environmental Science & Technology. 48, 5493-5500.

142. Roth, H.C., Schwaminger, S.P., Schindler, M., Wagner, F.E., Berensmeier, S. 2015. Influencing factors in the CO-precipitation process of superparamagnetic iron oxide nanoparticles: A model-based study. Journal of Magnetism and Magnetic Materials. 377, 81-89.

143. Ruankaew, N., Yoshida, N., Watanabe, Y., Nakano, H., Phongphanphanee, S. 2017. Size-dependent adsorption sites in a Prussian blue nanoparticle: A 3D-RISM study. Chemical Physics Letters 684, 117–125.

144. Saha, B., Das, S., Saikia, J., Das, G. 2011. Preferential and Enhanced Adsorption of Different Dyes on Iron Oxide Nanoparticles: A Comparative Study. Journal of Physical Chemistry C. 115, 8024-8033.

145. Sarkar, M., Acharya, P.K., Bhattacharya, B. J. 2003. Modeling the adsorption kinetics of some priority organic pollutants in water from diffusion and activation energy parameters. Journal of Colloid and Interface Science. 266, 28–32.

146. Schneemeyer, L.F., Spengler, S.E., Murphy, D.W. 1985. Ion selectivity in nickel hexacyanoferrate films on electrode surfaces. Inorganic Chemistry. 24, 3044– 3046.

147. Seenivasan, R., Chang, W.J., Gunasekaran, J.S. 2015. Highly sensitive detection and removal of lead ions in water using cysteine-functionalized graphene oxide/polypyrrole nanocomposite film electrode, ACS Applied Material and Interfaces. 7, 15935–15943.

148. Sharma, V.K., Mitra, S., Thakur, N., Yusuf, S.M., Juranyi, F., Mukhopadhyay, R. 2014. Dynamics of water in prussian blue analogues: Neutron scattering study. Journal of applied physics 116, 15-23.

149. Shen, Y.F., Tang, J., Nie, Z.H., Wang, Y.D., Ren, Y., Zuo, L. 2009. Preparation and application of magnetic Fe3O4 nanoparticles for wastewater purification. Separation and Purification Technology. 68, 312–319.

150. Showalter, A.R.,1, Duster, T.A., Szymanowski, J.E., Na, C., Fein, J., Bunker, B. 2016. Sorption mechanisms of metals to graphene oxide. Journal of Physics: Conference Series 712.

151. Si, Y., Samulski, E.T. 2008. Synthesis of water soluble graphene. Nano Letters. 8, 1679–1682.

152. Singh, S, Barick, K C., Bahadur, D. 2011. Surface engineered magnetic nanoparticles for removal of toxic metal ions and bacterial pathogens. The Journal of Hazardous Materials. 192, 1539–1547.

153. Singh, S., Barick, K. C., Bahadu,r D. 2013. Functional Oxide Nanomaterials and Nanocomposites for the Removal of Heavy Metals and Dyes. Nanomaterials and Nanotechnology, 1-15.

154. Sipos, P., Berkesi, O., Tombacz, E., St. Pierre, T. G., Webb, J. J. 2003. Formation of spherical iron(III) oxyhydroxide nanoparticles sterically stabilized by chitosan in aqueous solutions. The Journal of Inorganic Biochemistry Inorg. 95, 55-63.

155. Sitko, R., Turek, E., Zawisza, B., Malicka, E., Talik, E., Heimann, J., Gagor, A., Feista, B., Wrzalik, R. 2013. Adsorption of divalent metal ions from aqueous solutions using graphene oxide. Dalton Transactions. 42, 5682-5691.

156. Soares, P.I.P., Alves, A.M.R., Pereira, L.C.J. 2014. Effects of surfactants on the magnetic properties of iron oxide colloids. Journal of Colloid and Interface Science. 419, 46–51.

157. Sun, J., Liang, Q., Han, Q., Zhang, X., Ding, M. 2015. One-step synthesis of magnetic graphene oxide nanocomposite and its application in magnetic solid phase extraction of heavy metal ions from biological samples. Talanta 132, 557-563.

158. Sun, Y., Duan, L., Guo, Z., DuanMu, Y., Ma, M., Xu, L., Zhang, Y., Gu, N. J. 2005. An improved way to prepare superparamagnetic magnetite-.silica core−shell nanoparticles for possible biological application. The Journal of Magnetism and Magnetic Materials. 285, 65-70.

159. Swedish EPA. 2000. Coasts and Seas. Environmental quality criteria. Swedish Environmental Protection Agency, Uppsala. 138

160. Takahiro, S., Shunitz, T. 2012. Magnetic Separation of Cesium Ion Using Prussian Blue Modified Magnetite. Chemistry Letters. 41, 32-34.

161. Tan, P., Sun, J., Hu, Y., Fang, Z., Bi, Q., Chen, Y., Cheng, J. 2015. Adsorption of Cu^{2+}, Cd^{2+} and Ni^{2+} from aqueous single metal solutions on graphene oxide membranes. Journal of Hazardous Materials. 297, 251-260.

162. Tanga, B., Yuana, L., Shib, T., Yua, L., Zhua, Y. 2009. Preparation of nano-sized magnetic particles from spent pickling liquors by ultrasonic-assisted chemical co-precipitation. Journal of Hazardous Materials. 163, 1173-1178.

163. Tartaj, P., Morales, M. P., Veintemillas-Verdaguer, S., Gonzalez- Carreno, T., Serna, C. J. 2006. Synthesis, properties and biomedical applications of magnetic nanoparticles. Handbook of Magnetic Materials; Elsevier: Amsterdam, The Netherlands, 403.

164. Teja, A.S., Koh, P.Y. 2009. Synthesis, properties, and applications of magnetic iron oxide nanoparticles. Progress in Crystal Growth and Characterization of Materials 55, 22-45.

165. Thammawong, C., Opaprakasit, P., Tangboriboonrat, P., Sreearunothai, P. 2013. Prussian blue-coated magnetic nanoparticles for removal of cesium from contaminated environment. The Journal of Nanoparticle Research. 15, 1689-1695.

166. Tiwari, D., Kim, H.U., Lee, S.M. 2007. Removal behavior of sericite for Cu(II) and Pb(II) from aqueous solutions: batch and column studies. Separation and Purification Technology. 57, 11–16.

167. Tiwari, D., Yang, J.K., Lee, H.Y., Cho,i K.M., Lee, S.M. 2009. Removal of Mn(II) from aqueous solutions using manganese coated sand. Journal of Chemical Engineering data. 54, 1823–1828.

168. Tran, H.V.,Tran, L.D., Nguyen, N.T. 2010. Preparation of chitosan/magnetite composite beads and their application for removal of Pb(II) and Ni(II) from aqueous solution. Materials Science and Engineering C. 30, 304–310.

169. Treybal, R.E. 1981. Mass-Transfer Operations, third ed., McGraw-Hill international, Singapore.

170. Unsoy, G., Gunduz, U., Opres, O., Ficai, D., Sonmez, M., Radulescu, M., Alexie, M., Ficai, A. 2015. Magnetite: from synthesis to applications. Current Topics in Medicinal Chemistry. 15, 1622-1640.

171. Uzun, L., Türkmen, D., Yılmaz, E., Bektas, S., Denizli, A. 2008. Cysteine functionalized poly(hydroxyethylmethacrylate)monolith for heavy metal removal. Colloids and Surfaces A: Physicochemical and Engineering Aspects. 330, 161–167.

172. van Ewijk, G. A., Vroege, G. J., Philipse, A. P. 1999. Convenient preparation methods for magnetic colloids. Journal of Magnetism and Magnetic Materials. 21, 31-33.

173. Vayssières, L., Chanéac, C., Tronc, E., Jolivet, J.P. 1998. Size tailoring of magnetite particles formed by aqueous precipitation: an example of thermodynamic stability of nanometric oxide particles. The Journal of Colloid and Interface Science. 205, 205–212.

174. Vincent, T., Vincent, C., Guibal, E. 2015. Immobilization of metal hexacyanoferrate ion exchangers for the synthesis of metal ion sorbents - a mini-review. Molecules 20, 20582–20613.

175. Wang, H.J., Zhou, A.L., Peng, F., Yu, H., Yang, J. 2007. Mechanism study on adsorption of acidified multiwalled carbon nanotubes to Pb(II). The Journal of Colloid and Interface Science. 316, 277-283.

176. Wang, J., Chen, C. 2006. Biosorption of heavy metals by Saccharomyces cerevisiae: A review. Biotechnology Advances. 24, 427–451.

177. Wang, L., Li, J., Jiang, Q., Zhao, L. 2012. Water soluble Fe_3O_4 nanoparticles with high solubility for removal of heavy-metal ions from waste water. Dalton Transactions. 41, 4544–4551.

178. Wang, X B, Cai, W P, Lin, Y X, Wang, G Z., Liang, C H. 2010. Mass production of micro/nanostructured porous ZnO plates and their strong structurally enhanced and selective adsorption performance for environmental remediation. The Journal of Materials Chemistry. 20, 8582–8590.

179. Warner, C L, Addleman, R S, Cinson, A D, Droubay, T C, Engelhard, M H, Nash, M A, Yantasee, W., Warner, M. G. 2010. High-performance, superparamagnetic, nanoparticle-based heavy metal sorbents for removal of contaminants from natural waters. ChemSusChem. 3, 749–757.

180. Weber, W.J., Moriss, J.C. 1963. Kinetics of adsorption on carbon from solutions. Journal of Sanitary Engineering Division. 89, 31-60.

181. White, B.R., Stackhouse, B.T., Holcombe, J.A. 2009. Magnetic-Fe_2O_3 nanoparticles coated with poly-l-cysteine for chelation of As(III), Cu(II), Cd(II), Ni(II), Pb(II) and Zn(II), The Journal of Hazardous Materials. 161, 848–853.

182. Williams, G., Seger, B., Kamat, P.V. 2008. TiO_2-Graphene Nanocomposites. UV-Assisted Photocatalytic Reduction of Graphene Oxide. Nano. 2, 1487–1491.

183. Woo, K., Hong, J., Ahn, J.-P. 2005. Synthesis and surface modification of hydrophobic magnetite to processible magnetite@silica-propylamine. The Journal of Magnetism and Magnetic Materials . 293, 177-181.

184. Wu, W., He, Q., Jiang, C. 2008. Magnetic iron oxide particles: synthesis and surface functionalization strategies. Nanoscale Research Letters. 3, 397-415.

185. Wu, W., Yang, Y., Zhou, H., Ye, T., Huang, Z., Liu, R., Y. Kuan,g Y. 2012. Highly efficient removal of Cu(II) from aqueous solution by using graphene oxide. Water Air Soil Pollut. 224, 1–8.

186. Xin, X., Wei, q., Yang, J., Yan, L., Feng, R., Chen, G., Du, B., Li, H. 2012. Highly efficient removal of heavy metal ions by amine-functionalized mesoporous Fe_3O_4 nanoparticles. Chemical Engineering Journal. 184, 132-140.

187. Xu, F., Zhang, P., Navrotsky, A., Yuan, Z-Y., Ren, T-Z., Halasa, M., Su, B-L. 2007. Hierarchically assembled porous ZnO nanoparticles: Synthesis, surface energy, and photocatalytic activity. Chemistry of Materials. 19, 5680–5686.

188. Xue, Y. H. et al. 2011. Oxidizing metal ions with graphene oxide: the in-situ formation of magnetic nanoparticles on self-reduced graphene sheets for multifunctional applications. ChemComm. 47, 11689–11691.

189. Yan, G., T Viraraghavan, T. 2003. Heavy-metal removal from aqueous solution by fungus Mucor rouxii, Water Research. 37, 4486–4496.

190. Yang, H., Sun, L., Zhai, J., Li, H., Zhaoa, Y., Yu, H. 2014. In situ controllable synthesis of magnetic Prussian blue/graphene oxide nanocomposites for removal of radioactive cesium in water. Journal of Materials Chemistry A. 2, 326-332.

191. Yang, H.M., Jang, S.C., Hong, S.B., Lee, K.W., Roh, C., Huh, Y.S., Seo, B.K. 2016. Prussian blue-functionalized magnetic nanoclusters for the removal of radioactive cesium from water. Journal of Alloys and Compaunds. 657, 387-393.

192. Yang L., Ren X., Tang F., Zhang L. A practical glucose biosensor based on Fe3O4 nanoparticles and chitosan/Nafion composite film. Biosensors and Bioelectronics. 25 2009 p. 889- 895.

193. Yang, S.T., Chang, Y., Wang, H., Liu, G., Chen, S., Wang, Y., Liu, Y., Cao, A. 2010. Folding/ affrefation of graphene oxide and its application in Cu^{2+} removal. The Journal of Colloid and Interface Science. 351, 122-127.

194. Yantasee, W., Warner, C L., Sangvanich, T., Addleman, R S., Carter, G T., Wiacek, R J., Fryxell, G E., Timchalk, C., Warner, M G. 2007. Removal of heavy metals from aqueous systems with thiol functionalized superparamagnetic nanoparticles. Environmental Science & Technology. 41, 5114-5119.

195. Yasutaka, T., Kawamoto, T., Kawabe, Y., Sato, T., Sato, M., Suzuki, Y., Nakamura, K., Komai, T. 2013. Rapid measurement of radiocesium in water using a Prussian blue impregnated nonwoven fabric Journal of Nuclear Science and Technology. 50, 674–681.

196. Yavuz, C T, Mayo, J T, Yu, W W, Prakash, A, Falkne, J C, Yean, S, Cong, L, Shipley, H J, Kan, A, Tomson, M, Natelson, D., Colvin, V L. 2006. Low-field magnetic separation of monodisperse Fe$_3$O$_4$ nanocrystals. Science. 314, 964–967.

197. Yean, S, Cong, L, Yavuz, C T, Mayo, J T, Yu, W W, Kan, A T, Colvin, V L., Tomson, M B. 2005. Effect of magnetite particle size on adsorption and desorption of arsenite and arsenate. The Journal of Materials Research and Technology. 20, 3255-3266.

198. Yu, J. H., Lee, C.-W., Im, S.-S., Lee, J.-S. 2003. Structure and magnetic properties of SiO2 coated Fe2O3 nanoparticles synthesized by chemical vapor condensation process. Reviews on advanced materials science. 4, 55-59.

199. Yu, S., Wei, Q., Du, B., Wu, D., Li, H., Yan, L., Ma, H., Zhang, Y. 2013. Label-free immunosensor for the detection of kanamycin using Ag@Fe3O4 nanoparticles and thionine mixed graphene sheet Biosensors and Bioelectronics. 48, 224-229.

200. Yuan, Q., L,i N., Chi, Y., Geng, W., Yan, W., Zhao, Y., Li, X., Dong, B. 2013. Effect of large pore size of multifunctional mesoporous microsphere on removal of heavy metal ions. The Journal of Hazardous Materials. 254, 157–165.

201. Zhang, C., Sui, J. 2012. Efficient removal of heavy metal ions by thiol-functionalized superparamagnetic carbon nanotubes Chemical Engineering Journal. 210, 45-52.

202. Zhang, C., Wangler, B., Morgenstern, B., Zentgraf, H., Eisenhut, M., Untenecker, H., Kruger, R., Huss, R., Seliger, C., Semmler, W., Kiessling, F. 2007. Silica- and alkoxysilane-coated ultrasmall superparamagnetic iron oxide particles: a promising tool to label cells for magnetic resonance imaging. Langmuir 23, 1427-1434.

203. Zhang, G. Qu, J, Liu, H, Cooper, At, We, R. 2007. CuFe$_2$O$_4$/activated carbon composite: a novel magnetic adsorbent for the removal of acid orange II and catalytic regeneration. Chemosphere 68, 1058-1066.

204. Zhao, G., Li, J., Ren, X., Chen, C., Wang, X. 2011. Study of Graphene Oxide Structural Features for Catalytic, Antibacterial, Gas Sensing, and Metals Decontamination Environmental Applications. Environmental Science & Technology. 45, 10454-10462.

205. Zhao, G., Wen, T., Yang, X., Hu, J., Shao, D., Wang, X. 2012. Preconcentration of U(VI) ions on few-layered graphene oxide nanosheets from aqueous solutions. Dalton Transactions. 41, 6182-6188.

206. Zhao, G.X., Li, J.X., Ren, X.M., Chen, C.L., Wang, X.K. 2011. Few-layered graphene oxide nanosheets as superior sorbents for heavy metal ion pollution management. Environmental Science & Technology, 45, 10454–10462.

207. Zhao, Y -G., Shen, H -Y., Pan, S -D., Hu, M -Q. 2010. Synthesis, characterization and properties of ethylenediamine-functionalized Fe$_3$O$_4$ magnetic polymers for removal of Cr(VI) in wastewater. The Journal of Hazardous Materials. 182, 295–302.

208. Zhou, Y.T., Nie, H.L., Branford-White, C., He, Z.Y., Zhu, L.M. 2009. Removal of Cu^{2+} from aqueous solution by chitosan-coated magnetic nanoparticles modified with α-ketoglutaric acid Journal of Colloid and Interface Science. 330, 29-37.

209. Zhu, Y., Murali, S., Cai, W., Suk, J.W. Potts, J.R. Ruoff, R.S. 2010. Graphene and graphene oxide: synthesis, properties and applications. Advanced Materials. 1-19.

210. Zhuo, Y., Yuan, P.X., Yuan, R., Chai, Y.Q., Hong, C.L.2009. Bienzyme functionalized three-layer composite magnetic nanoparticles for electrochemical immunosensors. Biomaterials. 30, 2284–2290.

211. Zou, X.Y., Yin, Y.B., Zhao, Y.B., Chen, D.Y., Dong, S. 2015. Synthesis of ferriferrous oxide/L-cysteine magnetic microspheres and their adsorption capacity for Pb(II) ions. Materials Letters. 150, 59–61.